

Functional Characterization of Type II Secretion in *Chlamydia*

by

Emily Snavely

Department of Molecular Genetics and Microbiology
Duke University

Date: _____

Approved:

Raphael H. Valdivia, Supervisor

Jörn Coers

Gregory Taylor

David Tobin

Meta Kuehn

Dissertation submitted in partial fulfillment of
the requirements for the degree of Doctor
of Philosophy in the Department of
Molecular Genetics and Microbiology in the Graduate School
of Duke University

2017

ABSTRACT

Functional Characterization of Type II Secretion in *Chlamydia*

by

Emily Snavely

Department of Molecular Genetics and Microbiology
Duke University

Date: _____
Approved: _____

Raphael H. Valdivia, Supervisor

Jörn Coers

Gregory Taylor

David Tobin

Meta Kuehn

An abstract of a dissertation submitted in partial
fulfillment of the requirements for the degree
of Doctor of Philosophy in the Department of
Molecular Genetics and Microbiology in the Graduate School of
Duke University

2017

Copyright by
Emily Snavelly
2017

Abstract

Chlamydiae are obligate intracellular bacteria that infect a wide range of animal hosts. For a successful infection, interaction with the host cell by use of the type II (T2), type III (T3), and type V (T5) secretion systems is needed to secure nutrients and subvert the host innate-immune responses. While some the substrates and functions of the T3 and T5 secretion systems are known, a comprehensive understanding of what proteins constitute T2S substrates is largely lacking. Only one protein has been confirmed to be a T2S effector in *C. trachomatis*, the protease CPAF. In this work, we investigate the role of the T2SS and CPAF during *C. trachomatis* infection.

CPAF cleaves a defined set of mammalian and *Chlamydia* proteins in vitro. As a result, this protease has been proposed to modulate a range of bacterial and host cellular functions. However, it has recently come into question the extent to which many of its identified substrates constitute bona fide targets of proteolysis in infected host cells, rather than artifacts of post lysis degradation. Here we clarify the role played by CPAF in cellular models of infection by analyzing *Chlamydia trachomatis* mutants deficient for CPAF activity. We identified a mutant in Type II secretion (T2S) that accumulates unprocessed CPAF and two strains with nonsense, loss-of-function mutations in *cpa*. HeLa cells infected with these mutants did not display cleavage of previously reported CPAF substrates and lysates from HeLa cells infected with either T2S- or CPAF- *C. trachomatis* did not possess any detectable in vitro CPAF proteolytic activity. CPAF-deficient mutants displayed impaired generation of infectious elementary bodies (EBs), indicating an important role for this protease in the full replicative potential of *C. trachomatis*. HeLa cells infected with *cpa* mutant strains were not defective for

cellular traits that have been previously attributed to CPAF activity, including resistance to staurosporine-induced apoptosis, altered NF κ B-dependent gene expression, and resistance to reinfection. However, these observations do not imply that previously identified substrates are not targets of processing by CPAF in infected cells. We provide evidence in live cells that CPAF-mediated protein processing of at least two protein targets, vimentin filaments and the nuclear envelope protein Lamin-associated protein 1 (LAP1), a new CPAF substrate, occurs rapidly after the loss of the inclusion membrane integrity, but before loss of plasma membrane permeability and cell lysis. We postulate that CPAF plays a role late in infection, possibly during the stages leading to the dismantling of the infected cell prior to the release of EBs during cell lysis.

We further show defects in T2S impact bacterial attachment to host cells, intracellular growth, the properties of glycogen, and lytic exit. We sought to understand the basis of these phenotypes and identify additional substrates of the T2SS which contribute towards them. We use label-free quantitative liquid chromatography-tandem mass spectrometry (LC-MS/MS) for a comprehensive analysis of proteins present within WT and T2S-defective *C. trachomatis* bacteria. In combination with immunofluorescence analyses, we present evidence of a defined set of secreted proteins that associate with glycogen in the inclusion during infection and propose this polymer functions in regulating proteins secreted into the inclusion lumen.

Table of Contents

Abstract	iv
List of Tables	xi
List of Figures.....	xii
Acknowledgements	xiv
1. Introduction	1
1.1 Predicting and identifying substrates of the T2SS and their role in pathogenesis	4
1.1.1 Predicting T2S substrates	4
1.1.2 T2S substrates: from enzymatic activity to identity.....	7
1.1.3 Proteomic and genetic approaches to identify T2S exoproteins	8
1.1.4 T2S chaperones	9
1.1.5 Challenges faced in identifying secreted proteins during intracellular infection	10
1.1.6 The role of T2S and its substrates: survival and pathogenesis	12
1.2 Protein secretion during <i>Chlamydia</i> infection	14
1.2.2 Genetic tools for studying <i>Chlamydia</i>	16
1.2.3 The Chlamydial protease/proteasome-like activity factor CPAF	18
1.2.4 <i>C. trachomatis</i> accumulates extra-bacterial glycogen in the inclusion lumen	20
2. Reassessing the role of the secreted protease CPAF in <i>C. trachomatis</i> infection through genetic approaches.....	23
2.1 Introduction.....	23
2.2 Identification of <i>C. trachomatis</i> strains deficient in CPAF secretion or expression	26
2.2.1 A <i>Chlamydia</i> mutant defective for type II secretion accumulates unprocessed CPAF zymogen	26

2.2.2 Identification and generation of <i>Chlamydia</i> strains with loss-of-function mutations in CPAF	27
2.3 CPAF mutants are defective for the generation of infectious EBs	32
2.4 Phenotypes of CPAF-deficient <i>Chlamydia</i>	33
2.4.1 Cells infected with CPAF-deficient <i>Chlamydia</i> are resistant to staurosporine-induced apoptosis	33
2.4.2 CPAF is not required for protection from reinfection	34
2.4.3 CPAF is not required for dampening NFκB activity during infection.....	35
2.4.4 OmcB processing is reduced in cells infected with CPAF-deficient strains but not T2S mutants	36
2.4.5 HMGB1 cleavage during infection is partially dependent on CPAF	38
2.4.6 Golgin-84 is not cleaved during <i>C. trachomatis</i> infection	39
2.5 CPAF mediates cleavage of intermediate filaments late in infection.....	39
2.6 CPAF mediates cleavage of the nuclear envelope protein LAP1	45
2.7 Discussion	46
2.8 Materials and Methods	50
2.8.1 Reagents	50
2.8.2 Cell Culture and <i>Chlamydia</i> Infections	51
2.8.3 Plaque Assays.....	52
2.8.4 Identification and whole genome sequencing of CPAF-deficient LGV-L2 strains	52
2.8.5 Generation of M169 RST recombinant strains	53
2.8.6 Western blot analyses	54
2.8.7 In Vitro CPAF cleavage assays	55
2.8.8 IFU burst assays	56
2.8.9 Immunofluorescence	57

2.8.10 Detergent Extraction Assays	57
2.8.11 NFκB Reporter Assays	58
2.8.12 Apoptosis Induction Assay	59
2.8.13 Assessment of secondary infections	59
2.8.14 EGFP-Vimentin and LAP1-EGFP transfection and live cell microscopy	60
3. Investigating the role of the T2SS during <i>C. trachomatis</i> infection.....	61
3.1 Introduction.....	61
3.2 Impaired growth, glycogen granule production, and CPAF mis-localization are the result of a mutation in <i>gspE</i>	64
3.3 <i>C. trachomatis</i> mutants defective for type II secretion have decreased attachment to and exit from A2EN cells	68
3.4 Proteins accumulate in RstE4 bacteria	71
3.5 Proteome differences between RstE4 and WT bacteria	76
3.5.1 General secretory pathway in RSTE4 bacteria	76
3.5.2 Stress response proteins do not accumulate in RSTE4 bacteria	78
3.5.3 Predicted T2SS substrates do not accumulate in RSTE4 EBs	79
3.4.4 T2S-dependent differences in the abundance of virulence and T3S-related proteins.....	80
3.4.4.1 Glycogen biosynthesis proteins.....	81
3.5.5 Outer membrane protein levels differ in T2S deficient EBs.....	82
3.5.6 Accumulated proteins in RSTE4 bacteria have varied functions.....	84
3.6 Identifying candidate substrates of the type II secretion system	90
3.6.1 Using an alkaline phosphatase secretion assay to assess if predicted <i>Chlamydia</i> Sec signal sequences can drive secretion in <i>E. coli</i>	96
3.7 Localization of T2S candidate substrates during infection	97
3.7.1 CT017/Ctd1 and CT783 localize to <i>C. trachomatis</i> in infected cells.....	98

3.7.2	<i>C. trachomatis</i> proteins localize to glycogen during infection.....	99
3.7.3	CPAF expression levels are responsive to glycogen	103
3.8	<i>C. trachomatis</i> lytic exit is dependent on glycogen	103
3.9	Discussion	106
3.10	Materials and Methods	109
3.10.1	Reagents	109
3.9.2	Cell Culture and <i>Chlamydia</i> Infections	110
3.9.3	Identification of LGV-L2 mutant strains	110
3.9.4	Western blot analyses	111
3.9.5	Bacterial growth assays	111
3.9.6	Microscopy	111
3.9.7	Attachment and Entry Assays	112
3.9.8	Quantification of Exit	113
3.9.9	Preparation of <i>C. trachomatis</i> Total Protein Extracts	113
3.9.10	LC-MC Data Collection.....	114
3.9.11	LC-MS Data Processing and Protein Quantification.....	116
3.9.12	Sec Signal Prediction and Assessment.....	117
3.9.13	Glycogen Quantification Assays.....	118
4.	Future Perspectives	119
4.1	The path forward with CPAF	119
4.1.1	Using Rst5 and Rst17 to define the function of CPAF during <i>C. trachomatis</i> infection	119
4.2	The <i>C. trachomatis</i> type II secretion system	120
4.2.1	Identifying components of the T2SS.....	121

4.2.2 Identifying novel effector proteins.....	121
4.2.3 Investigating the role of glycogen during <i>C. trachomatis</i> infection	122
References.....	125
Biography	151

List of Tables

Table 1: Non synonymous single nucleotide variants identified in strains CTL2-M169 (CPAF-) and CTL2-M532 (CPAF-)	29
Table 2: Single nucleotide variants identified in strain RSTE4	65
Table 3: Proteome differences in the general secretory pathway between WT and RSTE4 EBs	77
Table 4: Stress response proteins do not accumulate in T2S-deficient bacteria	78
Table 5: HtrA and CT311 are not accumulated in T2S-deficient EBs	79
Table 6: Proteins involved in glycogenesis and glycogenolysis do not change between WT and RSTE4 EBs	82
Table 7: Outer membrane protein differences between RSTE4 and WT EBs	83
Table 8: Proteins accumulated greater than 1.5-fold in RSTE4 EBs compared to WT EBs	85
Table 9: <i>C. trachomatis</i> proteins predicted to contain Sec signal peptides using SignalP v3.0	91
Table 10: T2S candidate substrates	94

List of Figures

Figure 1: Schematic representation of the T2SS architecture.....	3
Figure 2: <i>C. trachomatis</i> developmental cycle.	15
Figure 3: Glycogen biosynthesis and breakdown.	21
Figure 4: Identification of <i>C. trachomatis</i> strains deficient in CPAF secretion or expression.....	28
Figure 5: Map of single nucleotide variants identified in CPAF-mutant and isogenic control strains.....	31
Figure 6: CTL2 <i>cpa::cat</i> is deficient in CPAF secretion and expression.	32
Figure 7: <i>C. trachomatis</i> mutants deficient in CPAF expression are impaired for the generation of infectious progeny.	33
Figure 8: CPAF is not required for many of the cellular phenotypes associated with <i>C. trachomatis</i> infection.	35
Figure 9: OmcB processing is diminished in cells infected with CPAF-deficient strains, but enhanced in T2S mutants.	37
Figure 10: Evidence for CPAF mediated processing of vimentin in intact cells.	40
Figure 11: The filament forming properties of vimentin are altered in a CPAF-dependent manner at late stages of infection.	42
Figure 12: Cleavage of vimentin in live infected cells occurs after inclusion rupture and is dependent on CPAF and T2S.	44
Figure 13: CPAF cleaves LAP1 during infection.....	45
Figure 14: Cleavage of LAP1 in live infected cells occurs after inclusion rupture and is dependent on CPAF and T2S.	47
Figure 15: Impaired growth, glycogen granule production, and CPAF localization result from a the mutation in <i>gspE</i>	67
Figure 16: HeLa cells deficient for <i>Gys1</i> have decreased levels of glycogen within the cells.	68
Figure 17: T2S mutants are defective in attachment to and exit from host cells.....	70

Figure 18: Proteins accumulate in RSTE4 bacteria.	71
Figure 19: <i>Chlamydia</i> protein contribution to the total based on peak intensities.	73
Figure 20: Principal component analysis of samples submitted for EB proteomics.	74
Figure 21: Immunoblot analysis of selected <i>C. trachomatis</i> proteins from WT and RSTE4 EB lysates.	75
Figure 22: Functional grouping of proteins accumulated in RSTE4 EBs.	90
Figure 23: Putative N-terminal signal peptides of T2S candidate substrates are sufficient for translocation of PhoA into the bacterial periplasm.	97
Figure 24: CT783 and CT017 localize prominently to the bacteria during <i>C. trachomatis</i> infection.	100
Figure 25: A subset of proteins are localized to glycogen granules during infection with RSTE4 or glgB <i>C. trachomatis</i> mutants.	102
Figure 26: Localization of CT733, CT600, and CT355 within the inclusion is dependent on the presence of glycogen.	104
Figure 27: CPAF expression is increased in strains with reduced levels of glycogen...	105
Figure 28: Glcogen synthesis regulates lytic exit.	106

Acknowledgements

I would like to thank my advisor Raphael Valdivia and my committee members for their support and influx of ideas. I also thank the Duke Light Microscopy Core Facility and the Proteomics and Metabolomics Shared Resource, along with my collaborator on Chapter 3, Dr. Guangming Zhong from the University of Texas Health Science Center at San Antonio. Additional contributions are as follows: Raphael Valdivia contributed to data analysis and manuscript preparation, Victoria Carpenter constructed the Gys1 KO cell lines, Marcela Kokes performed experiments and data analysis for Figures 4, 12, and 14, JD Dunn contributed toward experiments for Figure 13, and Robert Bastidas assisted with whole genome sequencing of Rst5 and Rst17.

Past and present members of the Valdivia laboratory, including Bidong Nyugen, Ine Jorgensen, Barbara Sixt, and Victoria Carpenter have been an invaluable resource for the completion of this work. In addition, I express my sincerest gratitude to both Sherilynn Black and Nancy Henshaw for their continued support and guidance as I sought to find my future career path. Finally, this work would not have been possible without the unceasing encouragement and love from family and friends, especially my amazing husband Kyle.

1. Introduction

To interact with the extracellular environment, bacteria have evolved numerous, highly specialized secretory pathways to release bacterial proteins and DNA across the cell envelope. Gram-negative bacteria have three principal layers that separate the interior of the cell from the outside environment: the outer membrane (OM), the peptidoglycan cell wall, and the inner or cytoplasmic membrane (IM) [1]. The molecular machines required for translocation from the interior to exterior of Gram-negative bacteria include the single OM spanning type V secretion system (T5SS) and the IM and OM spanning type 1 secretion system (T1SS), T2SS, T3SS, T4SS, and T6SS (reviewed in [2]). The substrates secreted by these various systems are required for bacterial survival, adhesion, invasion and establishment of infection, and adaptation to varying environments.

With the exclusion of secretion systems for one-step transport from the cytoplasm to the outside of the bacterial cell, proteins located outside of the cytoplasm, as well as substrates of the T2SS and T5SS, must first transit beyond the IM [3]. The Sec or twin-arginine translocation (Tat) pathways translocate proteins in an unfolded or folded state across the IM, respectively (reviewed in [4, 5]). Once in the periplasm, proteins transported via Sec will fold prior to interaction with the T2SS, which exports folded proteins from the periplasmic space to the exterior of the bacteria [6].

In the T2SS 12 to 15 *gsp* (general secretion pathway) genes are known encode components of the secretion machinery [6], with several additional proteins required for the assembly and proper localization of T2S components [7-10]. The use of the *gsp* nomenclature is not universal. While the genetic organization of large operons containing *gspC-gspO* is commonly found, some bacteria such as numerous

Acinetobacter species, have T2S genes dispersed in smaller clusters throughout the genome, similar to the organization of type IV pili (TFP) [6, 11, 12]. The pre-pilin peptidase, GspO, can also be located near TFP encoding genes and its function shared amongst the T2S and TFP systems, as is the case in *Pseudomonas aeruginosa* [13, 14]. The T2S and TFP systems are structurally similar and may be regulated in a comparable fashion. Work by Roelofs et al. suggests a class of ATPases, found in both the T2SS and TFP, bind to the signaling molecule cyclic diguanosine monophosphate (c-di-GMP); they identify a c-di-GMP binding T2S ATPase in *P. aeruginosa*, PA14_29490, and propose this may be a common regulation mechanism of some T2 and TFP systems [15].

The T2S apparatus likely spans both the inner and outer membranes, with the majority of the T2S components located in the cytoplasmic membrane or associated with the cytoplasmic side of the IM. Four parts compose the T2SS: the inner-membrane platform, the ATPase, the pseudopilus, and the outer-membrane complex (Fig. 1) [16, 17]. Unlike TFP, the pseudopilus in the T2SS remains confined to the periplasm. The four minor pseudopilins (GspH, I, J, and K) contain an N-terminus that is processed by the prepilin peptidase (GspO) prior to forming the pseudopilus tip [18]. Polymerization of the pseudopilins, including processing and addition of major pilin subunits (GspG) underneath the tip, requires the function of an ATPase, GspE [19, 20]. Interactions between GspE and bitopic IM platform protein GspL [21-24], along with GspL and GspG interactions [25], suggest GspL is the linker that allows for association between the ATPase and the pseudopilus through the IM platform. The other components of the IM platform form a complex and include the polytopic membrane protein GspF and the bitopic protein GspM [26-29]. The OM protein GspD is connected to the IM platform

through interactions with the transperiplasmic protein GspC [30, 31]. GspD is a member of the secretin family and forms a ring shaped structure in the outer membrane [7].

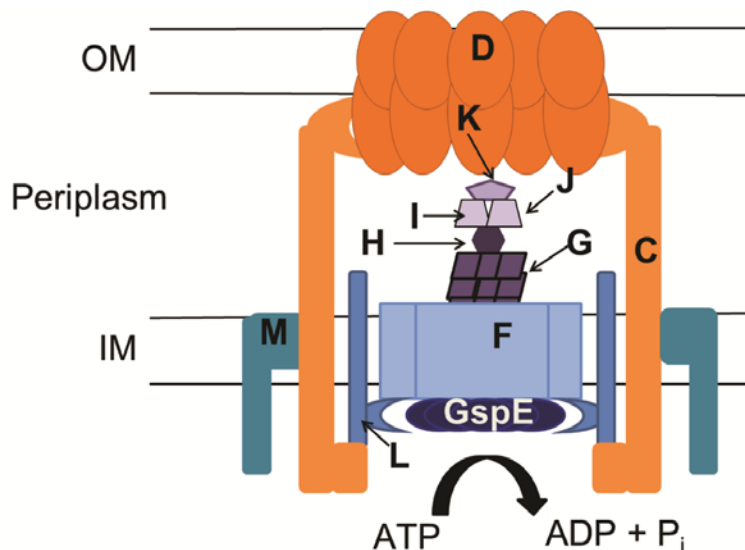


Figure 1: Schematic representation of the T2SS architecture. The inner membrane platform components are in blue, the outer membrane complex proteins are in orange, and the components of the pseudopilus are in purple. T2S substrates are first translocated across the inner membrane using a Sec-dependent pathway. Once in the periplasm, substrate recognition by GspC or GspD results in a signal transmitted to GspE to induce ATP hydrolysis. Conformational changes in GspE, transferred to GspL, aid in the formation and elongation of the pseudopilus, expelling the substrate through the GspD pore.

Proper localization and assembly of the secretin channel is accomplished in multiple ways. Some secretins, such as the *P. aeruginosa* HxcQ, are lipoproteins that contain an N-terminal lipid anchor allowing for self-transport to OM [32]. Conversely, additional proteins may be required for proper OM localization. Two distinct groups of OM targeting lipoprotein chaperones (pilotins) for GspD have been identified: the PulS-OutS family of proteins from organisms such as *Klebsiella oxytoca* and *Dickeya dadantii* [33, 34], and the AspS/YghG-type pilotins found in species of *Vibrio*, enteropathogenic *Escherichia coli* O127:H6 str. E2348/69 (EPEC), and enterotoxigenic *E. coli* (ETEC) str. H10407 [9, 10]. The GspAB-like complex may also be needed for correct secretin

assembly to occur; these proteins are believed to modify the organization of peptidoglycan to allow space for the transport and assembly of GspD [8]. Interestingly, mutations in *gspA* do not prevent the secretion of T2S substrates in numerous *Vibrio* species, but do result in decreased amounts of secretin multimer assembled, suggesting both GspAB and AspS may play a role in optimal GspD localization and assembly in certain bacteria [8].

The proton motive force and ATP hydrolysis provide the energy for T2 protein secretion [35, 36]. One mechanism for T2S involves the recognition by GspD or GspC of a T2S substrate, followed by substrate entry into the secretion channel. Cycles of ATP hydrolysis via GspE can convey conformational changes through the IM platform, allowing for the assembly of the pseudopilus. The growing pseudopilus is hypothesized to act as a piston and push the proteins through the secretin channel. Additional information regarding the structural and mechanistic aspect of T2S has been covered in numerous recent reviews [16, 17, 37].

1.1 Predicting and identifying substrates of the T2SS and their role in pathogenesis

The T2SS was first described in *Klebsiella* and since then has been shown to be conserved across numerous Gram-negative bacteria, including environmental, mammalian, and plant pathogenic strains [6, 38]. Throughout years of study, multiple methods have been employed to predict and identify proteins secreted by the T2SS. These strategies and the various confirmed substrates will be discussed below.

1.1.1 Predicting T2S substrates

Substrates of the T2SS use the Sec and Tat machineries to first cross the cytoplasmic membrane. The Sec pathway is thought to function as the major IM protein

transport system and is widely conserved across all bacteria, even present in the endoplasmic reticulum membrane of eukaryotic cells [5]. Two pathways of Sec-dependent protein translocation have been identified: co-translational and post-translational translocation [5]. Secretory proteins that reside in the periplasm or outer membrane are typically targeted post-translationally by the SecA/SecB pathway, while the co-translational signal recognition particle (SRP) targeting pathway is used by most inner membrane proteins, including the T2S pseudopilins [3, 39]. Translocating folded proteins across the IM using the Tat system allows for hetero-oligomeric complexes that form in the cytoplasm to be transported when only one of the subunits possesses a Tat-targeting signal peptide; folding in the cytoplasmic environment may also enable proteins to acquire a cofactor or obtain metal ions before translocation into the periplasm [4, 40].

Bioinformatical approaches, in combination with studies that employ bacterial strains containing mutations in either the Sec or Tat pathway, have been used to generate a catalog of proteins and activities that occur outside of the bacterial cytoplasm. Cleavable signal peptides present at the amino-terminal end of T2S substrates allow for targeting to either of these IM translocase systems [39]. A tripartite organization including a positively charged N-terminal region, followed by a hydrophobic then C-terminal domain, is found in both types of signal peptides [39]. Unlike Sec, Tat recognizes peptides that are longer and less hydrophobic and contain a distinctive pattern of two consecutive arginines in the N-terminal region [41]. By elucidating the structure of these signal sequences (ss), multiple groups have created computational prediction programs to differentiate between Sec and Tat signal peptides, while also discriminating these signals from possible transmembrane segments and lipoprotein signal peptides [41-46]. Voulhoux and colleagues identified putative substrates of the Tat

machinery by screening the genome of *P. aeruginosa* for the consecutive arginine motif [47]. Subsequent studies confirmed Tat-dependent secretion of the known T2S phospholipase C (PLC) proteins, PlcH and PlcN [47, 48]. In *Legionella pneumophila* strains 130b and Lens, the PlcA protein also contains twin arginines in the signal peptide and a portion of the secreted PLC activity is facilitated by the Tat system; Rossier and Cianciotto hypothesize PlcA export by the Sec pathway may occur in the absence of the Tat system [49].

Various experiments have confirmed T2SS substrates are translocated outside of the bacteria in a folded conformation, however no common primary amino acid sequence between substrates has been described [50, 51]. In *Pectobacterium carotovorum* and *Dickeya dadantii* (formerly known as *Erwinia carotovora* and *Erwinia chrysanthemi*), mutations in the last four residues at the C-terminal end of a polygalacturonase (PehA) β -lactamase hybrid or in a single tryptophan residue in Cel5 are sufficient to prevent T2-dependent secretion, respectively [52, 53]. Multiple, non-adjacent regions have been found to be necessary for the secretion of the *K. oxytoca* pullulanase, *P. aeruginosa* exotoxin A, and *P. carotovorum* PehA [54-57]. These regions vary in length and composition, suggesting a structural signal brought together during substrate folding may be recognized by the T2SS instead of a single portion of a protein.

The components of the T2SS required for exoprotein recognition vary based on organism and substrate, but include GspD, GspC, and the pseudopillins (reviewed in [6]). Recently, Pineau et al. used the *D. dadantii* pectate lyase Pell, along with the *P. carotovorum* orthologue Pel3, to define structural motifs that interact with the T2SS [58]. They observed direct interaction between multiple domains of OutC (GspC) and OutD (GspD) with an Fn3 domain of Pell that contains a loop region with a 3_{10} -helix.

Interestingly, the interaction between the PDZ domain of OutC and Fn3 was stronger in the presence of the N1 domain of OutD, suggesting interactions with this domain of OutD may increase the affinity of Fn3 to PDZ [58]. However, it remains unclear if a common T2S targeting motif is used for the recognition of secreted substrates from the milieu of proteins present in the periplasm.

1.1.2 T2S substrates: from enzymatic activity to identity

The T2SS secretes a wide variety of monomeric and oligomeric proteins, including toxins and degradative enzymes. While the T2SS was first described as exporting the *Klebsiella pneumoniae* pullulanase, a starch-debranching enzyme, the presence of this extra-bacterial enzymatic activity was known for many years prior [38, 59]. Additionally, the presence of cholera toxin (CT) in cell-free *Vibrio cholera* culture filtrate [60], the secreted pectinase and cellulase activities of *D. dadantii* [61], and chlamydia-dependent proteasome-like degradation activity in *Chlamydia trachomatis* infected cells [62] were all documented well before the proteins responsible were identified as substrates of the T2SS [63, 64]. Similarly, preceding the identification of a *L. pneumophila* strain with a mutation in the prepilin peptidase, PilD, several proteins were known to be secreted into the extracellular media [65, 66]. Identifying type II secretion genes and constructing strains deficient in secretion has allowed for observable enzymatic activities to be linked to substrates dependent on T2S in numerous bacteria.

By using homology searches with the T2S genes from organisms such as *V. cholerae*, *E. coli*, and *P. aeruginosa*, numerous T2S genes in other bacteria have been identified and subsequently mutated to determine if the system is functional. A similar homology search has been used by multiple groups to identify potential T2S substrates. In *A. baumannii*, $\Delta gspD$ and $\Delta gspE1$ mutants grew similarly to WT on LB agar, but failed

to grow on minimal agar in which olive oil was the sole carbon source [12]. Other bacterial strains defective in T2- dependent lipase secretion show similar phenotypes, and the presence of extracellular lipase activity was observed nearly 20 years ago in the related organism *Acinetobacter calcoaceticus* [67, 68]. Sequence searches using *P. aeruginosa* *lipA* and *lipB* identified homologous genes in *A. baumannii*; LipA was further shown to be secreted by the T2SS [12]. Prior knowledge regarding the types of enzymatic activities that occur in similar bacteria is often a jumping point toward identifying potential T2 exoproteins. For example, chitinase production in other *Vibrionaceae* [69] prompted the observation of chitinase activity in *V. cholerae*, the identification of the *chiA* gene, and the use of a *gspE* mutant to verify dependence of ChiA on the T2SS for extracellular transport [70].

1.1.3 Proteomic and genetic approaches to identify T2S exoproteins

Recent work has focused on proteomic approaches to capture a broader picture of the T2 secretome. For example, by comparing the supernatants of WT to T2SS deficient M2 Δ *gspD*::kan cultures, the secretome of *Acinetobacter nosocomialis* strain M2 was determined [11]. Using two-dimensional difference gel electrophoresis (2D-DIGE) analysis coupled with capillary-liquid chromatography-nanospray tandem mass spectrometry for protein identification, the authors identified and characterized three T2S-dependent effectors in detail: a metallopeptidase (CpaA), an ortholog to the *A. calcoaceticus* lipase LipA, and newly characterized lipase, LipH [11]. Comparable approaches have been used to identify secreted proteins in human and plant pathogens, along with non-pathogenic environmental bacteria. Some of bacteria in which proteomic approaches have identified novel T2S substrates include: *A. baumannii* [11, 12], *A. nosocomialis* [11], *Burkholderia pseudomallei* [71], *Burkholderia glumae* [72, 73], *V.*

cholera [74, 75], *Ralstonia solanacearum* [76, 77], *Pseudoalteromonas tunicate* [78], and *L. pneumophila* [79]. These substrates have a wide variety of functions, not all of which are known, and are required for processes such as: biofilm formation, nutrient acquisition, adherence to cell surfaces, suppression of host innate immunity, and extracellular respiration, just to name a few.

1.1.4 T2S chaperones

Similar to the T3SS, certain T2 substrates require additional proteins for their secretion. Within bacteria, molecular chaperones are proteins that assist in the folding or unfolding of individual proteins or protein complexes and can aid in preventing protein degradation or aggregation; chaperones are found in both the bacterial cytosol and periplasm. The first T2S chaperones were identified as being required for the secretion of extracellular lipases. These chaperones, termed Lif for lipase-specific foldases, have since been described in *Pseudomonas*, *Burkholderia*, *Aeromonas*, and *Acinetobacter*, among others [12, 67]. Lif's supply the steric information necessary for the proper folding of lipases, but as they contain a hydrophobic N-terminal membrane anchor they cannot be secreted by the T2S machinery [72].

Periplasmic formation of disulfide bonds is also known to be important for the secretion of certain T2 exoproteins [80, 81], including cholera toxin from *V. cholera* [82] and enterotoxin II from *E. coli* [83]. While disulfide bond formation is not universally required for the secretion of substrates [84], it can be important to maintain the extracellular enzymatic function of an exoprotein [85, 86]. Additionally, not all substrates contain intramolecular disulfide bonds [51, 85].

Recent studies have shown that T2S-dependent lipases are not the only proteins that require chaperones. Two of the three T2 secreted proteins identified by Harding et

al. in *A. nosocomialis* were adjacent to proteins that were demonstrated to be required for their secretion [11]. Consistent with studies in other *Acinetobacter* spp. [12, 67], one of these two T2S proteins was the lipase LipA, whose secretion is dependent on LipB [11]. However, this study was the first to identify a T2S chaperone (CpaB) required for the secretion of a protease (CpaA) [11]. Analysis by Domain Enhanced Lookup Time Accelerated (DELTA) BLASTp identified a domain from the SRPBCC superfamily in CpaB, members of which contain a deep hydrophobic ligand-binding pocket and are predicted to have chaperone activity. Furthermore, by searching ORFs that contain a predicted N-terminal transmembrane domain and are adjacent to known T2S effectors from other bacteria, the authors identified several putative T2S effector chaperones [11].

While the bulk of previously identified T2S chaperones are located adjacent to their proposed effectors, the LipC lipase from *P. aeruginosa* requires the presence of LipB, a protein that is located elsewhere in the genome downstream of a different lipase, LipA [87]. Chaperone-effector interactions have been used in other secretion systems, such as the T3SS from *C. trachomatis* [88], to identify new effector proteins. In combination with the new bioinformatical approach taken by Harding et al. to identify chaperones, similar biochemical approaches may be used to identify novel T2 chaperone-effector complexes.

1.1.5 Challenges faced in identifying secreted proteins during intracellular infection

The T2SS is important for bacterial survival in a diverse set of environments. In some bacteria, multiple T2SS are present and secrete proteins in response to varying conditions [89-92]. For example, a second T2SS present in *P. aeruginosa*, HcX, secretes low molecular weight alkaline phosphatases in response to phosphate limitation

[91]. Similarly, *Yersinia ruckeri* and *Yersinia enterocolitica* both possess the Yts1 and Yts2 T2SSs; the activation of the Yts1 system occurs at temperatures below that of a human host, indicating its secreted substrates may be important for environmental survival [89]. The *L. pneumophila* Lsp T2SS is also required for optimal low temperature growth and it is proposed the peptidyl-prolyl cis-trans isomerase, PpiB, functions as an isomerase or chaperone for the T2S apparatus and/or its substrates at these temperatures [93-95].

Establishing the conditions under which various secretion systems are active poses a challenge towards identifying their substrates. However, as showcased by *L. pneumophila*, secretion of effectors and their contribution to infection is also dependent on the specific host. In the environment, *Legionella* infects and grows in amoebae belonging to the *Acanthamoeba*, *Naegleria*, and *Hartmannella* genera [96]. Of the numerous secreted effectors analyzed, the metalloprotease ProA, RNase SrnA, and glycerophospholipid:cholesterol acyltransferase PlaC, are required for intracellular infection of *Hartmannella vermiformis* and *Naegleria lovaniensis*, but not for *Acanthamoeba castellanii* infection [97, 98]. In contrast, a *nttA* mutant exhibited reduced survival in *A. castellanii*, but was not defective for growth in *H. vermiformis* or *N. lovaniensis* [97]. ProA directly processes PlaC and is required for its activity [99]. Intriguingly, even though both ProA and PlaC are important for intracellular growth in *H. vermiformis* and *N. lovaniensis*, a *proA* mutant or *proAplaC* double mutant is more defective in growth compared a *plaC* mutant in *N. lovaniensis*; all three mutants are similarly impaired for growth in *H. vermiformis* [97]. This suggests ProA may be active beyond processing PlaC in certain hosts.

Many of the T2S substrates in *L. pneumophila* were identified by comparing the

supernatant of WT and *lsp* mutants [79, 100]. Unlike facultative intracellular organisms, analysis of secreted proteins in obligate intracellular bacteria is complicated by the need to separate extra-bacterial proteins present in the vacuole and/or host cytosol from those remaining inside the bacteria. In *Coxiella burnetii* the introduction of host cell-free growth medium has enabled mass spectrometry approaches to identify proteins present in culture supernatants [101-103]. However, it is probable only a subset of substrates are secreted in an environment lacking host-cell feedback. An axenic medium that supports some metabolic activity of *C. trachomatis* has also been developed, however bacterial growth and the secretion of proteins has yet to be assessed under these conditions [115]. If conditions where secretion is active are identified, this approach still will not identify substrates secreted over time during the lifecycle. As discussed later, new methods for genetic manipulation, combined with indirect immunofluorescence and proteomics, have advanced the discovery of secreted proteins in *Chlamydia*.

1.1.6 The role of T2S and its substrates: survival and pathogenesis

Functional T2SSs have been identified in human and animal pathogens, along with numerous plant pathogenic species. The genera that infect humans are: *Acinetobacter*, *Aeromonas*, *Burkholderia*, *Chlamydia*, *Escherichia*, *Klebsiella*, *Legionella*, *Pseudomonas*, *Stenotrophomonas*, *Vibrio*, and *Yersinia* [11, 12, 33, 37, 56, 64, 91, 104-113]. These bacteria facilitate disease at diverse anatomical locations, including the lungs, gastrointestinal tract, genital tract, and bloodstream. For each of these genera, mutations in genes of the T2SS or in confirmed effectors impacts growth and/or virulence in animal models of disease [71, 79, 89, 109, 114-123]. For example, in a modified experimentally-induced leukopenic mouse model of *A. baumannii* infection, a Δ *gspD* mutant and a strain containing the deletion of a T2 lipase LipA, were out

competed by the WT strain and exhibited colonization defects in the liver and spleen [12]. All three strains grow similarly in LB broth, suggesting a role for lipases and T2S in the *in vivo* environment. In a murine acute pulmonary infection model, mice intranasally inoculated with an *A. nosocomialis* $\Delta gspD$ mutant displayed significantly lower bacterial burdens in the lung and spleen, providing further evidence for the role of T2S in *Acinetobacter* pathogenesis [11].

The T2SS is also required to cause disease in flowers, fruit, rice, and vegetables [61, 124-126]. To begin and sustain a successful infection, *Xanthomonas oryzae* pv. *oryzae* (*Xoo*) must first degrade the plant cell wall. Ethyl methane sulfonate (EMS) mutagenesis identified *Xoo* strains with mutations in *gspD* and *gspF* that did not secrete the cell wall degrading xylanase, resulting in infection defects in both rice and tomato leaf models [127].

Not all T2S genes are required for secretion. In *A. baumannii*, $\Delta gspN$ strains grew similarly to WT on LB agar and on minimal agar with olive oil as the sole carbon source, the latter suggesting lipase secretion remains intact [12]. Consistent with these observations, in a mouse pulmonary infection model the $\Delta gspN$ mutant showed no virulence defects in survival or competition assays, compared to the parental strain [128]. This observation is congruent with studies in *K. oxytoca* where Gsp proteins B, H, and N are not required for pullulanase secretion [29].

The number of substrates secreted by various T2SSs ranges from 1 in *Klebsiella* to over 20 in *L. pneumophila*, with most secreted proteins having an enzymatic activity. In plant pathogens, T2-dependent degradative enzymes are common as they release carbohydrates and nutrients necessary for bacterial growth and survival. Some of the cell wall degrading enzymes secreted are polygalacturonases, cellulases, xylanases,

and pectate or pectin lyases [90, 127, 129]. Correspondingly, in human pathogens T2 secreted enzymes include: phosphatases [92], proteases [11, 64, 130, 131], lipases [12, 73, 86, 87], chitinases [69, 70], phospholipases [99, 132-136], and even an RNase [137] and DNase [120]. Another class of T2S exoproteins are outer membrane surface-anchored proteins that are either lipoproteins or associated with lipopolysaccharides [138]. Well known toxins such as the aerolysin from *Aeromonas spp* [36, 51], heat-labile enterotoxin from *E. coli* [84, 139, 140], exotoxin A from *P. aeruginosa* [48, 136], and cholera toxin from *V. cholerae* are also secreted by the T2SS [63, 96, 141]. Further studies are required to ascribe functions to novel T2-depending proteins that have been identified using proteomic approaches.

1.2 Protein secretion during Chlamydia infection

Chlamydiae represent a group of obligate intracellular bacteria that can infect a wide range of eukaryotic hosts; in particular, *C. trachomatis* infects both the ocular epithelia and the urogenital tract epithelia of humans[142]. Despite antibiotic regimens and sexually transmitted disease (STD) prevention education, *C. trachomatis* remains the most common notifiable disease in the United States, with the Centers for Disease Control and Prevention reporting over 1.5 million cases of infection in 2015, representing a 5.9% increase in the rate of reported cases since 2014 [143]. The continued rise in *Chlamydia* cases is concerning considering infections are long lasting if untreated and are often asymptomatic. Untreated urogenital infections can result in serious complications, including chronic pelvic pain, pelvic inflammatory disease, ectopic pregnancy, and infertility[144]. Understanding how *Chlamydia* manipulates its host to develop and maintain a specialized replicative niche will aid in the development of new methods for treatment and control of *Chlamydia* disease.

C. trachomatis has a complex biphasic developmental cycle that takes place within a parasitophorous vacuole termed the inclusion (Fig. 2). Infection begins when the infectious form of the bacteria, the elementary body (EB), attaches to a host cell. Once internalized, EBs differentiate to the reticulate body (RB) form and replicate. Prior to release and reinfection, RBs revert asynchronously back to EBs[145].

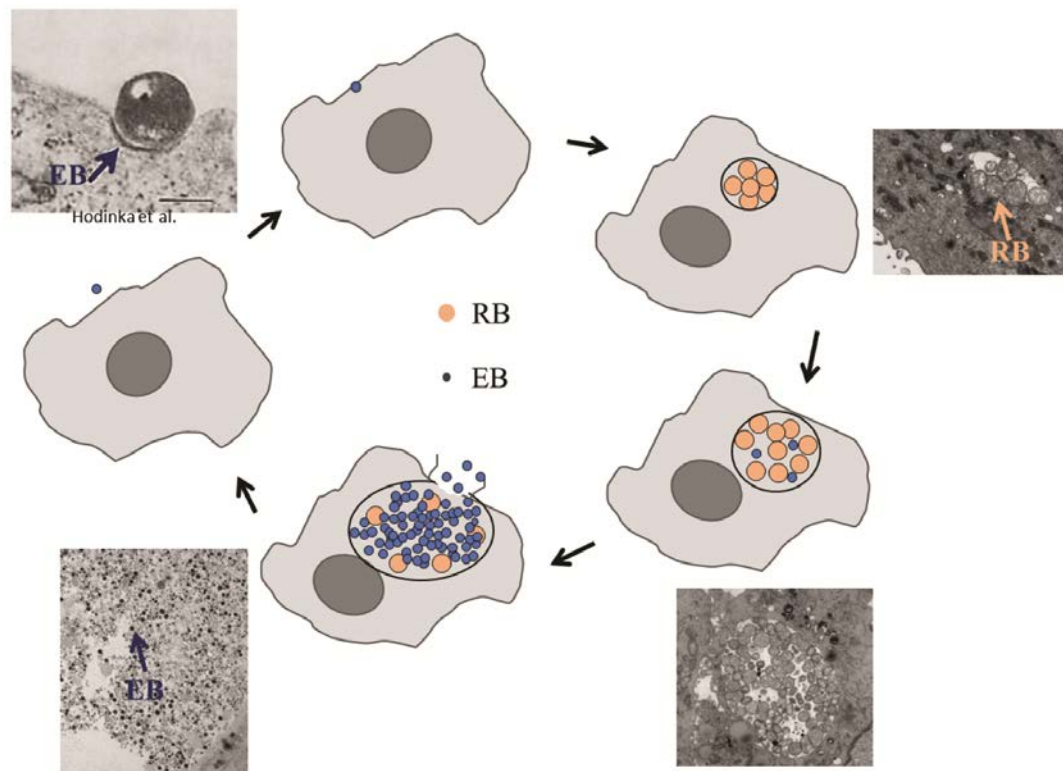


Figure 2: *C. trachomatis* developmental cycle. *Chlamydiae* convert between two morphologically and functionally discrete forms, the elementary body (EB) and the reticulate body (RB). The basic life cycle starts with the attachment and internalization of the EB (blue arrow-[146]). Once the EB is internalized, EBs will differentiate to RBs (peach arrow), the replicative form of the bacteria. The inclusion will grow as the RBs replicate and at later stages of infection asynchronous transition of RBs back into EB will occur. At the end of infection, the inclusion and host cell will lyse and released EBs can target a new cell.

As an intracellular pathogen, successful infection requires interaction with the host cell to secure nutrients and subvert the host innate-immune response [147]. Even

though the *Chlamydia* genomes are relatively small (~1Mb), studies predict 10-15% of the genome encodes effector proteins that can be secreted from the bacteria into the inclusion membrane, inclusion lumen or host cytosol [148-150]. *C. trachomatis* uses multiple secretion mechanisms to access the host cytosol, including the nonflagellar type III secretion (nfT3S) and the T5S systems. The T3S system and its substrates are vital for *Chlamydia* survival and pathogenesis and are known to interfere with host cellular processes such as cytoskeletal rearrangements, organelle trafficking, and signaling (reviewed in [151]). The *C. trachomatis* genome also encodes for homologues of components required for a T2SS that can work in concert with the Sec system [150]. Previous work by our laboratory and work presented here shows the T2S system in *C. trachomatis* is functional and important for intracellular survival and replication [64, 152].

1.2.2 Genetic tools for studying *Chlamydia*

The obligate intracellular nature of *Chlamydia* combined with the complex life cycle complicates elucidating the role of individual proteins to pathogenesis. Strategies for the identification of *Chlamydia* secreted proteins are varied, but include identifying effectors based on host-derived effector protein modification during infection, detecting secreted proteins during infection using immunolocalization assays, and immunoprecipitation and mass spectrometry approaches to identify effectors complexed with chaperones [88, 153-159]. Verification of and screening for T3 effectors has been accomplished using various heterologous T3SSs combined with the localization of the effector outside the bacteria, although studies have also used small molecule inhibitors INP0400 and N'-(3,5-dibromo-2-hydroxybenzylidene)-4-nitrobenzohydrazide (compound 1) to block secretion during *C. trachomatis* infection [160, 161]. While inhibitors of the T2SS have yet to be identified, the compound arylomycin C16, an inhibitor that targets

signal peptidase I, has been successfully used to block the *Chlamydia* general secretory pathway [157, 162, 163].

Recent progress in molecular genetic manipulation of *Chlamydiae* facilitates characterization of specific genes (reviewed in [164]). Major advances in the genetic toolbox include the introduction of systems for group II intron insertions to disrupt open reading frames and plasmid-based transformation protocols allowing for the expression of genes during the *Chlamydia* life cycle [165-168]. Mueller et al. recently described the use of fluorescence-reported allelic exchange mutagenesis (FRAEM) for targeted genomic sequence deletion and allelic exchange; they successfully used this approach to delete the open reading frames *trpA*, *ctl0063*, *ctl0064*, and *ctl0065* [169]. The use of the chemical mutagen ethyl methanesulfonate (EMS) has been used to create mutant libraries containing an array of point mutations in the *Chlamydia* genome. These libraries have been used for forward and reverse genetic applications [152, 170-173]. The generation of a diverse range of alleles for genetic analysis, including not only loss- or gain-of-function mutants, but also the potential to generate weak nonlethal alleles, is an advantage of chemical mutagenesis as it allows for the study of essential genes [64, 88, 152, 171, 172]. This last approach is key, as it is unlikely a section system will be able to be knocked out in its entirety.

In light of the recent advances allowing for the genetic manipulation of *Chlamydiae*, Bauler and colleagues devised a method of verifying protein access to the host cytosol by constructing a shuttle vector system that allows for the expression of candidate secreted effector proteins that have been tagged with various reporters [174]. The fusion of the known secreted proteins to a C-terminal FLAG tag, glycogen synthase kinase (GSK) tag, or the adenylate cyclase (*CyaA*) gene and subsequent assays

allowed for the confirmation that known effectors IncD and the CPAF access the host cytosol; however, CPAF's location was only verified by immunofluorescence with anti-FLAG antibodies, it was not fused to GSK or CyaA [174]. Secretion of some effector proteins in the intracellular pathogen *C. burnetii* has been confirmed with the use of β -lactamase (BlaM) translational fusions [175]. This approach, adapted by Mueller and Fields for *C. trachomatis* to verify the secretion of effectors CT694 and CT695, opens the possibility of screening for secreted proteins in the context of *Chlamydia* infection [176].

1.2.3 The Chlamydial protease/proteasome-like activity factor CPAF

Proteasome-like activity was first detected in the cytosol of *Chlamydia* infected cells as corresponding with the degradation of host transcription factors RFX5 and USF-1 [62]. This degradation was observed to be dependent on *Chlamydia* protein synthesis and could be inhibited by the proteasome inhibitor lactacystin; other proteasome and protease inhibitors were not effective against this activity [62]. Using column chromatography, Zhong et al. purified two protein bands responsible for the protease activity and matched the sequence of both bands to a protein encoded by CT858 (CTLO233), designated CPAF for chlamydial proteasome-like activity factor [177].

CPAF is a serine protease that is synthesized as a 70kDa proprotein prior to processing into two shorter polypeptides: a 35kDa CPAFc and a 25kDa CPAFn fragment, corresponding to the C-terminal and N-terminal halves of the protein, respectively [178]. Both polypeptides remain complexed together (CPAFc/n) and two of these complexes dimerize to form the catalytically active molecule (CPAFc/n:CPAFc/n) [156, 178]. Activation of CPAF occurs in three steps. Transient dimerization between two CPAF zymogens allows for cleavage between Met242 and Arg243, stabilizing the

formation of the homodimer and freeing the activation switch. Conformational changes then bring together the water-mediated catalytic triad, allowing for cleavage after Met264 and release of a portion of the inhibitory segment present within each CPAFc/n complex. The remaining inhibitory peptide portion is released following cleavage at Ser283 [179]. The sequence of this inhibitory peptide has been used to help define the role of CPAF in *Chlamydia* pathogenesis [180, 181], however it can have off-target effects [182].

CPAF is conserved amongst the *Chlamydiaceae* and processing into the CPAFc/n is observed in clinical isolates [156, 178, 183]. Cellular fractionation and immunofluorescence confirmed CPAF is localized to the host cell cytosol during infection [177] and requires the Sec translocation machinery to access the bacterial periplasm [163]. Prior to the introduction of methods for genetic manipulation of *Chlamydia*, CPAF was proposed to cause a number of effects on the infected host cell. Many of these connections were based on phenotypes observed during infection and corresponding cleavage or degradation of host and bacterial proteins by CPAF. For example, downregulation of major histocompatibility complex (MHC) class I, MHC class II, and CD1d antigen presentation was believed to be due to CPAF-mediated degradation of RFX5 and USF1, along with direct processing of the heavy chain of CD1d by CPAF, leading to its degradation by the host proteasome [178, 184]. Recent evidence suggests CPAF remains active during standard protein harvesting procedures and that some of the substrates previously thought to be cleaved by CPAF during infection are mostly cleaved during sample preparation [182]. However, many of the previously observed *Chlamydia*-host interactions still occur under conditions where CPAF is not active, opening up exciting opportunities to discover CPAF-independent manipulation mechanisms.

1.2.4 *C. trachomatis* accumulates extra-bacterial glycogen in the inclusion lumen

Glycogen is a polysaccharide that contains branched glucose (Glc) units and is known to be a major energy reserve in both eukaryotes and bacteria. In accordance with numerous other bacteria, *Chlamydia* possess the genes required for glycogen biosynthesis (Fig. 3) [185] [150]. The pathway begins when glucose-1-phosphate (Glc1P) is converted to ADP-glucose (ADP-Glc) via the ADP-Glc pyrophosphorylase GlgC. The glycogen synthase, GlgA, can use both ADP-Glc and host-derived UDP-Glc as a substrate to form a linear chain of α 1,4-linked Glc molecules [186]. The linear molecules are branched through α 1,6-glucosidic bonds introduced via the branching enzyme GlgB, increasing the solubility of glycogen. Glycogen catabolism to Glc1P utilizes the debranching enzyme GlgX, along with the glycogen phosphorylase GlgP. The phosphoglucomutase MrsA can convert Glc1P to Glc6P, the latter of which can be imported into the bacteria using the hexose phosphate transporter UhpC [186]. Curiously, Glc6P is thought to be the main energy source of EBs, as opposed to RBs which use ATP [187]; however, multiple proteomic studies suggest the Glc6P importer UhpC is up to five-fold more abundant in RBs, compared to EBs [188, 189]. This discrepancy is not fully understood.

In addition to glycogen inside the bacteria, both *C. trachomatis* and *C. muridarum* are unique in their ability to accumulate extra-bacterial glycogen within the inclusion lumen during infection; this occurs before glycogen appears in EBs and a timepoint (16-20 hpi) when very few EBs are present within the inclusion [186, 190, 191]. Previous studies by our laboratory hinted that glycogen enzymes may act outside of the bacteria as mutations in the branching enzyme, GlgB, led to the accumulation of glycogen

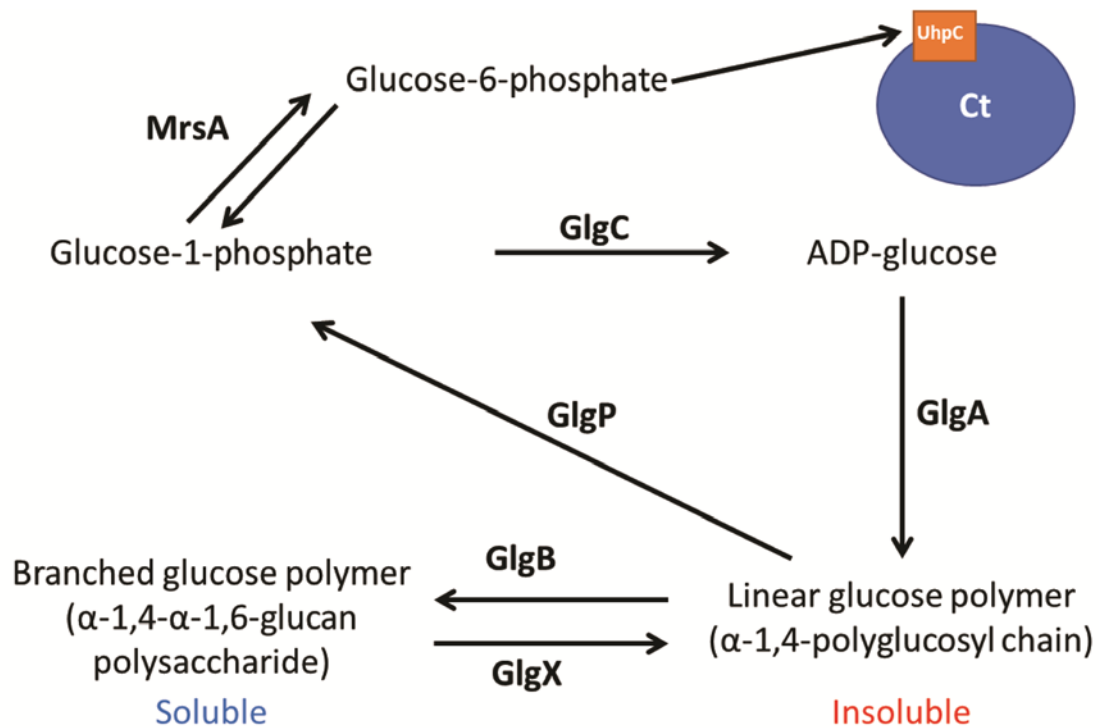


Figure 3: Glycogen biosynthesis and breakdown. Glc1P is converted to ADP-Glc using the enzyme GlgC. Linear glycogen chains are then formed by the glycogen synthase GlgA using both ADP-glucose derived from the bacteria and UDP-glucose imported from the host cell. These linear chains are insoluble until they are branched by GlgB. During catabolism, the debranching enzyme GlgX and the phosphorylase GlgP generate Glc1P. MrsA converts Glc1P to Glc6P which can be imported by the bacteria using UhpC.

granules within the inclusion lumen; the granules are thought to be composed of linear, insoluble glycogen. Additionally, these *glgB* mutant strains did not differ in the production of infectious progeny compared to WT, suggesting bacterial lysis was not the source of the extra-bacterial glycogen [152]. Further studies confirmed the localization of various glycogen enzymes: Lu et al. localized GlgA outside of the bacteria, while Gehre et al. expanded this observation to include GlgX [159, 186]. Using a heterologous *Shigella flexneri* assay, Gehre et al. fused the N-termini of various *C. trachomatis* glycogen enzymes to a calmodulin-dependent adenylate cyclase from *Bordetella pertussis* and tested for the ability of the fusion enzymes to be secreted in the supernatant [186]. Their

work supports secretion of GlgA, GlgB, GlgX, GlgP, and MrsA (but not GlgC) into the inclusion lumen via the type III secretion system [186]. Build-up of glycogen in the inclusion is also accomplished by the bulk translocation of glycogen from the host cytoplasm [186]. When host-glycogen is imported into the inclusion, the host glycogen synthase, Gys1, is also localized within the inclusion lumen [186].

Chlamydia possess a conserved 7.5 Kb plasmid that encodes eight open reading frames. Plasmid encoded protein Pgp4 is a known transcriptional regulator of chromosomal genes, including *glgA* [192, 193]. Plasmid-free organisms have been created in *C. muridarum* by curing the plasmid with novobiocin treatment [190] and naturally occurring plasmidless strains have been isolated from clinical samples of *C. trachomatis* [194]. One notable phenotype of plasmid-free *C. muridarum* and *C. trachomatis* strains is the lack of glycogen within the inclusion lumen, presumably due to the downregulation of *glgA* in the absence of Pgp4 [190, 191, 195]. The plasmid is dispensable for *C. trachomatis* and *C. muridarum* growth *in vitro*. However, *in vivo* studies have shown the plasmid is required for upper genital tract pathology in mice during *C. muridarum* infection and for the ability of *C. trachomatis* to colonize and sustain an infection in the mouse genital tract [191, 196]. Numerous plasmid-regulated chromosomal genes may contribute towards the growth of *Chlamydia in vivo* and further studies are needed to delineate the individual contribution of *glgA*, and therefore glycogen, to this phenotype.

In this work, we investigate the role of the only confirmed T2S substrate, CPAF, during *C. trachomatis* infection, use quantitative proteomics to identify proteins that accumulate in a *C. trachomatis* T2S-mutant strain, and propose a new function for glycogen within the inclusion lumen.

2. Reassessing the role of the secreted protease CPAF in *C. trachomatis* infection through genetic approaches¹

2.1 Introduction

The obligate, intracellular bacterial pathogen *Chlamydia trachomatis* primarily infects epithelial cells of the urogenital tract and the conjunctiva, leading to sexually transmitted diseases and conjunctivitis [197]. Disease is often associated with immune damage resulting from chronic inflammation due to repeated and recurring infections. In women, this can result in severe sequelae such as pelvic inflammatory disease, ectopic pregnancies and infertility [198]. Similarly, recurrent and untreated *C. trachomatis* conjunctival infections can lead to trachoma, a prominent cause of blindness worldwide [199].

C. trachomatis infection begins with the attachment and entry of elementary bodies (EB), the invasive form of *Chlamydia*, onto epithelial cells. Upon entry, the EB form transitions into the replicative reticulate body (RB) form, and establishes a parasitophorous vacuole (“inclusion”) that avoids fusion with lysosomal compartments [197]. At mid-to-late stages of infection, RB replication becomes asynchronous to generate more RBs and intermediary forms that transition back to the EB form. By the end of the cycle, bacteria within the inclusion are released to infect neighboring cells. The process of exit from infected cells can occur through a lytic phase, where there is a programmed dismantling of the inclusion membrane that precedes loss of plasma

¹ Parts of Chapter 2 are reused and edited with permission from the following published research paper: Snavely EA, Kokes M, Dunn JD, Saka HA, Nguyen BD, Bastidas RJ, et al. Reassessing the role of the secreted protease CPAF in *Chlamydia trachomatis* infection through genetic approaches. *Pathog Dis.* 2014;71(3):336-51. doi: 10.1111/2049-632X.12179.

membrane integrity, and a non lytic, “extrusion” exit mechanism that leads to the exocytosis of the entire inclusion or inclusion fragments [200].

To modulate host cellular functions, *Chlamydia* employs a type III secretion (T3S) system to translocate “effector” proteins that mediate cell invasion, re-routing of lipid transport, and manipulation of signaling pathways important in immunity [148]. In addition, some *Chlamydia* virulence proteins contain “classical” signal peptides and presumably use the Sec system to cross the bacterial cytoplasmic membrane [163]. How these signal peptide-containing proteins are further translocated from the bacterial periplasmic space to the inclusion lumen and eventually across the inclusion membrane is unclear. Potential delivery pathways include: outer membrane vesicles, which have been observed and purified during *C. trachomatis* infection, [201, 202] and Type II secretion (T2S), which in Gram-negative bacteria is required to secrete a subset of folded proteins across the outer membrane [203]. One prominent example of a protein that may follow this secretion pathway is the *chlamydial* *protease-like activity factor* (CPAF), a serine protease [177]. Late in infection, CPAF localizes to the inclusion lumen and the host cell cytoplasm as assessed by immunofluorescence microscopy and subcellular fractionation [204, 205]. CPAF can cleave in vitro two transcription factors (RFX5 and USF1) required for the expression of antigen presentation molecules (MHC), the pro-apoptotic factors Bim and Puma [177, 206], p65/RelA, a transcription factor required for NFκB signaling [207], intermediate filaments, [208, 209], the adherence junction protein nectin1 [210], the MHC-like lipid presentation protein CD1d [184], the pro-inflammatory mediator HMGB1 [211], the mitotic cell cycle regulator CyclinB1 [212], securin [213, 214], the Golgi tethering factor Golgin 84 [214], and PARP – a mediator of DNA-damage during apoptosis [215].

Because of CPAF's apparent preference for proteins important in host immunity and signaling, it has been proposed that CPAF-mediated proteolysis represents a core strategy employed by *Chlamydia* to modify host-signaling pathways and usurp the cellular machinery for its own benefit [216, 217]. Additional functions of CPAF may include death of the infected host cell, as ectopic over expression of CPAF in mammalian cells initiates a host cell death pathway that mimics the necrotic cell death observed at the end of the *Chlamydia* life cycle [215]. Similarly, *Chlamydia* proteins, including early and midcycle T3S effectors, have also been reported to be targets of CPAF-mediated processing [218, 219]. We postulated cleavage of early effectors plays a role in protection from re-infection [218, 219]. CPAF is also thought to process the abundant outer membrane protein OmcB [220], which may represent a mechanism to generate soluble form(s) of OmcB that can access the host cell cytoplasm [221].

CPAF is fairly selective in its target specificity and broad degradation of proteins is not observed when crude cell lysates are treated with recombinant CPAF [218]. However, the significance of CPAF-dependent proteolysis *in vivo* has recently come into question as degradation can occur during routine sample preparation [222]. As a result, it is unclear the extent to which CPAF cleaves any of its reported substrates in intact infected cells [222]. Definitive experimental evidence for the *in vivo* target specificity of CPAF and the consequences of its proteolytic activity has been hampered by the difficulty in identifying CPAF substrate recognition sites that can be mutated, the redundancies in the function of host cell targets, and the lack of a system to generate defined mutations in *Chlamydia*. Furthermore, cell permeable inhibitors of CPAF have yielded conflicting results with possible off-target effects that are difficult to anticipate or control [214, 218, 220].

In this study, we sought to clarify the role played by CPAF by performing a phenotypic analysis of *C. trachomatis* mutants that are either defective for CPAF secretion or have loss-of-function mutations in *cpa*. In this manner, we confirm that CPAF is required for the efficient generation of *Chlamydia* infectious progeny. We also report that many of the cellular phenotypes of *Chlamydia*-infected cells that had been previously ascribed to CPAF, are not CPAF-dependent. However, this does not mean that all identified CPAF substrates are not targeted for proteolysis *in vivo*. We provide evidence for CPAF-mediated processing of vimentin as well as a new CPAF substrate we identified *in vitro*, the nuclear envelope protein Lamin Associated protein-1 (LAP1). These proteolytic events occurred in intact live cells, late in infection, soon after loss of inclusion membrane integrity, suggesting that the bulk of active CPAF is sequestered within the inclusion lumen.

2.2 Identification of *C. trachomatis* strains deficient in CPAF secretion or expression

2.2.1 A *Chlamydia* mutant defective for type II secretion accumulates unprocessed CPAF zymogen

We recently identified a *C. trachomatis* LGV-L2 variant (RSTE4 (T2S-)) bearing a point mutation in the Type II secretion ATPase GspE [223]. This mutant is attenuated for growth and accumulates insoluble glycogen granules within inclusions, presumably because of the impaired secretion of glycogen processing enzymes [223]. Given the known role of T2S in the export of folded hydrolases from the bacterial periplasm [203], we hypothesized that this secretion system is also responsible for the export of CPAF. Indeed, immunofluorescence analysis with anti-CPAF antibodies of HeLa cells infected with *C. trachomatis* RSTE4 (T2S-) mutants revealed that all CPAF was exclusively associated with bacteria within the inclusion and no immunoreactive material was

present in the host cytoplasm (Fig. 4A-B). During infection with the wild type strain, 80% of infected cells show CPAF localization to the host cytoplasm, with only 20% of infected cells displaying bacterial-only localization (Fig. 4B). An immunoblot analysis of total protein lysates from cells infected with RSTE4 (T2S⁻) further showed that the processed 35kDa and 29kDa bands of mature CPAF [224], which are prominent in cells infected with wild type *C. trachomatis*, are absent. Instead, a higher molecular weight 70kDa band consistent with the size of unprocessed CPAF zymogen [224] was detected, albeit at lower abundance (Fig. 4C). Lysates from cells infected with an unrelated *C. trachomatis* slow-growing mutant (SPQ6-2 (TrxB*)) [223] also showed the processed forms of CPAF, indicating that the accumulation of unprocessed CPAF in cells infected with the T2S⁻ mutants is not due to a slower replication rate. Overall these results suggest that CPAF is a substrate of T2S and that secretion is coupled to its processing into an active form. Consistent with this observation, crude lysates from cells infected with a *gspE* mutant lacked *in vitro* CPAF activity against a purified substrate (recombinant GST-CT695) (Fig. 4D).

2.2.2 Identification and generation of *Chlamydia* strains with loss-of-function mutations in CPAF

The finding that RSTE4 (T2S⁻) mutants did not possess CPAF activity suggested that CPAF is not absolutely essential for bacterial viability. This is consistent with previous observations made with CPAF-inhibitors where 5-10 fold differences in the yield of infectious units were reported [214, 218, 220]. We generated a bank of chemically mutagenized *C. trachomatis* LGV-L2 strains and screened for mutants that consistently formed small plaques on Vero cell monolayers overlaid with soft agar. We isolated ~1000 small plaque forming mutants. These mutants were amplified in Vero cells, and

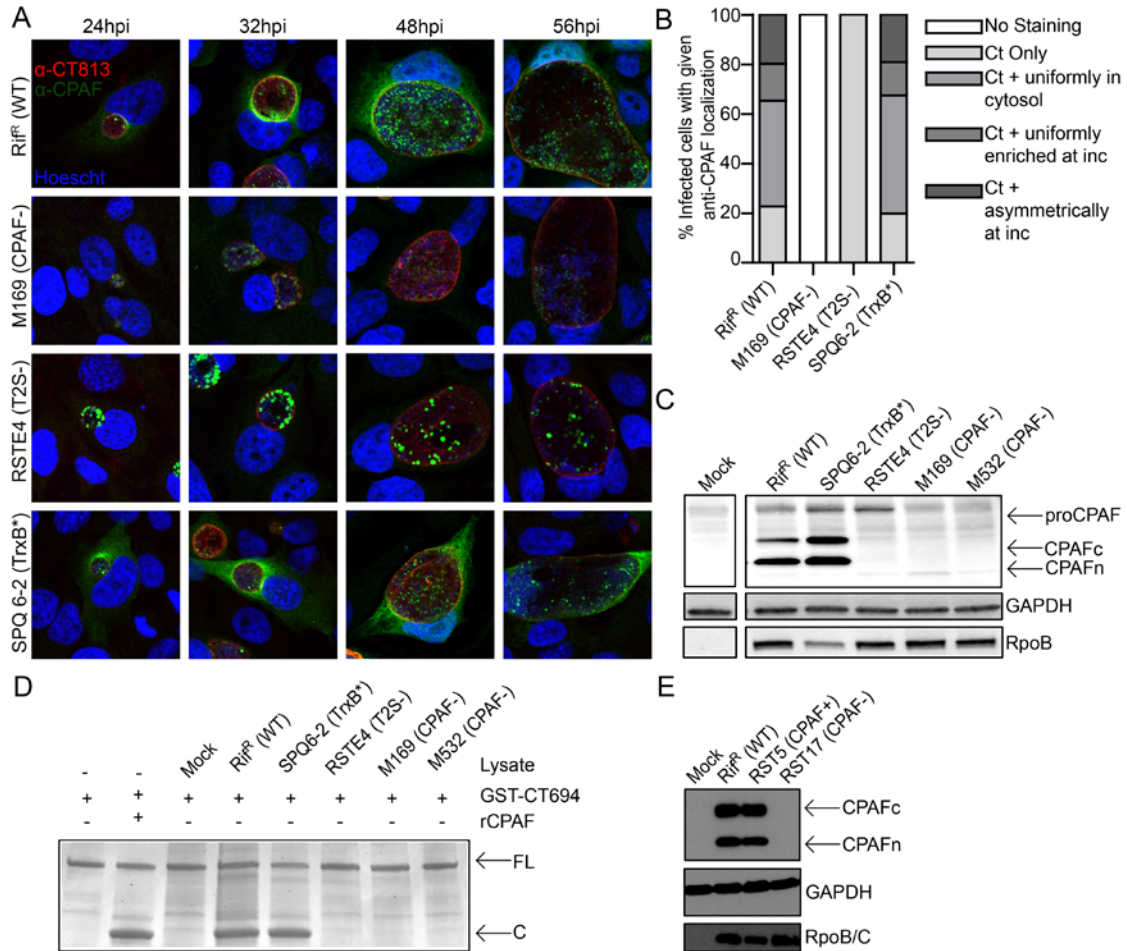


Figure 4: Identification of *C. trachomatis* strains deficient in CPAF secretion or expression. A-B). CPAF fails to accumulate in the cytoplasm of cells infected with a T2S-deficient mutant and is not detectable in a CPAF-truncation mutant (M169). The subcellular localization of CPAF in HeLa cells infected with the indicated *C. trachomatis* mutant strains was assessed by indirect immunofluorescence with polyclonal anti-CPAF antibodies. Immunoreactive material could not be detected in cells infected with a CPAF-deficient strain, or in the cytoplasm of cells infected with a T2S-deficient strain. The relative distribution of CPAF at 32 hpi in infected cells (n=100) is shown in panel B. C) T2S-deficient mutants fail to process CPAF into its active form. Immunoblot analysis of total protein lysates from HeLa cells infected with the indicated strains at 48 hpi. Strains containing mutations in *cpa* that do not express CPAF and T2S-deficient strains exhibit accumulation of a larger molecular weight band consistent with the size of unprocessed CPAF (proCPAF). D) Lysates from cells infected with CPAF or T2S-deficient *C. trachomatis* mutants do not process CPAF substrates in vitro. Purified recombinant CPAF (rCPAF) or lysates from HeLa cells that were mock infected or infected with the indicated strain were harvested at 40 hpi and incubated with recombinant GST-CT695, an in vitro CPAF substrate. Cleavage products were monitored by SDS PAGE and staining with Coomassie Blue. FL: full length GST-CT695;

C: cleavage product. E) M169-derived recombinant *C. trachomatis* strains retaining the *cpa* mutation do not express CPAF. Immunoblot analysis of total protein lysates of HeLa cells infected with RST17 (CPAF-) or its nearly co-isogenic recombinant sibling RST5 (CPAF+) for 48 hours. CPAF expression is restored in RST5 (CPAF+) bacteria but still absent in the RST17 (CPAF-) strain. The genotypes of these strains are shown in Table 1 and Figure 5.

their DNA isolated and sequenced in pools of 20 [172]. Among this collection of mutants, we identified two strains (M169 and M532) with nonsense mutations in *cpa* and isolated these individual strains from the pool of 20 using TILLING (Targeting Induced Local Lesions in Genomes) (Table 1, Fig. 6). We determined that a representative CPAF truncation mutant (M169) had no detectable CPAF protein by immunofluorescence microscopy (Fig. 4A-B) or western blots (Fig. 4C). Furthermore, as observed for the T2S-deficient *Chlamydia* mutant, lysates of HeLa cells infected with the strains M169 and M532 lacked *in vitro* protease activity (Fig. 4D).

Table 1: Non synonymous single nucleotide variants identified in strains CTL2-M169 (CPAF-) and CTL2-M532 (CPAF-).

CTL2-M169 (CPAF-)				
Reference genome location ¹	Amino Acid change	434/Bu locus tag ²	Ser. D locus tag ³	Gene
8,918	I571V	CTL0007	CT639	<i>recB</i>
35,718	E174K	CTL0029	CT660	<i>gyrA2</i>
102,990	D619N	CTL0080	CT711	
270,665	L295F	CTL0213	CT841	<i>ftsH</i>
290,514	W294*	CTL0233	CT858	<i>cpa</i>
306,954	D442N	CTL0248	CT869	<i>pmpE</i>
406,553	A136T	CTL0327	CT071	<i>dxr</i>
436,534	E497K	CTL0353	CT098	<i>rpsA</i>
763,691	T207I	CTL0646	CT390	<i>dapL</i>
869,346	G786E	CTL0736	CT475	<i>pheT</i>
1,004,316	L85S	CTL0869	CT606	
1,020,947	G207S	CTL0884	CT620	

CTL2-M532 (CPAF-)				
Reference genome location ¹	Amino Acid change	434/Bu locus tag ²	Ser. D locus tag ³	Gene
141,972	S188F	CTL0111	CT643	<i>topA</i>
144,164	E224K	CTL0113	CT744	
289,759	Q43*	CTL0233	CT858	<i>cpa</i>
374,717	G71S	CTL0303	CT047	
493,667	A128V	CTL0403	CT148	<i>mhpA</i>
601,361	G264E	CTL0503	CT251	<i>oxaA</i>
631,979	G615S	CTL0535	CT283	
928,436	E295K	CTL0805	CT543	<i>hisS</i>
998,156	T301M	CTL0862	CT599	<i>tolB</i>
1,014,167	D50N	CTL0879	CT615	<i>rpoD</i>

¹ Nucleotide position in *C. trachomatis* LGV L2 434/Bu reference strain genome (GenBank number NC_010287).

² Locus designation in *C. trachomatis* LGV L2 434/Bu reference strain.

³ Locus designation in *C. trachomatis* D/UW-3/CX (Serotype D) reference strain (GenBank number NC_000117.1).

We sequenced the genome of the CPAF-deficient isolate M169 and M532 and identified non-parental SNVs; the non-synonymous SNVs identified in both strains are listed in Table1. To segregate the *cpa* mutation from these other mutations, we co-infected Vero cells with M169, which was generated in a Rif^R background, and a wild type Spc^R LGV-L2 strain. Progeny from this co-infection were amplified in the presence of rifampicin and spectinomycin to isolate recombinant strains as previously described [223]. In this manner, we generated Spc^RRif^R recombinants where only four mutations were inherited from the parental M169 strain. These strains were further “crossed” to a Tmp^R LGV-L2 strain by co-infections to further decrease the number of extraneous mutations. As a result, we generated two strains RST5 (CPAF+) and RST17 (CPAF-) (Fig. 5). The only significant differences between the genotypes of RST5 (CPAF+) and RST17 (CPAF-), in addition to the nonsense mutation in *cpa* (*CTL0233*) in

RST17(CPAF-), is the presence of an L to F substitution in a non-conserved residue of FtsH (*CTL0213*) in RST5 (CPAF+) and a S to F substitution at residue 555 in CTL0884 in RST17 (CPAF-) that was present in the Spc^R strain used for crosses (Fig. 5).

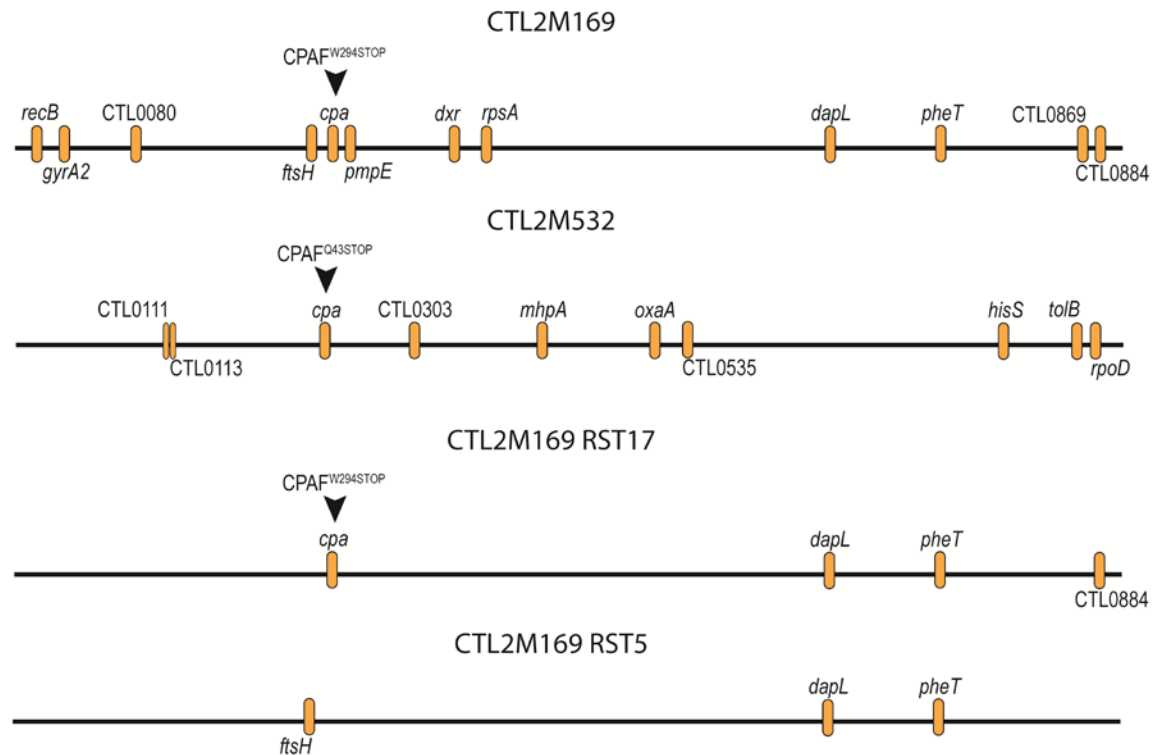


Figure 5: Map of single nucleotide variants identified in CPAF-mutant and isogenic control strains. The location of non-synonymous SNVs present within the genomes of M169 and M532, along with the RST17 and RST5 strains resulting from the “crosses” of the M169 mutant.

For the remainder of this chapter, the Rst5 (CPAF+) and Rst17 (CPAF-) *C. trachomatis* strains are used to assess the contribution of CPAF to a variety of phenotypes during infection. However, advances in *Chlamydia* genetics after the publication of the research paper from this chapter allowed us to create a CPAF mutant strain in a background that does not contain any other SNVs [165]. We disrupted *cpa* in the wild-type *C. trachomatis* strain CTL2 by insertional gene inactivation with a retargeted group II intron and chloramphenicol resistance cassette (*cat*), as recently

described [165]. Cells infected with CTL2 *cpa::cat* have no detectable CPAF protein present when assessed by immunofluorescence or immunoblot (Fig. 6A,B). When protein lysates are harvested under conditions in which CPAF is active post-lysis, Vimentin cleavage is only detected during WT infection, further supporting a loss of CPAF activity in the CTL2 *cpa::cat* mutant strain (Figure 6B). This strain will be used for future analysis of CPAF's activities during infection.

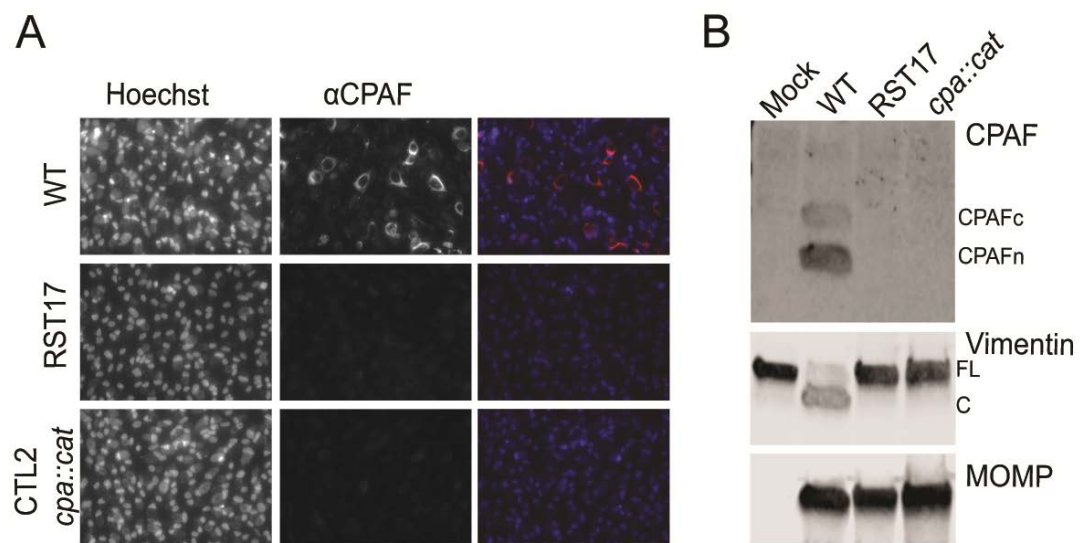


Figure 6: CTL2 *cpa::cat* is deficient in CPAF secretion and expression. A) CPAF is no longer in the host cytosol of cells infected with a CTL2M strain containing a group II intron disrupting *cpa*, the gene encoding CPAF. B) Immunoblot analysis of total protein lysates of HeLa cells infected with CTL2 *cpa::cat*, harvested in RIPA buffer after 48hpi. CPAF activity is not detected in CTL2 *cpa::cat* infected cells.

2.3 CPAF mutants are defective for the generation of infectious EBs

Next, we determined if RST5 (CPAF-) displayed any differences in growth potential as compared to its nearly co-isogenic partner RST17 (CPAF+). Cells infected with the *cpa* mutant RST5 (CPAF-) displayed a ~3-fold decrease in EB yields per input EB as compared to RST17 (CPAF+) (Fig. 7). These findings support a role for CPAF in the generation of fully infectious forms of *C. trachomatis*.

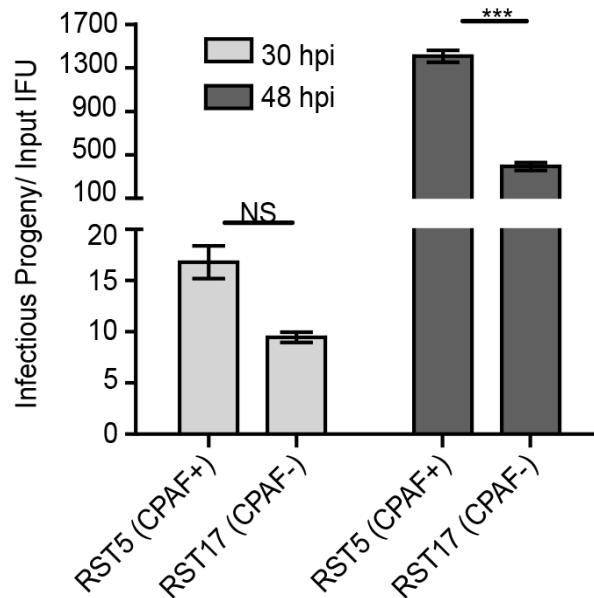


Figure 7: *C. trachomatis* mutants deficient in CPAF expression are impaired for the generation of infectious progeny. Vero cells were infected with the indicated strains at an MOI=0.3 and infectious progeny released per input IFU was calculated at 30hpi and 48hpi. RST17 (CPAF-) mutants produce a 3-fold lower yield of infectious units compared with RST5 (CPAF+) bacteria at 48hpi. Three independent experiments, SEM, two-way ANOVA with Bonferroni post-hoc, ***p<0.001.

2.4 Phenotypes of CPAF-deficient Chlamydia

Because the expected consequences of the degradation of known CPAF targets correlated with cellular phenotypes observed in *C. trachomatis* infected cells, and because these phenotypes were reversed by CPAF inhibitors, it has been widely assumed that CPAF is required for these cellular disruptions [214, 216, 218, 220]. We formally tested this premise using T2S- and CPAF- *C. trachomatis* mutants. We monitored the following cellular phenotypes associated with *Chlamydia* infections:

2.4.1 Cells infected with CPAF-deficient *Chlamydia* are resistant to staurosporine-induced apoptosis

Chlamydia infected cells are remarkably resistant to extrinsic and intrinsic pro-apoptotic stimuli [225, 226]. Because BH3-domain pro-apoptotic proteins have been

described as targets of CPAF-mediated degradation, it has been inferred that CPAF activity is required for host cell resistance to cell death, especially late in infection [212, 227, 228]. We formally tested this premise by infecting HeLa cells with wild type or CPAF-deficient mutants. At 18, 30 and 42h post infection, staurosporine was added for 6h to induce cell death [229]. Unlike mock infected control cells, where staurosporine treatment led to nuclear condensation in greater than 70% of cells, neither wild type nor CPAF-deficient mutants showed apparent signs of nuclear condensation or cell death (Fig. 8B). These findings imply that CPAF is not essential for the anti-apoptosis state of *Chlamydia*-infected cells.

2.4.2 CPAF is not required for protection from reinfection

We recently reported that early effector proteins like Tarp and CT694 are targets of CPAF-mediated degradation [218]. We postulated that one instance where such effectors would encounter CPAF is when effectors are delivered by an EB attempting to infect a cell that has an established inclusion. Consistent with this hypothesis, pre-infected cells are partially protected from reinfection [218]. Because this protection from re-infection is reversed by treating infected cells with a CPAF-specific inhibitory peptide, we postulated that CPAF plays a central role in niche protection [218]. To formally test this premise, we pre-infected cells with wild type and M169 (CPAF-) mutants for 30h, followed by a second round of infection with GFP-expressing LGV-L2 for 1h. Cells were fixed and immunostained with anti-phospho-tyrosine (Tyr) antibodies, which prominently labels Tarp translocated at EB entry sites. As previously reported, pre-infection decreased the number of phosphor-Tyr positive EBs [218]. However, this protection from re-infection is not dependent on CPAF as M169 (CPAF-) was not less susceptible to reinfection (Fig. 8C).

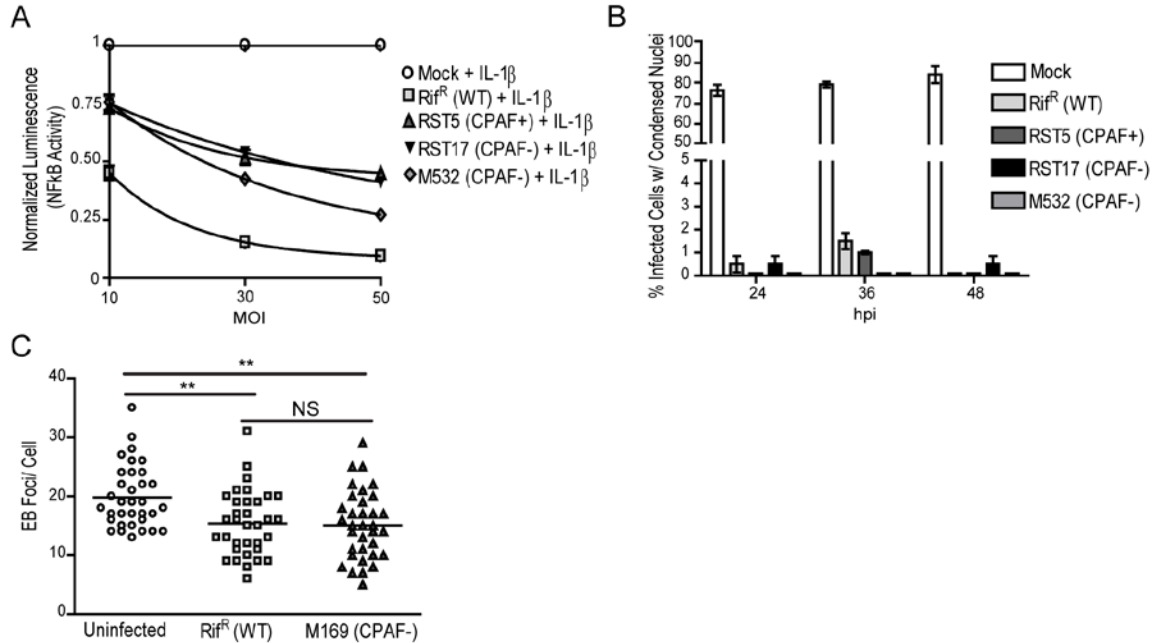


Figure 8: CPAF is not required for many of the cellular phenotypes associated with *C. trachomatis* infection. A) HeLa cells stably expressing an NFκB luciferase reporter were infected with the indicated strains at an MOI of 10, 30, or 50 for 24 hours and were simultaneously treated with 10 ng/ml IL-1β. Luciferase activity was measured in cell lysates and normalized to the treated mock-infected control. CPAF-deficient strains and Rif^R (WT) strains show an MOI dependent decrease in luciferase activity. B) Infected or mock-infected HeLa cells were treated with 2 μM staurosporine for 6 hours prior to the indicated time points and the percentage of infected cells with condensed nuclei determined. C) HeLa cells were either infected with the indicated strain or left uninfected for 29 hours prior to being infected at an MOI=25 with GFP-expressing LGV-L2 for 1 hour. The number of phospho-tyrosine foci per cell was determined for 35 cells. HeLa cells infected with the CPAF-deficient strain (M169) remain protected from superinfection. **: p < 0.01, SEM, n=3.

2.4.3 CPAF is not required for dampening NFκB activity during infection

The RelA/p65 subunit of the NFκB transcription factor has been identified as a CPAF target [230]. RelA/p65 is required for the expression of inflammatory genes during *Chlamydia* infections and *Chlamydia* infected cells are impaired in their ability to express NFκB-dependent genes upon stimulation with IL-1β [230]. These cleavage events and loss of responsiveness to IL-1β can be recapitulated in a cell line expressing active

CPAF [230]. To formally test the role of CPAF in this process, we infected HeLa cells stably expressing a luciferase reporter under the control of an NFκB-responsive promoter with increasing MOIs of RST5 (CPAF+), RST17 (CPAF-), and M532 (CPAF-) for 24h in the presence of 10ng/mL of IL-1β (Fig 8A). Mock infected cells displayed a robust activation of the luciferase reporter upon treatment with IL-1β. The expression of the NFκB-dependent reporter was inhibited by infection in a dose-dependent manner. However, this inhibition was independent of CPAF (Fig. 8A). Additionally, no detectable cleavage of p65/RelA occurs in the RST17 (CPAF-) infected cells; cleavage is only detected in RST5 when lysates are collected under conditions in which CPAF remains active (Figure 9A).

2.4.4 OmcB processing is reduced in cells infected with CPAF-deficient strains but not T2S mutants

Proteomic studies by our laboratory indicate OmcB is one of the most abundant proteins present within EBs [188] and it is highly conserved amongst *Chlamydia* species. OmcB is localized to the outer membrane protein, with a portion being surface exposed and the remainder being present within the periplasm [231, 232]. During early stages of infection, the N-terminus of OmcB binds to heparin helping to facilitate adhesion of *Chlamydia* to host cells [233, 234]. Intriguingly, OmcB can be processed into C-terminal and N-terminal fragments, with the C-terminal region of OmcB localized to the host cell cytosol during infection [232]. Previous studies suggest CPAF is required for this processing during infection [235]. We confirmed processing of OmcB occurs in infected cells harvested under stringent lysis conditions, indicating processing occurs prior to cell lysis (Figure 9A,B). However, OmcB cleavage was still observed in cells infected with the M169 and M532 CPAF-deficient strains, albeit to a lesser extent than the processing

observed during WT infection (Figure 9B). These results suggest another factor may contribute towards the processing of OmcB during infection. Despite similar levels of the bacterial loading controls MOMP and RpoB, there is an increase in OmcB protein in

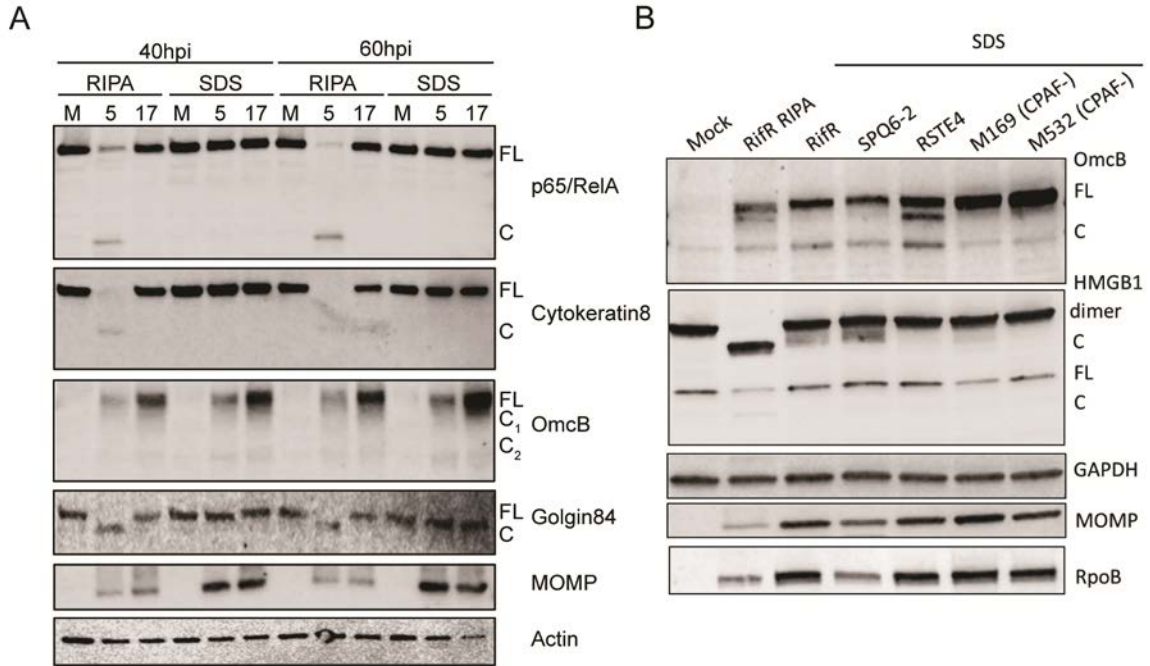


Figure 9: OmcB processing is diminished in cells infected with CPAF-deficient strains, but enhanced in T2S mutants. A) HeLa cells were either mock infected or infected with RST5 (CPAF+) or RST17 (CPAF-). M: mock, 5: RST5, 17: RST17. At 40 and 60 hpi cells were harvested in either RIPA buffer to keep CPAF active or 1% SDS buffer to prevent post-lysis CPAF activity. Degradation was assessed for p65/RelA, Cytokeratin 8, OmcB, and golgin-84. FL: full Length, C: cleavage product. B) HeLa cells were infected with the indicated strain and harvested at 48hpi in either RIPA buffer (to show expected cleavage products) or 1% SDS buffer. Minimal processing of OmcB is still evident in cells infected with M169 or M532, however no processing of HMGB1 is detected. OmcB processing is detected in greater amount in the RSTE4 (T2S-) mutant, compared to the RifR WT control.

CPAF-deficient *Chlamydia*, possibly due to a subset of FL-OmcB remaining unprocessed in these strains.

We previously demonstrated the T2S- mutant strain RSTE4 has no detectable CPAF activity against recombinant GST-CT694 (Fig. 4D). Additionally, only unprocessed, full length CPAF is detected during infection with RSTE4 (Fig. 4C).

Nevertheless, infection with RSTE4 results in the increased processing of OmcB (Fig. 9B). The CPAF zymogen present within the periplasm is hypothesized to possess minimal activity, as purified recombinant CPAF undergoes trans-autocatalytic cleavage [179]. Furthermore, forced clustering of CPAF in uninfected cells results in its activation [212]. One possibility is that the CPAF zymogen has activity against periplasmic substrates such as OmcB; OmcB processing may also occur by multiple mechanisms or in multiple steps that include, but are not dependent on the presence of CPAF. T2S mutants accumulate material in the periplasmic space [152] and the retention of another T2S substrate within the bacterial periplasm may enhance or stabilize the function of the CPAF zymogen or be independently responsible for OmcB cleavage.

2.4.5 HMGB1 cleavage during infection is partially dependent on CPAF

High-mobility group box 1 protein (HMGB1) functions to stabilize nucleosome formation and can be secreted by activated macrophages or natural killer cells in response to infection; it can also be released by cells during necrosis [236]. Yu and colleagues first identified a decrease in secreted HMGB1 levels in culture supernatants by ELISA during *C. trachomatis* infection [211]. They further showed CPAF was sufficient to degrade HMGB1. To test if CPAF cleaves HMGB1 under cell processing conditions where CPAF is inactive, we infected HeLa cells with Rif^R (WT), RSTE4 (T2S), M169 (CPAF⁻) and M532 (CPAF⁻) strains and harvested cell lysates in 1% SDS buffer 48hpi. We observed degradation of HMGB1 to a lesser extent in WT infected cells harvested in 1%SDS buffer, compared to the RIPA buffer control (Figure 9B). Cleavage of HMGB1 was not noticeable during infection with the M532 CPAF-deficient strain,

suggesting the processing seen in RifR (WT) and the slow-growing mutant SPQ6-2 of HMGB1 may be due to CPAF.

2.4.6 Golgin-84 is not cleaved during *C. trachomatis* infection

C. trachomatis infection leads to fragmentation of the Golgi apparatus into mini-stacks [237], a phenotype that can be recapitulated by expression of active CPAF in infected cells [214, 237]. Golgi fragmentation in infected cells correlates with the cleavage of golgin-84 [237]. However, cleavage of golgin-84 occurs during or after cell processing, as RST5 infected cells do not show processing when harvested in CPAF inhibiting conditions; cleavage is also not seen in cells infected with RST17 harvested in any condition (Figure 9A). These results suggest CPAF-dependent cleavage of golgin-84 is not the cause of Golgi fragmentation in *Chlamydia*-infected cells.

2.5 CPAF mediates cleavage of intermediate filaments late in infection

CPAF cleaves the head domain at the amino terminus of intermediate filaments [181, 238, 239]. Given the evidence that post lysis proteolysis can exaggerate the extent to which any true processing occurs in live cells [222, 240], we reassessed our protein harvesting protocols. Because we found variability on the effectiveness of commercial batches of lactacystin (data not shown), we shifted to protein extractions either in hot 1% SDS at pH 7.0 or in normal sample buffer supplemented with a CPAF-inhibitory peptide [218], conditions under which the activity of recombinant CPAF activity is completely inhibited (Fig. 10A). We performed a time course of infection with *C. trachomatis* from 12-56h and harvested total protein under these conditions. An immunoblot analysis of total protein lysates indicated that a vimentin cleavage product is detected, but later during infection and to a lesser extent than previously described [239]. The example

shown in Fig 10B highlights an experiment where the *least* amount of vimentin processing was observed. In parallel, we monitored the release of LDH from wells with infected cells and did not observe significant differences in LDH release suggesting that cells remained intact during the course of infection (Fig. 10C). These findings are consistent with vimentin and other CPAF targets (see below) being processed late during the course of infection.

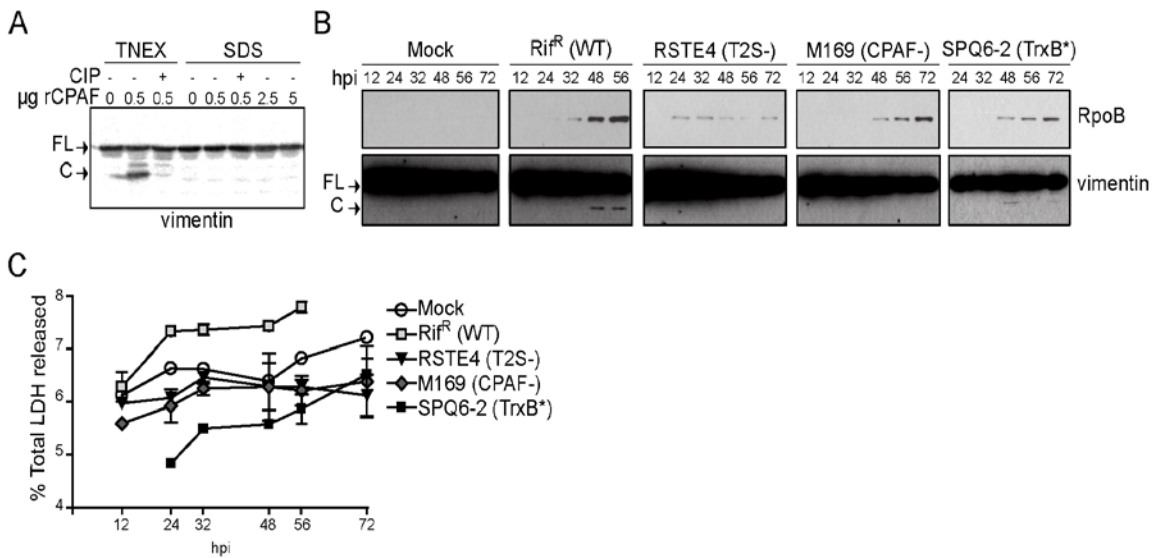


Figure 10: Evidence for CPAF mediated processing of vimentin in intact cells. A) CPAF is not active in 1% SDS buffer. HeLa cell lysates prepared under denaturing conditions in 1% SDS buffer were incubated with the 0.5, 2.5, and 5 µg recombinant CPAF (rCPAF) for 20 minutes at 37°C. As a positive control, rCPAF was also incubated with HeLa lysates prepared under non-denaturing conditions in TNEX buffer. Where indicated, 100 µM CPAF inhibitor peptide (CIP) was included as a control. CPAF activity was assessed by monitoring the generation of vimentin cleavage products by immunoblot analysis. B) Proteolytic processing of vimentin at later stages of infection is dependent on CPAF. FL: full-length vimentin; C: cleavage product. C) LDH release by cells infected with wild type and CPAF-deficient *C. trachomatis* strains. The supernatants of infected cells were collected at the indicated time points and the amount of LDH release was measured and compared to total LDH levels. Error bars represent standard deviation, n=3.

We previously observed that extraction of live cells with 0.5% Triton X-100 on ice for 5 minutes preferentially extracted filaments proximal to the inclusion but not those at

the periphery within the same cell or within adjacent cells [239]. We interpreted these findings as evidence of spatially constrained alteration of the cytoskeletal properties of intermediate filaments by CPAF. Although these detergent extractions were performed in the presence of lactacystin, the effectiveness of this inhibitor is difficult to control. To address potential issues arising from CPAF proteolysis during the detergent extraction process, we repeated these experiments in the presence of a CPAF-inhibitory peptide [181]. HeLa cells were infected with *C. trachomatis* for 44, 52 and 60h, chilled on ice and extracted with 0.5% Triton X-100 with excess amounts of the CPAF-inhibitory peptide. Under these conditions, we did not observe solubilization of filaments proximal to the inclusion for the majority of infected cells (Fig. 11A lower left panel). These results indicate that either processing does not occur in all infected cells or that the extent of processing in the averaged infected cell does not lead to gross alterations in the physical properties of filaments.

Nonetheless, we observed that in a significant subset of infected cells the vimentin filament network was completely extractable with Triton X-100 even when CPAF activity was carefully inhibited during the extraction process (Fig 11A lower right panel). The proportion of these cells increased to ~7% of all cells as infection progressed to >60h. To determine if CPAF played a role in this processing, we infected HeLa cells with RST5 (CPAF+) or the CPAF-deficient mutants RST17 and M532 and recorded the number of cells with Tx100-extractable vimentin filaments in the presence of CPAF-inhibitory peptide (Fig. 11B). The presence of these “detergent-sensitive” vimentin filaments in infected cells was completely dependent on CPAF. These results suggested that at late stages of infection a subset of infected cells display CPAF-mediated degradation of one of its well-described substrates.

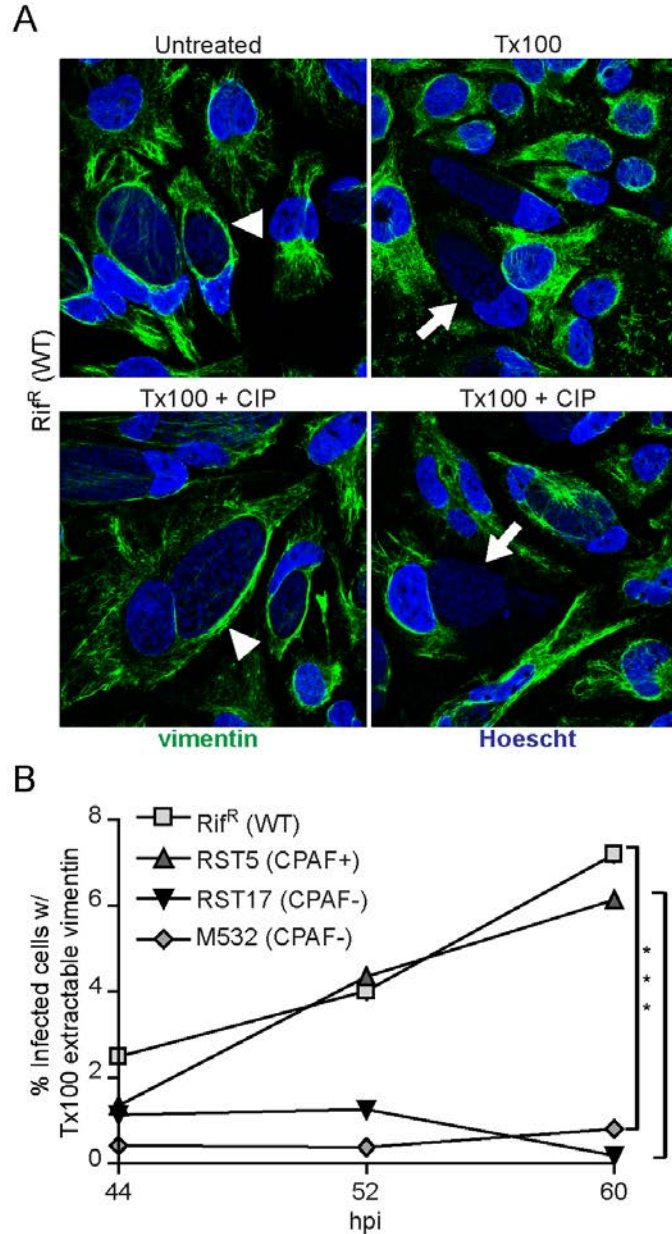


Figure 11: The filament forming properties of vimentin are altered in a CPAF-dependent manner at late stages of infection. A) A subset of infected cells contain vimentin filaments that are sensitive to detergent extraction. Top panel: Immunofluorescence images of HeLa cells infected with Rif^R (WT) at 52 hpi. Infected cells were either untreated or treated with 0.5% Tx100 for 5 minutes on ice, prior to fixation and immunostaining for vimentin localization. Vimentin cage forms around the inclusion of infected cells (arrowhead), which are sensitive to Tx100 extraction (arrow). Bottom panel: Infected HeLa cells were treated with 0.5 % Tx100 in the presence of 100 μ M CPAF-inhibitory peptide (CIP). Note the presence of inclusions with both detergent resistant (arrowhead) and detergent sensitive (arrow) vimentin filaments. Blue: Hoescht;

Green: vimentin. B) The proportion of inclusions with detergent extractable vimentin filaments increases with infection times in a CPAF-dependent manner. Cells were infected with Rif^R (WT) or CPAF-mutant strains and the percentage of infected cells with Tx100 extractable vimentin (Figure 5A, bottom right) was quantified at 44 hpi, 52 hpi, and 60 hpi. All extractions were done in the presence of 100 μ M CIP. Cells with extractable intermediate filaments were not apparent in HeLa cells infected CPAF-deficient mutants. ***: $p < 0.001$, SEM, $n = 3$.

Given the observation that brief extractions (<5min) of live cells with cold Triton X-100 in the absence of robust inhibition of CPAF lead to the preferential solubilization of filaments at the inclusion periphery *post lysis* we inferred that the bulk of active CPAF is restricted to the inclusion lumen. We reasoned that active CPAF within the inclusion lumen would access most of its host substrates in a live cell when the integrity of the inclusion membrane is compromised. To formally test this premise, we performed live cell microscopy in HeLa cells co-expressing EGFP-vimentin and tdTomato during infection with either wild type (Rif^R) or a CPAF-deficient mutant (M532). tdTomato is a red fluorescent protein that localizes to the host cell cytoplasm and is excluded from the inclusion lumen. Upon loss of inclusion membrane integrity, tdTomato becomes evenly distributed throughout the infected cell. Similarly, loss of plasma membrane integrity can be monitored as the overall loss of cell-associated red fluorescence, when cytoplasmic proteins rapidly diffuse into the extracellular media. In this manner, we determined that on average, plasma membrane integrity is not compromised until >30 min after the loss of inclusion membrane integrity (data not shown). Time-lapse events captured by fluorescence microscopy showed that in cells infected with wild type *Chlamydia*, loss of inclusion membrane integrity at late stages of infection preceded the rapid (<7min) processing of vimentin filaments (Fig. 12). In contrast, in CPAF-deficient mutants, the vimentin network remained unaltered upon loss of inclusion membrane integrity or even after loss of plasma membrane integrity.

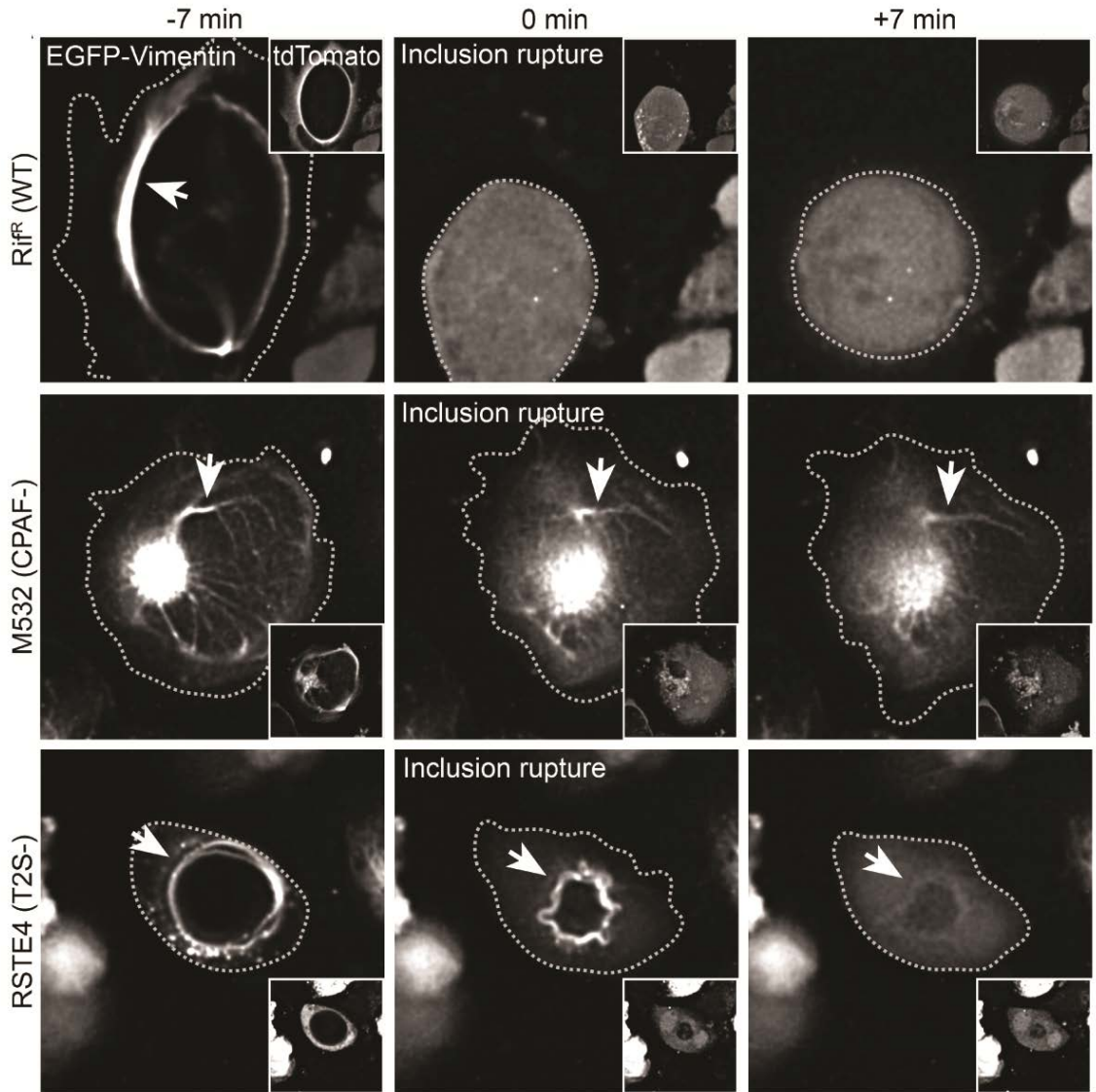


Figure 12: Cleavage of vimentin in live infected cells occurs after inclusion rupture and is dependent on CPAF and T2S. CPAF-dependent modification of vimentin filaments occurs immediately after inclusion rupture. HeLa cells were infected with the indicated strains and transfected with N-terminally EGFP-tagged vimentin and tdTomato vectors and imaged using widefield deconvolution live-cell microscopy every seven minutes after 54hpi for 14 hours. Inclusion rupture was assessed by the influx of dTomato signal into the inclusion lumen. Images acquired 7 min before and after inclusion rupture are shown. In cells infected with RifR (WT) LGV-L2, the filamentous EGFP-vimentin signal became diffuse immediately after inclusion rupture. EGFP-vimentin remained in a filamentous form after loss of inclusion integrity in cells infected with CPAF or T2S-deficient strains (arrows).

2.6 CPAF mediates cleavage of the nuclear envelope protein LAP1

During a proteomic analysis of inclusion membranes [241], we identified a new potential CPAF substrate, the laminin-associated protein-1 (LAP1)/Torsin 1A-interacting protein, a nuclear envelope protein that links the nuclear lamins to the ER ATPase Torsin1A [240]. Furthermore, mass spectrometry-based mapping of potential cleavage sites indicated that the CPAF cleavage site most likely localized to domains of the protein within the nucleoplasm (unpublished data). Consistent with these findings, we determined that endogenous LAP1 and EGFP-LAP1 are cleaved *in vitro* by recombinant CPAF (Fig. 12A). Importantly, LAP1 cleavage was also observed in cell lysates of *Chlamydia* infected cells that had been harvested under conditions that inhibited all CPAF activity. As with vimentin, LAP1 was cleaved late during infection (Fig. 13B) and these cleavage events were not observed in HeLa cells infected with the CPAF-deficient mutant M169 or T2S-defective mutants (Fig. 13B).

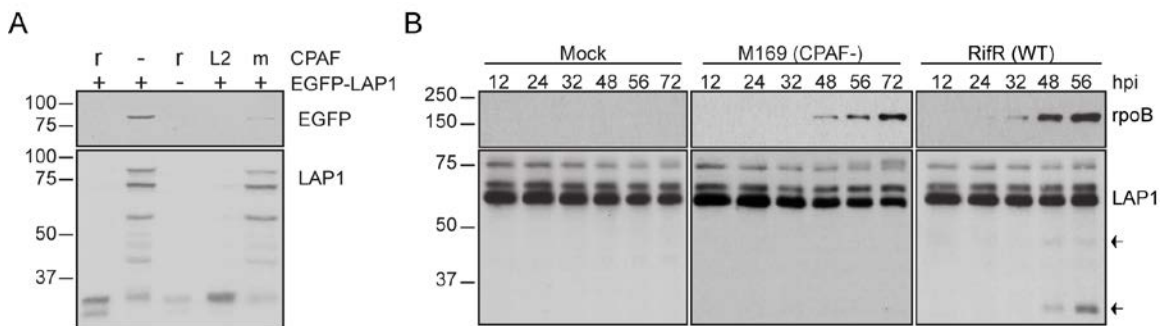


Figure 13: CPAF cleaves LAP1 during infection. A.) CPAF cleaves EGFP-LAP1. HeLa lysates transfected (+) or not (-) with EGFP-LAP1 were incubated with (r) or without (-) recombinant CPAF or with lysates from L2-infected HeLa cells (L2) or mock-infected (m) HeLa cells. Blots were probed with anti-EGFP (EGFP) or anti-LAP1 (LAP1). B.) LAP1 cleavage during infection is CPAF-dependent. HeLa cells infected with either the CPAF- strain or RifR (WT) strain or mock-infected were harvested in 1% SDS buffer at the indicated times post-infection. Blots were probed with anti-LAP1 and anti-rpoB. Arrows indicate LAP1 cleavage products.

Based on our observations with vimentin processing in live cells, we predicted that LAP1 cleavage would also occur upon loss of inclusion membrane integrity late in infection. We formally tested this prediction by infecting cells that had been co-transfected with tdTomato and EGFP-LAP1 with either RST17 (CPAF⁻) or RST5 (CPAF⁺) *Chlamydia* strains. As previously described [240], EGFP-LAP1 prominently labeled the nuclear envelope (Fig. 13). This localization pattern was not altered in infected cells. Time lapse microscopy of live infected cells revealed that upon loss of inclusion membrane integrity, as assessed by the influx of tdTomato into the inclusion lumen, the localization of EGFP-LAP1 rapidly changed from the nuclear envelope to the cytoplasm, which most likely resulted from the cleavage of the EGFP moiety from the portion of the protein anchored to the nuclear membrane (Fig. 14). As with vimentin cleavage, these proteolytic events occurred within cells in which the integrity of the plasma membrane was not compromised and were dependent on CPAF.

2.7 Discussion

The protease CPAF was the first *Chlamydia* virulence factor for which a biochemical activity (protease) and a target (transcription factors) had been established [204]. CPAF-mediated degradation of the transcription factors RFX-5 and USF-1 were linked to the loss of expression of MHC Class I and II - a cellular phenotype that had been observed in infected cells [242]. As more CPAF targets began to emerge, similar correlations were made between the degradation of these factors and cellular phenotypes of *Chlamydia*-infected cells. This list includes, but is not limited to, Golgi fragmentation, inclusion expansion, resistance to re-infection, modulation of apoptosis and pro-inflammatory signaling pathways, disruption of the cell cycle, cell junction defects, centrosomal abnormalities, and processing of the *Chlamydia* outer membrane

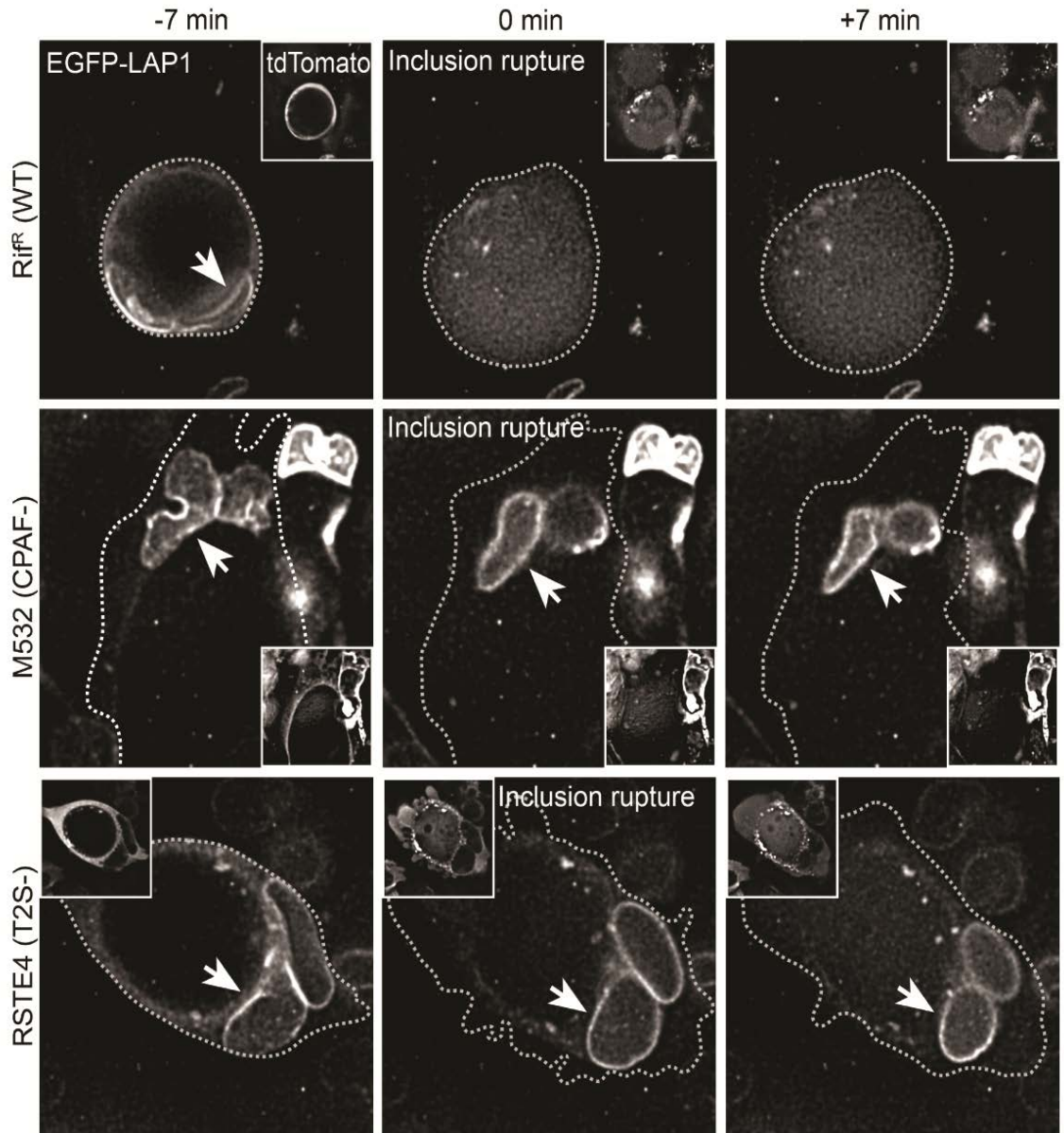


Figure 14: Cleavage of LAP1 in live infected cells occurs after inclusion rupture and is dependent on CPAF and T2S. CPAF-dependent processing of LAP1 occurs after inclusion rupture. HeLa cells were transfected with EGFP-LAP1 and tdTomato expression vectors and imaged using widefield deconvolution live-cell microscopy every seven minutes after 54hpi for 14 hours. Inclusion rupture was assessed by the influx of dTomato signal into the inclusion lumen. Images acquired 7 min before and after inclusion rupture are shown. Loss of EGFP-LAP1 localization to the nuclear membrane occurs rapidly following inclusion rupture in cells infected with Rif^R (WT) but not in cells infected with CPAF or T2S-deficient strains.

protein OmcB (reviewed in [216]). Because molecular genetic tools to specifically inactivate *Chlamydia* genes were not available, many of these correlations could not be formally tested in CPAF-deficient mutants. The development of small molecule and peptide inhibitors that blocked CPAF activity *in vitro* and *in vivo* promised to be helpful in assessing some of these questions. Indeed, these inhibitors blocked CPAF activity in cell culture infection models, decreased the replicative potential of *Chlamydia* [214, 218, 220] and often reversed cellular phenotypes of infected cells that have been associated with CPAF. However, these CPAF inhibitors also varied in their effect in cells and displayed varied levels of toxicity [214, 218].

In the last two years, there has been remarkable advances in the development of systems for genetic analysis in *C. trachomatis*. This includes the generation and mapping of chemically generated mutants as well as the stable delivery of recombinant DNA into *C. trachomatis* [171, 223, 243, 244]. We had previously identified and characterized a mutant defective in T2S [223], which we now report is also defective for CPAF secretion (Fig. 4A). In addition, we identified two *C. trachomatis* LGV-L2 strains with nonsense mutations in *cpa* (Fig. 4, Table 1). Equipped with these mutants we can now clarify the role that CPAF plays in the various unique cellular phenotypes that have been attributed to *Chlamydia* infections. Overall, our findings suggest that CPAF is not essential for blocking apoptosis, Golgi fragmentation, resistance to re-infection, or inhibition of pro-inflammatory signaling pathways. However, while CPAF does not appear necessary for these cellular processes to occur, it is important to note that we cannot exclude the possibility that this protease plays an axillary role.

Tan and colleagues brought to the forefront the issue that the unique challenges of inhibiting CPAF's proteolytic activity post lysis can confound the degree of proteolytic

activity that occurs within live infected cells [222]. Indeed, the level of true CPAF-mediated proteolysis that occurs within infected cells has come into doubt with an understandable impulse to label most proteolytic events observed to date as artifacts [244]. Our findings indicate that it is premature to assume that traditional targets of CPAF are not cleaved during infection. We presented evidence that the bulk of CPAF activity resides within the inclusion lumen and that CPAF rapidly cleaves at least one of its described targets when the inclusion membrane is compromised during late stages of infection (Fig. 12). Our results also indicate that the new CPAF substrate we identified, LAP1, is similarly processed upon loss of inclusion membrane integrity. Yu et al. detected decreased levels of released HMGB1, as measured by ELISA, at late stages of infection when the inclusion membrane may be ruptured in some infected cells [211]. Our immunoblot analysis suggests minimal processing of HMGB1 occurs under conditions where CPAF is inhibited and the processing is almost undetectable in CPAF-deficient strains (Fig. 9B). Further studies are needed to confirm the observation that HMGB1 processing is partially dependent on CPAF. Overall, this could represent a pathogenic strategy to destroy key components in the cytoplasm or subcellular structures (e.g. nuclear envelope for LAP1) prior to bacterial exit from a lysing cell or a transient response to mechanical or immune stress on the integrity of the inclusion. Such a strategy may help degrade or modify factors that constitute danger signals to be sensed by immune cells, or modify physical barriers that limit bacterial dispersal. CPAF mutants display a small (~2.5 fold) decrease in the generation of IFUs (Fig. 7), suggesting that CPAF also performs functions important for replication *before* the late exit stages. These functions could include the processing and turnover of bacterial

proteins within the inclusion, as has been suggested for the outer membrane protein OmcB [220].

In addition, CPAF released from infected cells may play a prominent role in tissue colonization or dissemination in infected animals. Indeed, experimentally infected animals and human patients develop a strong humoral response to CPAF, and immunization with recombinant CPAF is protective against infections [245, 246], suggesting that this protein may have extracellular roles in tissue infections.

At this stage, there are many unresolved questions as to the function of CPAF. Prominent among these is why CPAF is detected in the cytoplasm when activity on its described substrates is not apparent. Is CPAF activity in the host cytosol regulated? Could there be additional structural motifs that are only present in a subset of 'true' CPAF substrates that are cleaved in the cytoplasm of cells with intact inclusions? In such a scenario, CPAF in the cytoplasm could act as a molecular "scalpel" to specifically modify host cellular processes and as a "hammer" when inclusion membrane integrity is compromised and the bulk of active CPAF is released into the cytoplasm. Future work with *Chlamydia* expressing modified forms of CPAF should help address some of the outstanding questions remaining as to the function of this unusual protease.

2.8 Materials and Methods

2.8.1 Reagents

Reagents were obtained from the following sources: mouse anti-GM130 (BD Biosciences), rabbit anti-*Chlamydia* MOMP (gift of K. Fields, U. of Miami), mouse anti-vimentin (Invitrogen, clone V6630), rabbit anti-GAPDH (Abcam), mouse anti-EGFP monoclonal antibody (Clontech), rabbit anti-LAP1 antibodies (kindly provided by William Dauer, U. of Michigan), rabbit anti-RpoB/C (gift of M. Tan, UC Irvine), rabbit anti-CPAF

(27), mouse anti-phosphotyrosine (Cell signaling), Alexa Fluor 555-conjugated anti-mouse, Alexa Fluor 488-conjugated anti-rabbit, Hoescht 33258 (Invitrogen), FluorSave Reagent (Calbiochem), Staurosporine (Cell Signaling), IL-1 β (Biolegend), Cyclohexamide (Sigma-Aldrich), Rifampicin (Sigma-Aldrich), Trimethoprim (Sigma-Aldrich), Slow Fade Gold Antifade Reagent (Invitrogen), JetPrime (Polyplus transfection). Enhanced green fluorescent protein (EGFP)-tagged rat vimentin was provided by Ronald Liem (Columbia University, NY), and tandem dimer Tomato (tdTomato) was provided by Marc Caron (Duke University, NC). Full-length lamin-associated protein 1 (LAP1) was PCR-amplified from MGC Human sequence-verified cDNA clone 3458117 (Thermo Fisher) and inserted into pLEGFP-C1 (Clontech) downstream of EGFP to express an EGFP-LAP1 fusion protein. To enable genetic disruption of CTL0233 (*cpa*), *Chlamydia* were transformed with derivatives of the *E. coli*-*Chlamydia* TargeTron vector pDFTT3 [165] containing the chloramphenicol acetyltransferase (or CAT) gene instead of the beta-lactamase (*bla*) gene.

2.8.2 Cell Culture and *Chlamydia* Infections

HeLa cells (CCL-2: ATCC) and Vero cells (CCL-81: ATCC) were maintained in DMEM HG supplemented with 10% FBS (CellGro Mediatech). *C. trachomatis* LGV-L2 434/Bu and *C. trachomatis* mutant strains were propagated by infecting HeLa cells with elementary bodies (EBs) that had been stored in sucrose-phosphate-glutamate (SPG) buffer (0.25 M sucrose, 10 mM sodium phosphate, 5 mM L-glutamic acid, pH7.0) and purified on Omnipaque (GE Healthcare) density gradients [241]. EBs were added to HeLa cells at the indicated multiplicities of infection (MOIs), and infections were synchronized by centrifugation at 2500 \times *g* for 30 min at 10°C. Rifampin, spectinomycin, and trimethoprim resistant *C. trachomatis* LGV-L2 variants were generated as previously

described [247]. The mutations leading to antibiotic resistance in these strains were determined by whole genome sequencing: H471Y in *CTL0567* (*rpoB*), G1197 in *CTL_r01/CTL_r02* (16S rRNA copies 1 and 2), and G408R in *CTL0369* lead to Rif^R, Spc^R, and Tmp^R, respectively.

2.8.3 Plaque Assays

Plaque assays were performed as previously described [223]. Briefly, monolayers of Vero cells grown in a 6-well plate were infected with ~100 inclusion-forming units (IFUs) per well. Cells were incubated for 2 hours at 37 °C and 5% CO₂, allowing for bacterial internalization. The growth medium in infected cell monolayers was replaced with 6 mL of a DMEM/agarose overlay/well (DMEM HG, 10% FBS, 50 µg/mL Gentamicin, 500 ng/mL cyclohexamide, 1X nonessential amino acids (Gibco), 0.5% SeaKem LE agarose (Lonza)) allowed to solidify for 10 minutes, and dried in a sterile cabinet without lids for 15 minutes. Cells were incubated for 10 to 14 days until plaques were observed. Plaques were isolated using a pipette tip and transferred to Vero cell monolayers for amplification.

2.8.4 Identification and whole genome sequencing of CPAF-deficient LGV-L2 strains

Identification of cpa mutants. LGV-L2 strains containing the null alleles *C127T* (Q43*) and *G882A* (W294*) in *cpa* (CTL0233) were initially identified by whole genome sequencing of pools of chemically-mutagenized and plaque-purified *C. trachomatis* LVG-L2 434/Bu strains (Bastidas R. J. and Valdivia R. H. unpublished results). Strain CTL2-M532 harboring the *cpaC127T* allele and strain CTL2-M169 harboring the *cpaG882A* allele were identified from among two independent pools of mutants by PCR-amplifying the target regions, reannealed by slow cooling to promote formation of dsDNA

heteroduplexes, digested by CEL I, and visualized by DNA agarose gel electrophoresis. Lesions in the CTL0233 (*cpa*) locus were further confirmed by Sanger sequencing.

Whole genome sequencing. Strains were harvested from infected Vero cells grown in a 6-well cell culture plate by hypotonic lysis of host cells with 800 μ l of dH₂O per well (for 20 minutes) followed by addition of 200 μ l of 5X SPG buffer. Lysates were sonicated (2 x 10 seconds in ice water) and bacterial cells spun down at 14,000 rpm, for 15 minutes at 4 °C. Bacterial pellets were pooled and resuspended in 1X DNase I buffer (New England Biolabs, Ipswich, MA, USA). Depletion of host DNA was achieved by treating cell suspensions with 4 Units of DNase I (New England Biolabs,) for 1 hour at 37 °C. Bacterial pellets were washed with PBS buffer and total DNA isolated with a DNA isolation kit (DNeasy tissue and blood kit, Qiagen) following the manufacturers instructions. One μ g of M169 and M532 enriched DNA was sheared with an Adaptive Focused Acoustics S220 instrument (Covaris). DNA sequencing libraries were prepared with a library construction kit (TruSeq DNA Sample Preparation Kit v2, Illumina, Inc. San Diego, CA, USA) according to the manufacturer's instructions. Libraries were sequenced in a MiSeq DNA Sequencing Platform (Illumina) at the Duke University IGSP DNA Sequencing Core facility. Genome assembly and single nucleotide variant (SNV) identification was performed with Geneious Software version 6 (Biomatters - <http://www.geneious.com>). The *C. trachomatis* LGV L2 434/Bu genome (GenBank no. NC_010287) was used as reference sequence. All non-synonymous single nucleotide variants (SNVs) identified in M169 and M532 were verified by Sanger sequencing.

2.8.5 Generation of M169 RST recombinant strains

Recombinant LGV-L2 strains were generated as previously described [223]. Briefly, confluent Vero cells grown on a 24-well plate were co-infected with M169 (Rif^R)

and a Spc^R mapping strain at a MOI ratio of 3:3. Recombinant progeny were selected from among plaques that formed in the presence of 200 ng/mL Rif and 200 µg/mL Spc. Plaque-purified recombinants were further expanded in Vero cells and genotyped to assess the segregation of mutations present in the CTL2-M169 parental strain. Rif^R and Spc^R M169 recombinants harboring the *cpaG882A* allele were further backcrossed to a trimethoprim resistant (Tmp^R) mapping strain as described above and progeny selected from plaques that formed in the presence of Spc and 150 µg/mL Tmp. These second-generation, plaque-purified recombinants were further expanded in Vero cells and a M169-derived recombinant strain harboring the *cpaG882A* allele (M169 RST17 (CPAF-)) was identified by genotyping with SNV specific primers. A co-isogenic recombinant strain (RST5 (CPAF+)) that shares the same background SNVs as RST17 (CPAF-) and that inherited a wild type *cpa* allele was also identified. The genomes of both RST recombinant strains were re-sequenced as described above. The relevant SNVs identified are shown in Table 1.

2.8.6 Western blot analyses

HeLa cells were grown in 6-well plates to confluency and infected with the *C. trachomatis* LGV-L2 Rif^R parent or its derived mutant strains at an MOI of 1. At the indicated hours post infection, cells were washed with 1X PBS (Invitrogen), lysed with 1% SDS buffer (1% SDS, 150mM NaCl, 50mM Tris-HCL pH 7.5), heated in boiling water bath immediately before addition to cells. Lysates were incubated at 65°C for 10 minutes to solubilize and denature proteins and sonicated 2x10 seconds to shear DNA. Protein concentrations were determined by the DC protein assay (Bio-Rad). Equal amounts of lysate were loaded into SDS-PAGE 4-15% gradient gels (Bio-Rad), transferred to 0.45 µM nitrocellulose membranes using a Trans-Blot SD Semi-Dry Electrophoretic

Transfer Cell (Bio-Rad), blocked in Odyssey blocking buffer (LI-COR) and incubated in primary antibodies diluted in Odyssey blocking buffer, followed by incubation with goat anti-rabbit IRDye 680LT (LI-COR) or goat anti-mouse IRDye 800CW (LI-COR).

Membranes were imaged with the LI-COR Odyssey infrared imaging system.

2.8.7 In Vitro CPAF cleavage assays

HeLa cells grown in 6-well plates were mock-infected or infected with the *C. trachomatis* LGV-L2 Rif^R strain or with the indicated mutant strains at an MOI of 1. At 40 hours post infection (hpi) crude protein extract were prepared by lysing infected cells in RIPA buffer (50 mM Tris pH 7.5, 150 mM NaCl, 0.1% SDS, 0.5% sodium deoxycholate, 1% NP-40) supplemented with a protease inhibitor cocktail (Roche). 40µg recombinant CPAF (D. McCafferty, Duke University, NC) or crude protein extracts were prepared as described above and incubated with 20µg recombinant GST- CT695 for 1hr at 37°C, and cleavage was assessed by colloidal blue Commassie Blue staining (Invitrogen). Figures were compiled and intensities adjusted for display using Photoshop CS6.

To test the effectiveness of 1% SDS buffer in preventing post-lysis degradation by CPAF, the activity of recombinant CPAF in this denaturing buffer was assessed. Crude protein extracts were prepared from non-infected HeLa cells by rinsing monolayers with PBS, adding 1% SDS buffer pre-warmed to 100°C, transferring to a microfuge tube, heating at 65°C for 10 minutes, and then clarifying the lysate by centrifugation (10,000 x g, 15 minutes, room temperature). For the *in vitro* cleavage assays, 200 µg of total HeLa protein extract with or without 100 µM of a CPAF-inhibitory peptide [181] was mixed with 0.5, 2.5, or 5 ug recombinant CPAF in a final volume of 100 µl. The reactions were assembled at room temperature, incubated at 37°C for 20 minutes, and then inactivated with SDS-PAGE sample buffer and incubation at 65°C for

10 minutes. As a positive control, reactions were also performed under non-denaturing conditions. Crude protein extracts were generated from non-infected HeLa cells by rinsing monolayers with PBS, adding ice-cold TNEX buffer (20mM Tris-HCl, pH8, 150mM NaCl, 2mM EDTA, 1% Triton X-100, complete protease inhibitor cocktail (Roche)), incubating at 4°C for 10 minutes, transferring lysates to a microfuge tube, and then clarifying the lysate by centrifugation (10,000 x g, 15 minutes, 4°C). Reactions were assembled on ice, incubated at 37°C for 20 minutes, and subsequently processed as described for the reactions in 1% SDS buffer. CPAF activity was determined by monitoring vimentin cleavage via western blot analysis.

In vitro cleavage assays were used to demonstrate that CPAF cleaves EGFP-LAP1. HeLa cells transfected with the EGFP-LAP1 construct were harvested in TNEX buffer, and crude protein extracts were generated as described above. For the reactions, 100 ug of transfected or non-transfected extract was incubated with either recombinant CPAF or TNEX protein extracts prepared from mock-infected or LGV-L2 -infected (44 hours post-infection) HeLa cells. The reactions were assembled on ice, incubated at 37°C for 30 minutes, and then inactivated with SDS-PAGE sample buffer and incubation at 65°C for 10 minutes. Cleavage was assessed by western blot analysis with mouse anti-EGFP) and rabbit anti-LAP1 antibodies.

2.8.8 IFU burst assays

Vero cells were seeded onto 96 well plates (15,000 cells/well) and infected with each of the strains analyzed (six biological replicates per each timepoint) at a MOI~0.6. To determine the input inclusion forming units (IFUs), a set of infected wells were fixed with 100% Methanol (EMD Millipore) for 10 minutes on ice and stained with a polyclonal anti-LGV-L2 sera followed by Alexafluor-conjugated secondary antibodies and cells

samples mounted for fluorescence microscopy using the FluorSave reagent. Images were acquired in a Zeiss Axioskop 2 upright epifluorescence microscope and the number of inclusions in at least 5 different fields per replicate were counted. Output IFUs at 30 hpi and 48 hpi were determined by lysing infected cells by adding 160ul of ultra-pure water and incubating for 10 minutes before adding SPG to 1x. Vero cells were infected with serial dilutions of harvested cell lysates. After 40-42 hpi, cells were fixed, immunostained with anti-MOMP antibodies, and the number of inclusions determined as described above. To determine the infectious progeny generated per input bacteria ("IFU burst"), the total number of output IFUs was divided by the total number of input IFUs.

2.8.9 Immunofluorescence

For routine indirect immunofluorescence, HeLa cells were grown on glass coverslips and infected at the indicated MOIs. Cells were fixed with 3% formaldehyde/0.025% glutaraldehyde or 4% paraformaldehyde or methanol in phosphate-buffered saline (PBS) for 20 minutes and permeabilized with 0.1-0.2% Triton X-100 for 10 minutes at 4°C. After blocking with 5% bovine serum albumin (BSA)-PBS for 20 minutes, cells were stained with specific antibodies followed by Alexa-conjugated secondary antibodies at room temperature at 20 minutes. Host and bacterial DNA were stained with 1 µg/mL Hoechst at the same time. Coverslips were mounted with FluorSave, or Slow Fade prior to imaging with an upright Leica SP5 confocal microscope or a Zeiss Axioskop 2 upright epifluorescence microscope using Axiovision v3.0 software.

2.8.10 Detergent Extraction Assays

For immunofluorescence assays after detergent extraction, HeLa cells were seeded in wither 24-well plates for initial imaging (Figure 11A) or 96-well plates for time

course quantification (Figure 11B). Three biological replicates per condition (+Triton X-100 and -Triton X-100) were infected at an MOI of 1 with the indicated strains. At 44 hpi, 52 hpi, or 60 hpi cells in the untreated condition were washed twice with ice cold PBS and fixed with 3% formaldehyde/0.025% glutaraldehyde at room temperature for 20 minutes prior to permeabilization and blocking with BSA-PBS. For live cell samples extracted with Triton X-100, infected cells were first washed twice with ice cold PBS before incubation with pre-chilled 0.5% Triton X-100 in PBS supplemented with 100 μ M anti-CPAF peptide [181] on ice for 5 minutes. Cells were then fixed, blocked with BSA-PBS and immunostained with mouse monoclonal anti-vimentin antibodies, followed by fluorophore conjugated secondary anti-mouse antibodies; host and bacterial DNA were stained with 1 μ g/mL Hoechst. Samples were mounted with Slow Fade Gold Antifade reagent and images from at least 5 fields for each replicate were acquired with a Zeiss Axioskop 2 upright epifluorescence microscope using Axiovision v3.0 software. The number of infected cells with altered vimentin staining was calculated for each replicate in 0.5% Triton X-100 treated and untreated samples. The average percentage of infected cells with altered vimentin (6-8% of total cells) staining in the untreated samples was subtracted from the treated control for each replicate. Figures were compiled and intensities adjusted for display using Photoshop CS6. Two-way ANOVA with Bonferroni's post-test was performed using GraphPad Prism for Windows, GraphPad Software, San Diego California USA.

2.8.11 NF κ B Reporter Assays

The NF κ B luciferase HeLa reporter cell line used in this study was generated by stably transducing HeLa cells with an NF κ B -Luciferase reporter system (SABiosciences) following the manufacturer's instructions. NF κ B activity was assayed by

infecting confluent reporter cells in triplicate for each condition in 96-well plates with the indicated strains at an MOI of 10, 30, or 50. Experiments were performed in duplicate. At the time of infection, cells were treated with 10 ng/ml of IL-1 β (BioLegend). After 24 hours, cells were lysed and luciferase activity measured using the britelite plus reagent (PerkinElmer) according to manufacturer's instructions and luminescence values determined using a EnSpire 2300 Multilabel reader (PerkinElmer). Luminescence values obtained for each sample were normalized to the IL-1 β treated, mock-infected control. Data was analyzed and figures generated using GraphPad Prism (GraphPad Software, San Diego California USA).

2.8.12 Apoptosis Induction Assay

HeLa cells grown on glass coverslips were infected with an MOI of 0.5 with the indicated strains (two biological replicates and two technical replicates per condition). Six hours prior to fixation cells were treated with 2 μ M staurosporine (Cell Signaling). At 24 hpi, 36 hpi, and 48 hpi infected cells were fixed with methanol and stained with anti-LGV-L2 antibodies followed by Hoechst and Alexa-conjugated secondary antibodies. The number of infected or mock-infected cells with condensed nuclei was counted using a Zeiss Axioskop 2 upright epifluorescence microscope with Axiovision v3.0 software for 200 infected cells in each condition. Data was analyzed and figures generated using GraphPad Prism.

2.8.13 Assessment of secondary infections

HeLa cells were seeded on coverslips in 24-well plates (50,000 cells/well) and incubated overnight. For primary infections, cells were infected with purified EBs from either *C. trachomatis* L2 434/Bu or its mutant Rif^R derivatives, as indicated at an MOI of 1. At 29 hpi, secondary infections were performed using a *C. trachomatis* L2 434/Bu

strain transformed with the GFP-expressing plasmid pGFP-SW2 [243]. After 1h, cells were fixed (3% formaldehyde-0.025% glutaraldehyde, 20 min, RT) and immunostained with mouse anti-phospho tyrosine monoclonal antibodies without permeabilization and counter-stained with anti-mouse Alexafluor 555-conjugated secondary antibodies (Invitrogen). Coverslips were mounted in Slow Fade Gold Antifade media and images were acquired using a Zeiss Axioskop 2 upright epifluorescence microscope with Axiovision v3.0 software. Phospho-tyrosine foci were counted in 35 cells for each of two biological replicates, in two independent experiments performed by two independent observers. One-way ANOVA with Bonferroni's multiple comparison test was performed using GraphPad Prism.

2.8.14 EGFP-Vimentin and LAP1-EGFP transfection and live cell microscopy

Cells were seeded onto #1.5 glass-bottom plates, infected with Rif^R L2 434/Bu, M532 (CPAF⁻), M169 (CPAF⁻), RSTE4 (TS2⁻) strains, and co-transfected with either EGFP-Vimentin or EGFP-LAP1 and tdTomato using the lipid-based JetPrime reagent 4h after infection. Cells were imaged every seven minutes from 54-76hpi after infection at 37°C under 5% CO₂ using a motorized Zeiss Axio Observer Z1 widefield fluorescence microscope equipped with a 40x air objective. Fifteen stage positions at minimum were recorded with 6-23 instances of inclusion rupture in transfected cells observed for each condition. Only cells expressing moderate levels of the fluorescent reporters were included in the analysis. Images were viewed with Metamorph to manually assess inclusion rupture by tdTomato diffusion into the inclusion lumen and the structured or diffuse nature of the EGFP signal. Images were deconvolved using Huygens Essential, and processed with ImageJ and Photoshop for presentation.

3. Investigating the role of the T2SS during *C. trachomatis* infection

3.1 Introduction

Chlamydiae are obligate intracellular bacteria that infect a wide range of animal hosts. *C. trachomatis* infection with serovars A-C is commonly associated with ocular infection, while genital infection is typically caused by serovars D-K [248]. Serovars L1, L2, or L3 are responsible for lymphogranuloma venereum (LGV), a systemic infection of the lymphatic system. Genital infections are often asymptomatic but untreated and repeat infections can lead to serious complications in women, including pelvic inflammatory disease, ectopic pregnancy, and sterility. [144]. Despite antibiotic regimens and sexually transmitted disease (STD) prevention education, *C. trachomatis* infections are on the rise in the United States [143]. Improved knowledge regarding the pathogenic strategies employed *Chlamydia* may aid in the development of approaches to combat this growing threat.

C. trachomatis has a biphasic developmental cycle that takes place within a membrane bound compartment termed the inclusion. There are two morphologically and functionally distinct developmental forms of *Chlamydia*: the infectious elementary body (EB) and the replicative reticulate body (RB). Infection begins when the EB attaches to a host cell and is internalized. EBs can then differentiate into the RB form and replicate via binary fission inside a growing inclusion. At late stages of infection, prior to release and reinfection, RBs revert asynchronously back to EBs [145].

As an intracellular pathogen, successful infection requires interaction with the host cell to secure nutrients and subvert the host innate-immune response [147]. Even though the *Chlamydia* genome is relatively small (~1Mb), studies suggest 10-15% of the

genome encodes effector proteins that can be secreted from the bacteria [148-150]. *C. trachomatis* uses multiple secretion mechanisms to access the host cytosol, including the T2, T3 and T5 secretion systems. The *C. trachomatis* genome also encodes for homologues of components required for Sec-mediated translocation into the periplasm [150].

Substrates of the T2SS must first cross the inner membrane prior to translocation beyond the bacteria. The twin-arginine translocation (Tat) and Sec machineries have been characterized to perform this function, with proteins crossing the inner membrane in a folded or unfolded state, respectively [5]. Once in the periplasm, substrates are recognized by components of the T2S apparatus, which facilitates their entry into the secretion channel formed by the outer membrane protein GspD. Cycles of ATP hydrolysis via the ATPase GspE convey conformational changes through the secretion system, allowing for the assembly of the pseudopilus. The growing pseudopilus is hypothesized to act as a piston and push the effector proteins through the secretin channel [16, 17, 37].

While most T2SSs in Proteobacteria contain the core constituents T2S/Gsp CDEFGHIJKLMO, there may be different subclasses of T2SS that require a reduced set of proteins for a functional system. A set of T2S genes is present in the *C. trachomatis* genome, *gspCDEFG* (CTL0836-CTL0832/ CT573-CT569). These genes are widely conserved amongst all *Chlamydiae* and in *C. trachomatis* they are in an operon with CTL0831/CT568 and CTL0830/CT567 (data not shown). The N-terminal region of both CTL0830/CT567 and CTL0831/CT568 contains a leader peptide followed by a modified GFxxxE prepilin cleavage motif and a hydrophobic rich region. This structure is very characteristic of pseudopilins in other Gram-negative bacteria, suggesting

CTL0830/CT567 and CTL0831/CT568 may be minor pseudopilins. The minor pseudopilins (GspH, I, J, and K) are methylated and cleaved by the prepilin peptidase (GspO) prior to forming the pseudopilus tip [106, 249]. The addition of GspG major pilin subunits underneath the tip allows the for pseudopilus elongation during secretion. However, the prepilin peptidase responsible for removal of the pseudopilin leader peptide in *C. trachomatis* remains unknown. Additionally, structural or regulatory components required for a functional T2S in *Chlamydia* may be at other genomic locations.

The T2SS of *C. trachomatis* contributes to optimal bacterial growth in the intracellular environment [87]. However, a comprehensive understanding of what proteins constitute T2S substrates is largely lacking. Thus far, only one protein has been confirmed to be a T2SS effector in *C. trachomatis*, the protease CPAF [64]. Based on an alkaline phosphatase (*phoA* gene) fusion system and immunofluorescence studies, several *C. trachomatis* proteins are potential T2S candidate substrates; they are predicted to be dependent on Sec translocation into the periplasm and are suggested to localize to the host cytosol during infection. These proteins include the high temperature requirement protein A protease (cHtrA/CT823), the tail-specific protease (Tsp/CT441), CT311, and CT795 [93, 94, 99, 125]. However, their localization has not been assessed in a T2S-deficient *Chlamydia* strain.

As it remains unclear how T2S substrates are recognized for secretion from the milieu of proteins present in the periplasm, identifying which *Chlamydia* proteins are T2S substrates cannot be accomplished from bioinformatic studies alone [17]. An axenic medium that supports some metabolic activity of *C. trachomatis* EBs and RBs has been developed, however bacterial growth and the secretion of *Chlamydia* proteins has yet to

be assessed under these conditions [115]. As which T2 proteins are secreted varies in different host environments in other Gram-negative organisms, it is possible not all proteins may be secreted under axenic growth. In addition, much remains to be discovered about the extra-bacterial enzymatic activities that occur in the inclusion lumen during *Chlamydia* infection, precluding strategies to identify substrates by the presence or absence of a specific enzymatic activity in WT or T2S mutants.

Unlike facultative intracellular organisms, analysis of secreted proteins in obligate intracellular bacteria is complicated by the need to separate bacterial proteins present in the vacuole and/or host cytosol from those remaining inside the bacteria. However, nonfunctional T2S can lead to the accumulation of T2 substrates and other proteins in the bacterial periplasm; a phenotype which is seen in a *C. trachomatis* T2S-defective strain [152]. In this study, we use label-free quantitative liquid chromatography-tandem mass spectrometry (LC-MS/MS) for a comprehensive analysis of proteins present within WT and T2S-defective *C. trachomatis* bacteria and identify proteins that are preferentially accumulated in the T2S mutant strain. Using this approach, we described a subgroup of proteins whose localization within the inclusion lumen is dependent on the presence of glycogen.

3.2 Impaired growth, glycogen granule production, and CPAF mis-localization are the result of a mutation in *gspE*

Our laboratory reported the creation of a genetically defined library of *C. trachomatis* LGV-L2 mutants using chemical mutagenesis coupled with whole genome sequencing [152, 172]. A *C. trachomatis* LGV-L2 variant [RSTE4 (T2S⁻)] identified using this approach contains a point mutation in the type II secretion ATPase GspE (*CTL0834*) [152]. This mutant is attenuated in the production of infectious progeny, accumulates

insoluble glycogen granules within the inclusion lumen, and fails to secrete the protease CPAF outside of the bacteria during infection [64, 152]. While the SNVs identified in the genome of RSTE4, except for the mutation in *gspE*, are found in the parental Rif^R, Spc^R, or Tmp^R strains used to generate RSTE4 (Table 2), we wanted to confirm the phenotypes of RSTE4 are due to the G to E substitution at amino acid 425 in GspE.

Table 2: Single nucleotide variants identified in strain RSTE4

Reference genome location ¹	Amino Acid change	Variant Type ²	434/Bu locus tag ³	Ser. D locus tag ⁴	Gene
123,086		Non coding ⁸			
123,163		Non coding ⁷			
127,338	P219P	Synonymous ⁸	CTL0103	CT734	
135,167		Non coding ⁵			
157,211		Non coding ⁵			
456,892	G408R	Non synonymous ⁶	CTL0369	CT114	
959,281	G425E	Non synonymous	CTL0834	CT571	<i>gspE</i>

¹ Nucleotide position in *C. trachomatis* LGV L2 434/Bu reference strain genome (GenBank number NC_010287).

² Single nucleotide variant classification. Synonymous (silent substitution), non synonymous (substitution), nonsense (truncation), non coding (outside coding domain sequence).

³ Locus designation in *C. trachomatis* LGV L2 434/Bu reference strain.

⁴ Locus designation in *C. trachomatis* D/UW-3/CX (Serotype D) reference strain (GenBank number NC_000117.1).

⁵ Mutations leading to spectinomycin resistance.

⁶ Mutation leading to trimethoprim resistance.

⁷ SNV present in Rif^R parental strain.

⁸ SNV present in Tmp^R parental strain.

Introducing a shuttle vector into RSTE4 encoding a N-terminally FLAG tagged copy of *gspE* under the control of the IncD promoter (RSTE4^{pGspE}) partially restores the growth of this mutant (Fig. 15a). Additionally, immunofluorescence analysis with anti-CPAF antibodies of HeLa cells infected with RSTE4^{pGspE} show immunoreactive material

in the host cytosol, indicating the loss of CPAF localization out of the bacteria in RSTE4 infected cells is a result of the SNV in *gspE* (Fig. 15e). The loss of CPAF protein to the host cytosol is not due to the presence of glycogen granules within the inclusion lumen. CPAF is localized to the host cytosol during infection of HeLa cells with another glycogen granule accumulating L2 strain (M380) bearing a nonsense mutation in *glgB* (*CTL0245*), the *Chlamydia* glycogen branching enzyme (Fig. 15e) [172].

Gehre et al. recently observed glycogen inside the inclusion is both translocated in bulk from the host cell and synthesized within the inclusion using bacterial enzymes that are secreted via the T3SS [186]. Glycogen and glycogen granules can be visualized within the inclusion of infected cells by staining with Schiff reagent following periodic acid treatment (Fig. 15c). To determine if host glycogen synthesis is required for glycogen granule formation, we generated HeLa cell lines deficient for Gys1, the host glycogen synthase, by CRISPR/Cas-mediated gene editing (Fig. 16a). Gys1 knock out cells have a 14-fold reduction in the amount of measurable glycogen within the cell, compared to control cells (Fig. 16b).

Glycogen granules form within the inclusion of host cells infected with the RSTE4 mutant or M380, indicating granules are composed of bacterial-derived glycogen (Figure 15d). Interestingly, RSTE4^{pGspE} infected cells display a 9-fold decrease in the number of glycogen granules present within the inclusion of infected cells compared to RSTE4, suggesting defects in the T2SS can alter the properties of glycogen (Fig. 15b-c). These results suggest there may be an interplay between the T2 and T3 secretion systems of *C. trachomatis*. In support of this idea, recent work by Patton et al. found there was cooperation between T3 secreted effectors and CPAF in the suppression of the host innate immune signaling [219].

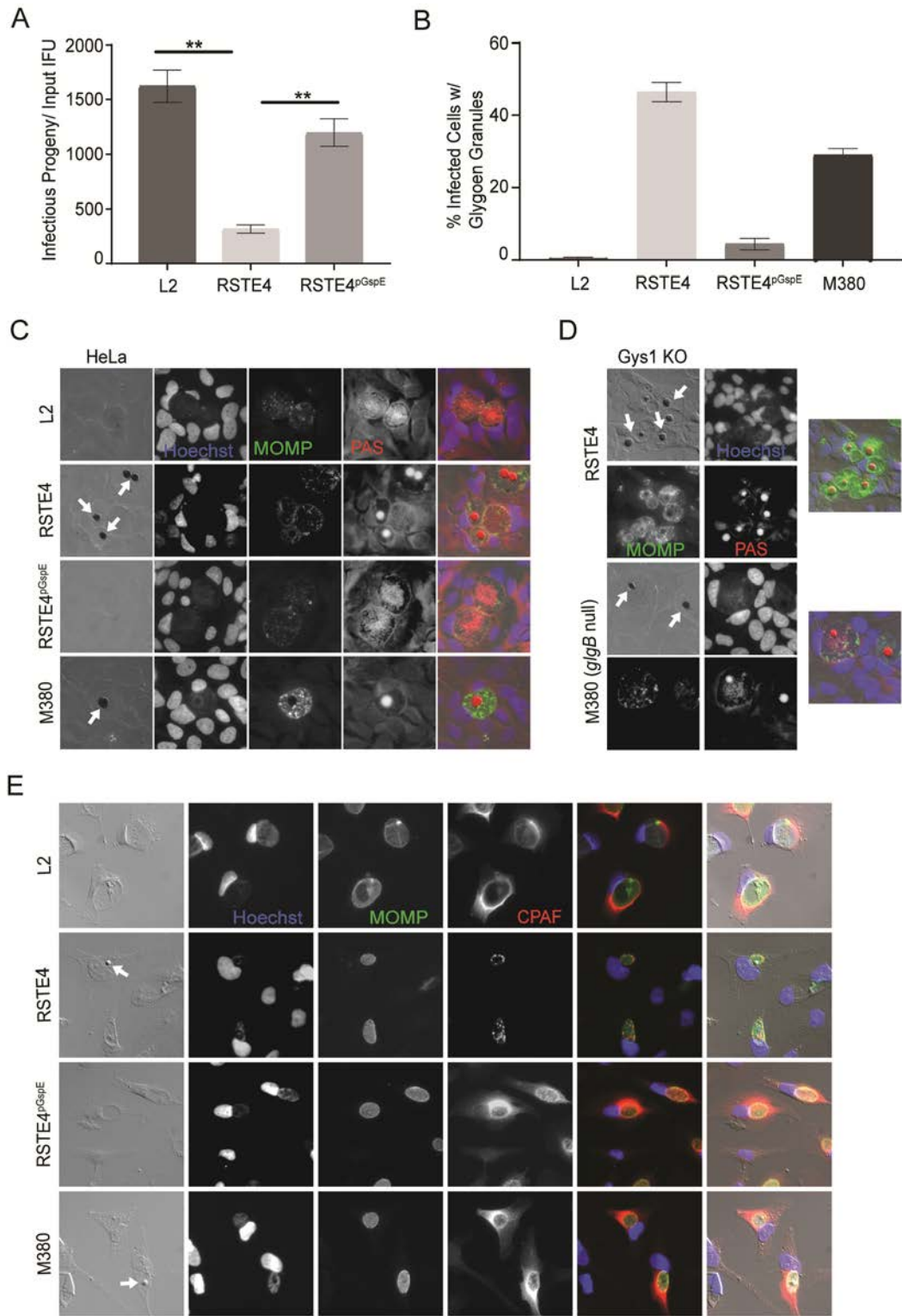


Figure 15: Impaired growth, glycogen granule production, and CPAF localization result from a the mutation in *gspE*. A) Vero cells were infected with the

indicated strains at an MOI=0.6 and infectious progeny released per input IFU was calculated at 44 hpi. Infection with the RSTE4^{pGspE} strain partially rescues the reduced production of infectious units seen in the RSTE4 mutant. **P<0.01, SEM, n=3. B-C) HeLa cells were infected with the indicated strains at an MOI=1 for 48 h. Glycogen within the cell was visualized by staining with Schiff reagent after periodic acid treatment (PAS-red; DNA-blue; MOMP-green). Glycogen granules (white arrows) within the inclusion of infected cells were counted for 5 fields, 2 biological replicates. RSTE4^{pGspE} infected cells have 10-fold fewer granules compared to RSTE4. D) Cells lacking the host glycogen synthase (Gys1) still form glycogen granules when infected with *C. trachomatis* strains with mutations in *gspE* or *glgB* (RSTE4 or M380, respectively). E) The subcellular localization of CPAF in HeLa cells infected with various *C. trachomatis* strains was assessed by indirect immunofluorescence with anti-CPAF antibodies (red), DNA with Hoechst, and the bacteria with anti-MOMP (green). CPAF localization to the host cytosol is restored in cells infected with the RSTE4^{pGspE} strain.

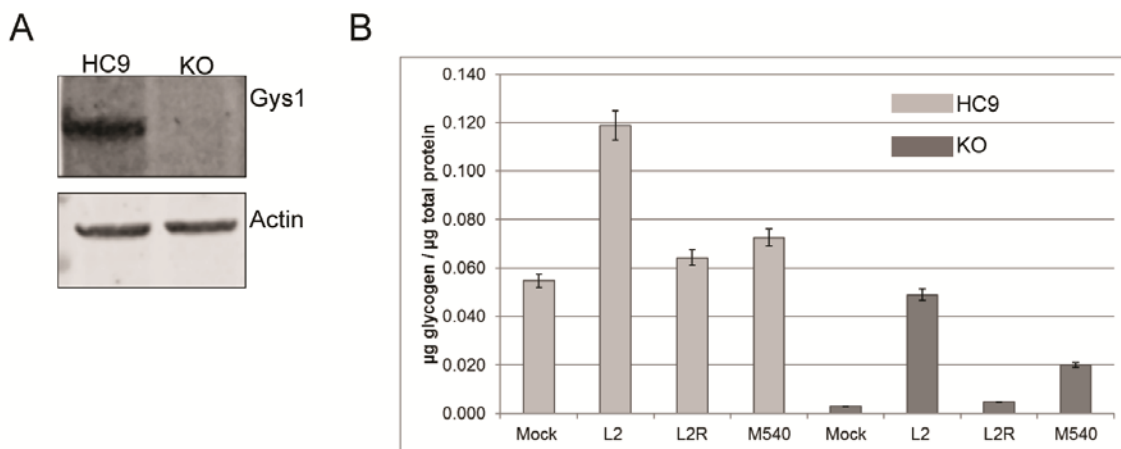


Figure 16: HeLa cells deficient for Gys1 have decreased levels of glycogen within the cells. A) Immunoblot analysis of the Gys1 deficient cell line and control HeLa Cas9 (HC9) using anti-Gys1 antibody. Gys1 protein is not detectable in the knock-out cell line. B) Gys1 KO cells have 10-15 fold less glycogen compared to HeLa Cas 9 control cells. Cells were also infected with the indicated *C. trachomatis* mutant strains at an MOI=1. 48hpi the total µg of glycogen normalized to the total protein within the cell was determined using a colorimetric glycogen assay kit and a DC protein assay. L25667R (L2 strain w/o plasmid) and *glgA* M540 mutant have decreased levels of glycogen during infection. Each experiment was performed with technical triplicates; 2 biological replicates.

3.3 *C. trachomatis* mutants defective for type II secretion have decreased attachment to and exit from A2EN cells

The use of centrifugation to enhance infections varies between species and strains of *Chlamydia*, but the effect is typically minimal for LGV biovars [250]. However,

we noticed infection efficiency with RSTE4 was markedly decreased in the absence of centrifugation, suggesting the RSTE4 mutant may have a defect in the attachment to and/or entry into host cells. To differentiate these possibilities, we tested the ability WT, RSTE4, or RSTE4^{pGspE} bacteria to attach to endocervical epithelial A2EN cells in the absence of centrifugation. We quantified the number of attached bacteria immediately following infection at a multiplicity of infection (MOI) of 50. There was a greater than 50% reduction in the number of RSTE4 bacteria attached to the surface of the cells compared to WT and reintroduction of GspE was capable of rescuing attachment (Fig. 17a). We further evaluated *Chlamydia*'s entry into host cells by shifting the infected cells to 37°C for 1 hour, allowing the attached bacteria to enter the cells. Using immunofluorescence, we discriminated external vs internal bacteria by staining with an anti-LPS antibody (external bacteria) prior to permeabilization and incubation with an antibody against *C. trachomatis* MOMP (total bacteria) [251]. We found no significant difference in the ability of RSTE4 bacteria to enter the cell, demonstrating the reduced infection efficiency is due to an attachment, not entry, defect in RSTE4 bacteria (Fig. 17b).

Both entry into and exit from a host cell are critical steps in the infection cycle of *Chlamydia*. Exit from the host occurs via two distinct mechanisms, lysis and extrusion [200]. We tested the ability of RSTE4 mutants to exit the host cell via lysis by monitoring infected monolayers for lysis and measuring the number of recoverable infectious units in the supernatant at various timepoints post infection. Cell lysis during infection with WT bacteria occurs by 52hpi with majority of infected cells having lysed completely by 65hpi (Fig. 17c). In contrast, lysis in RSTE4 infected cells is delayed and non-lysed cells are still visible after 120hpi, suggesting the T2SS or its substrates may play a role in the completion of the *Chlamydia* life cycle.

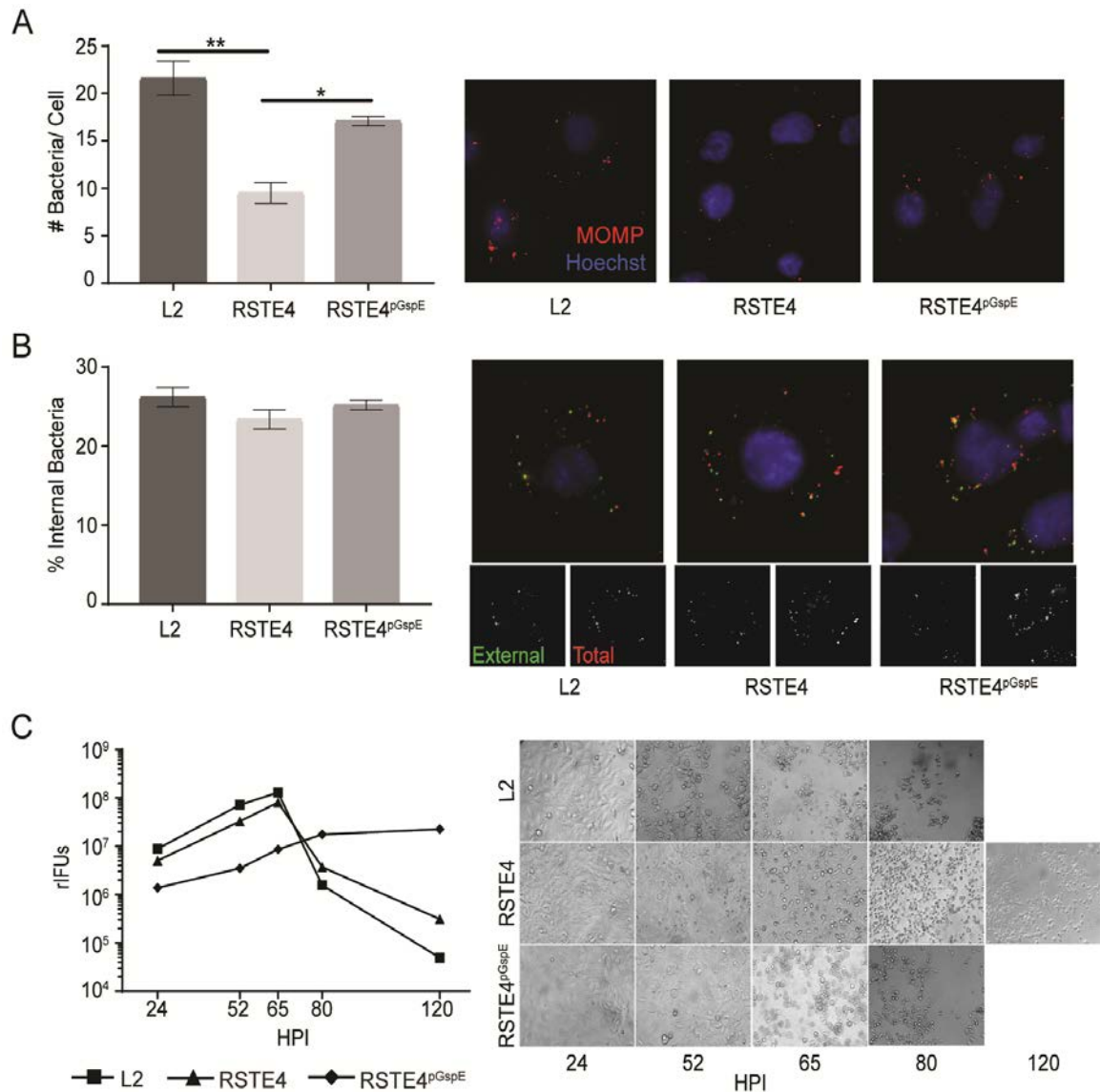


Figure 17: T2S mutants are defective in attachment to and exit from host cells. A) Attachment to A2EN cells was assessed immediately following infection at an MOI of 50 using immunofluorescence with anti-MOMP antibodies (red) and DNA with Hoechst. Bacteria attached to cells were quantified in a minimum of 5 fields for each replicate. RSTE4 bacteria are defective in the attachment to host cells. ****** $P < 0.01$, ***** $P < 0.05$, SEM, $n = 4$. B) Entry into host cells was assessed following infection at 37°C for 1 hour by differential staining of total (MOMP-red) vs external (LPS-green) bacteria for 5 fields, 2 biological replicates. There is no difference in the ability of T2S mutant bacteria to enter the host cell following attachment. C) HeLa cells were infected with the specified strains. Recoverable IFUs were determined and images were taken at the indicated timepoints post infection. The RSTE4 mutant has delayed lysis and sustained rIFUs at 80 and 120 hpi, compared to the WT and RSTE4^{pGspE} infected cells. Images are representative from one of three independent experiments.

3.4 Proteins accumulate in *RstE4* bacteria

Our electron microscopy studies reveal the RSTE4 mutant accumulates electron dense material in the periplasmic space of approximately 40% of RBs within the inclusion (Fig. 18a-b) [152]. Build-up of proteins in the periplasm is associated with mutations in T2S in in other Gram-negative bacteria [6, 252]. However, the abundance of material in the periplasm of *C. trachomatis* is unique, raising the possibility that bacterial products other than proteins may also accumulate in the RSTE4 strain. Nonetheless, we hypothesized a portion of the accumulating material in RBs may be T2S substrates. Due to the technical difficulties of harvesting RBs and the increased risk

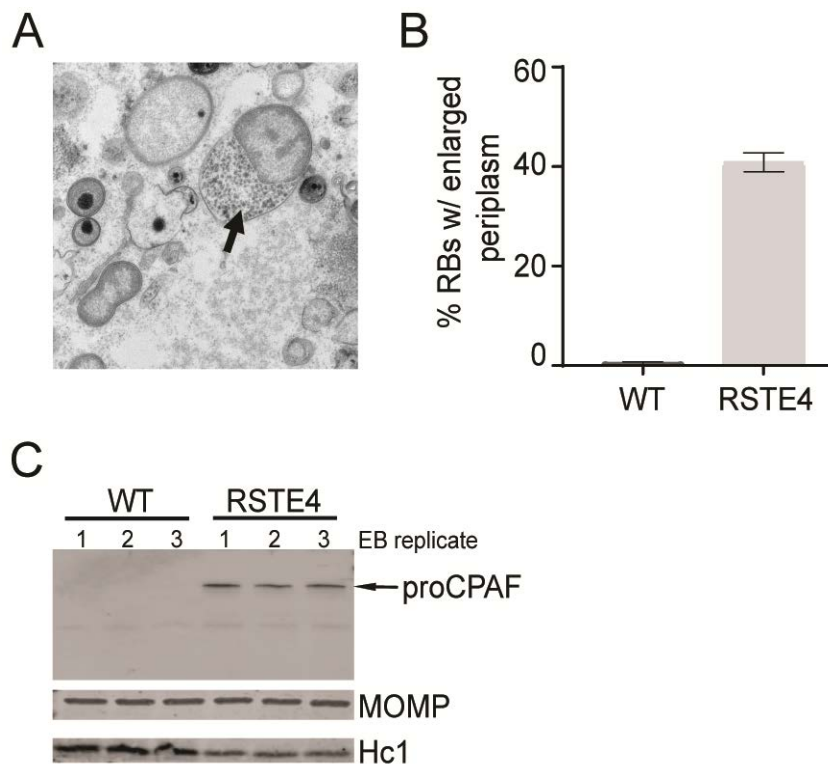


Figure 18: Proteins accumulate in RSTE4 bacteria. A-B) Using transmission electron microscopy, the number of RBs showing the accumulation of electron dense material in the periplasmic space was quantified for both WT and RSTE4 infected Vero cells. C) Immunoblot analysis of EB lysate from Vero cells infected with WT or T2S mutants. Unprocessed full length CPAF is only detected in RSTE4 EB lysate.

of lysis during the purification of RBs with an enlarged periplasm, we asked if proteins that accumulate in RBs also increase in EBs when the RBs differentiate back at the end of the life cycle. To test this hypothesis, we purified EBs from both WT and RSTE4 infected cells. Immunoblot analysis revealed the 70-kDa CPAF zymogen was only detectable in EB lysate from the RSTE4 bacteria and processed CPAF was not detected in either strain, consistent with previous studies that suggest CPAF is predominately present in RBs (Fig. 18c) [188, 189].

For a comprehensive analysis of the proteins present in both EB populations and identify proteins that are preferentially accumulated in the RSTE4 bacteria, we purified three biological replicates of EBs using sequential density gradients. Using purified bacteria, we prepared total EB protein lysates. Following trypsin digestion, peptides were submitted for quantitative two-dimensional liquid chromatography – tandem mass spectrometry (LC/LC-MS/MS) analysis. To test for technical reproducibility, 3 QC pools were made from portions of each of the samples submitted. Samples were also run in an order to minimize batch effect (QC pool, WT-1, RSTE4-1, WT-2, QC pool, RSTE4-2, WT-3, RSTE4-3, QC Pool).

The final quantitative dataset identified 6,917 peptides matching to 1,237 human and *Chlamydia* proteins, with 774 proteins containing at least 2 unique peptides. Human proteins are contamination from the preparation of purified EBs, therefore we utilized a method for mixed-species quantification of proteomic samples that was developed by Saka et al. [188]. During the first step of this process, peptides that are homologous between *Chlamydia* and the host are removed. Next, the average intensity across all 6 samples of each peptide identified for a protein is determined and peptides are ranked according to average intensity. The top three peptides are used to calculate that

protein's relative abundance in the sample. Due to the low molecular weight of many *Chlamydia* proteins, this calculation was also performed if there were only 2 peptides to match. The fmol of protein in each sample is then calculated based on the intensity of the top 2 or 3 peptides and the historic response factor of the instrument. This fmol value is then converted to nanograms using the molecular weight of the protein and the total amount of protein of each species is summed per sample. For the species-specific correction, the fmol of each *Chlamydia* protein present is divided by only the ng total of *Chlamydia* protein present in that sample. The average makeup of *Chlamydia* protein to total (human + *Chlamydia*) protein across all six samples is 75.5 +/- 3.3% (Figure 19). These values are consistent with previous studies by our laboratory [188].

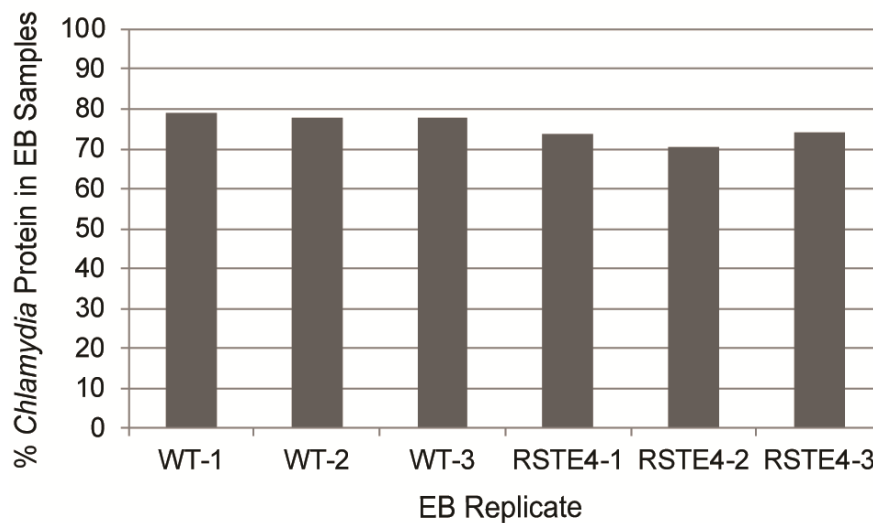


Figure 19: *Chlamydia* protein contribution to the total based on peak intensities. The total ng of *Chlamydia*-specific protein within each EB sample preparation was compared to the total ng of protein present within the sample.

To screen for potential outliers, a principal component analysis was performed using z-scored peptide intensities (Figure 20). As expected, the three QC pools were most similar. However, there is some separation between the WT (green) and RSTE4 (blue) samples along the PC1 axis.

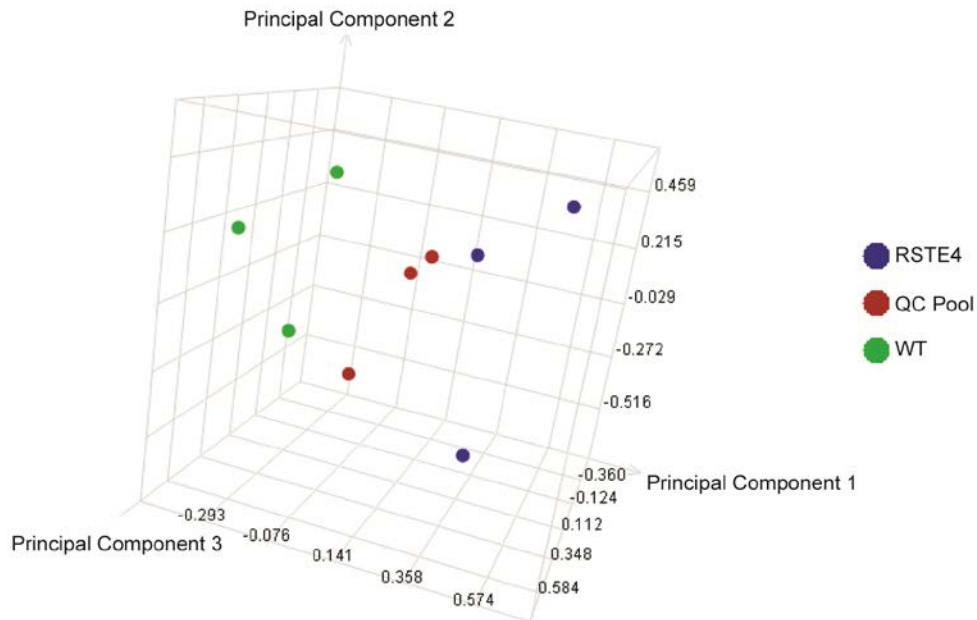


Figure 20: Principal component analysis of samples submitted for EB proteomics. WT and RSTE4 quantitative data was analyzed by principal component analysis for each independent sample measurement. The data was first summed to the expression values and z-score normalized, then 3 principal components were calculated for each of the 9 analyses (3 WT EB- green, 3 RSTE4 EB- blue, 3 QC pools- red).

Analysis of the proteome identified 515 non-redundant *C. trachomatis* proteins across both WT and RSTE4 EBs. Of these proteins 431 (84%) have two or more peptides to match, allowing for their quantification. By comparison, our previously published dataset from Saka et al. identified 485 total proteins and 373 reliably quantifiable proteins (n = 2 peptides or more) across both EB and RB developmental forms [188]. The current study represents a 16% increase in the coverage of the EB proteome.

To independently verify the MS-based quantification, we used immunoblot analysis on a group of selected proteins (Fig 21). Fold-change was calculated two ways:

based on the quantification (fmol/ug) of each protein with 2 or more peptides or by comparing the sum of the peptide intensities for each protein. Either way, fold change is




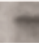
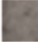
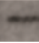






	Immunoblot		MS (fmol/μg)		FC
	WT	RSTE4	WT	RSTE4	(RSTE4/WT)
GspD			0.37 ± 0.06	1.32 ± 0.17	3.53
CPAF			15.52 ± 1.29	35.82 ± 6.84	2.31
IncG			1.27 ± 0.18	1.98 ± 0.26	1.56
HtrA			42.58 ± 4.13	46.02 ± 4.10	1.08
Tarp			27.33 ± 2.18	24.83 ± 1.07	-1.10
CopB			24.37 ± 1.47	16.30 ± 1.03	-1.49

Figure 21: Immunoblot analysis of selected *C. trachomatis* proteins from WT and RSTE4 EB lysates. The relative abundance in EBs from WT or RSTE4 for a subset of *Chlamydia* proteins was determined by immunoblot analysis and compared with the mass spectrometry (MS)-based quantification. Fold change is based on protein quantification; a negative fold change indicates the protein is accumulated in RSTE4 EBs.

represented as the ratio of average RSTE4 protein over the average of WT, or the inverse reciprocal, such that proteins upregulated in RSTE4 have positive fold-change and downregulated have negative fold-change. For example, the T2 outer membrane protein, GspD, was determined via immunoblot with anti-GspD antibodies to be accumulated in RSTE4 EBs, consistent with the MS data. Another component of the T2SS, GspG, the major pilin subunit of the pseudopilus, is also increased in abundance in T2S-defective EBs (Table 8). This perhaps represents a strategy by the bacteria to upregulate export out of the periplasms in response to the quantity of material present within. We similarly verified IncG, previously reported to be found mainly within RBs, is increased in RSTE4 EBs, while the type III secretion translocator protein CopB is

decreased in this strain (Fig. 21). Overall, the immunoblot results strongly agreed with the MS-based analysis.

3.5 Proteome differences between *RstE4* and WT bacteria

Of the proteins 92 that display a > 1.5-fold difference between RSTE4 and WT EBs, only 27 were increased in WT, with 18 having 1 or more peptide to match. Some of the notable proteins that are upregulated in WT, not including T3S-related proteins are: proteins involved in translation (CT021/CTL0276, CT436/CTL0695, CT833/CTL0205, CT752/CTL0121, and CT677/CTL0046), the histone like protein Hc1, the thioredoxin TrxA (CT539/CTL0801) and thioredoxin disulfide isomerase DsbH (CT780/CTL0149). There are many additional proteins and pathways we anticipated might differ between RSTE4 and WT bacteria. Below is a discussion of some of the more general findings from the proteomics dataset.

3.5.1 General secretory pathway in RSTE4 bacteria

As mentioned above, the Sec pathway translocates proteins across the inner membrane in an unfolded state. There are three parts of the Sec system: a membrane integrated channel, a protein targeting component, and a motor protein. The integral membrane complex is composed of SecY, SecE, and SecG. Proteins destined to cross the inner membrane are maintained in an unfolded state after translation through the actions of a cytoplasmic chaperone SecB. SecB can deliver substrates to the ATPase SecA, which provides the energy for protein translocation and also acts to target the protein to the SecYEG channel [253]. It is believed SecD/F maintains the proton motive force required for efficient protein translocation and prevents the emerging preprotein in the periplasm from backsliding into the SecYEG channel [254].

The *C. trachomatis* genome encodes for SecY (CT510/CTL0772), SecE (CT321/CTL0573), SecG (CT351a/CTL0606) and a SecDF fusion protein (CT448/CTL0708a). Additionally, *Chlamydia* has two SecA homologues: CT141/CTL0396 and CT701/CTL0070. As CT141 is significantly shorter in length, it is likely a SecA fragment and will be noted as SecA2. No SecB homologue has been identified, however other cytoplasmic chaperones, such as the GroELs (CT110/CTL0365, CT604/CTL0867, CT755/CTL0124), may function in its place [150].

Table 3: Proteome differences in the general secretory pathway between WT and RSTE4 EBs

434/BU	UW-3/ CX	Gene Name	Peptide Matches	Fold Change Intensity (RSTE4/WT)
CTL0708a	CT448	<i>secD/secF</i>	5	2.86
CTL0606	CT351a	<i>secG</i>	1	1.11
CTL0070	CT701	<i>secA</i>	32	1.08
CTL0867	CT604	<i>groEL2</i>	1	1.07
CTL0772	CT510	<i>secY</i>	3	1.06
CTL0573	CT321	<i>secE</i>	1	-1.09
CTL0365	CT110	<i>groEL</i>	43	-1.28
CTL0396	CT141	<i>secA2</i>	2	-1.96
CTL0124	CT755	<i>groEL3</i>	0	ND*

* No peptides found in dataset, fold change not determined

Of the components within this pathway, only one peptide was found to match for SecG, SecE, and GroEL2 (Table 3). Intriguingly, SecDF is accumulated in RSTE4 bacteria, while SecA2 (CT141) is downregulated in RSTE4 EBs. The remaining components are not significantly changing. Certain Gram-positive organisms also contain two SecA proteins; in these cases, the smaller homolog (SecA2) is regulated differently and is used to export a unique, typically reduced, set of proteins [253]. In *Chlamydia*, SecA2 may be important for translocating certain T2 substrates into the periplasm and bacterial

sensing of periplasmic contents could change SecA2 levels. Cells infected with Rst17, which lacks the T2 substrate CPAF, have more SecA2 present at 30hpi [219]. In this proteomics dataset, downregulation of SecA2 could represent an effort to reduce transport of specific proteins across the inner membrane.

3.5.2 Stress response proteins do not accumulate in RSTE4 bacteria

Numerous studies have shown disrupting T2S has the potential to alter other important cellular processes, resulting in oxidative stress and compromised outer membrane integrity [255]. Similar effects may result in increased stress response proteins being present in RSTE4 bacteria. In *C. trachomatis* infected cells, stresses such as heat shock increase *groEL*, *groES*, and *dnaK* expression [256-258]. Proteins responsible for degrading accumulated/misfolded proteins in the periplasm, such as the periplasmic proteases SohB or HtrA, may also be increased in T2S-deficient bacteria.

Table 4: Stress response proteins do not accumulate in T2S-deficient bacteria

434/BU	UW-3/ CX	Gene Name	Peptide Matches	Fold Change Intensity (RSTE4/WT)
CTL0650	CT394	<i>hrcA</i>	2	1.42
CTL0755	CT494	<i>sohB</i>	12	1.18
CTL0195	CT823	<i>htrA</i>	31	1.02
CTL0652	CT396	<i>dnaK</i>	42	-1.18
CTL0365	CT110	<i>groEL</i>	43	-1.28
CTL0366	CT111	<i>groES</i>	7	-1.41

Majority of the stress response proteins identified in the dataset are not significantly changing in RSTE4 EBs. Heat shock of *Chlamydia*-infected cells leads to loss of transcriptional repressor (HrcA) binding to the *groESL* and *dnaK* promoters [257]. The moderate increase in HrcA protein in RSTE4 bacteria could help explain the slight

decrease in GroEL, GroES, and DnaK in T2S mutant bacteria (Table 4). HtrA has protease and chaperone activities in the periplasm and its function increases in response to heat shock, however it does not change between WT and RSTE4 bacteria [259-261]. It is unexpected that the loss of the T2SS and increased abundance of proteins in the periplasm does not result in an increase in stress response proteins or periplasmic proteases. However, upregulation of other periplasmic chaperones may aid in stabilizing RSTE4 bacteria by promoting the proper folding of proteins.

3.5.3 Predicted T2SS substrates do not accumulate in RSTE4 EBs

Besides CPAF, we hypothesized that four other proteins could be T2S substrates and would accumulate in RSTE4 EBs. These proteins, HtrA, Tsp, CT311, and CT795 have been shown to have Sec signal peptides sufficient for translocation into the bacterial periplasm and are localized outside of the bacteria [157, 158, 261]. In accordance with two other published proteomic datasets, we did not identify any peptides matching Tsp/CT441 or CT795 and therefore cannot conclude whether these proteins are accumulated in RSTE4 EBs [188, 189]. Surprisingly, both CT311 and HtrA were not accumulated in RSTE4 bacteria (Table 5). There are numerous possibilities

Table 5: HtrA and CT311 are not accumulated in T2S-deficient EBs

434/BU	UW-3/ CX	Gene Name	Peptide Matches	Fold Change Intensity (RSTE4/WT)
CTL0195	CT823	<i>htrA</i>	31	1.02
CTL0563	CT311		1	-1.11
CTL0164	CT795		0	ND*
CTL0700	CT441	<i>tsp</i>	0	ND*

* No peptides found in dataset, fold change not determined

as to why HtrA and CT311 failed to accumulate in RSTE4 EBs. The proteins may be accumulated in RBs, but are degraded prior to transition back to EBs. Alternate

regulation mechanisms may also exist to decrease protein levels in response to increasing concentrations in the periplasm. Finally, T2S is not the only way out of the periplasm. Outer membrane vesicles (OMVs) bud off the outer membrane and contain selective periplasmic content [262].

Membrane vesicles have been observed via electron microscopy to be produced during *Chlamydia* infection, however their exact function remains to be determined [263-265]. OMVs produced by other Gram-negative bacteria have a wide variety of functions; they can contain proteins that contribute towards pathogenesis or be important for bacterial survival in response to envelope or oxidative stress [262, 266-268]. Envelope stress caused by the periplasmic accumulation of misfolded proteins in an *E. coli* strain lacking the periplasmic protease/chaperone DegP ($\Delta degP$ strain), results in an increased production of OMVs [267, 269]. An increase in the generation of OMVs is also seen under conditions of antibiotic exposure in *Shigella dysenteriae* and *P. aeruginosa* [270, 271]. Similarly, exposure of *C. trachomatis* to ampicillin increases the formation of OMVs and through TEM analysis these vesicles are found near the inclusion membrane and in the host cytosol [272]. Isolated *C. trachomatis* serovar F/Cal-I-13 vesicles contain the outer membrane protein MOMP, in addition to a predicted phospholipase D protein CT159, and the putative cytotoxin CT166 [265]. Further investigations are needed to determine if the abundant periplasmic material in the RSTE4 mutant induces envelope stress which results in an increase in the production of HtrA or CT311 containing OMVs.

3.4.4 T2S-dependent differences in the abundance of virulence and T3S-related proteins

The TEM images of RSTE4 bacteria show a large separation between the IM and OM due to the increase of electron dense material in the periplasm. We

hypothesized this membrane disturbance might disrupt other *C. trachomatis* secretion systems, including the T3SS. Of the 40 T3S-related proteins identified in the dataset, 30 remained unchanged (fold-change less than 1.49), 3 were decreased in RSTE4 bacteria, and 7 were increased in RSTE4 EBs. Majority of the structural components of the T3SS remained unchanged, except for a 1.5-fold decrease of translocator protein CopB in RSTE4. The other two proteins decreased are the T3S effector CT694/CTL0063 and the predicted inclusion membrane like protein CT565/CTL0828. Predicted mid to late-cycle T3 effectors, including CT142 and CT143 are increased RSTE4 bacteria [273]. The inclusion membrane proteins IncG, CT518/CTL0882, CT223/CTL0476, and CT147/CTL0402 are also upregulated in RSTE4 EBs. Despite these differences, various T3 effector proteins, such as Tarp, TepP, and InaC, are still secreted during infection, and bacterial-derived glycogen is still found in the inclusion lumen, suggesting the T3SS is functional throughout RSTE4 infection (data not shown).

3.4.4.1 Glycogen biosynthesis proteins

We previously hypothesized the accumulation of glycogen granules in the RSTE4 mutant was due to the failure of this strain to secrete a glycogen hydrolase [152]. The glycogen biosynthesis enzymes have since been shown to be secreted by the T3SS [186]. We assessed the protein levels of various enzymes involved in glycogenesis and glycogenolysis in both RSTE4 and WT bacteria to better understand if these pathways change in the absence of T2S (Table 6).

No significant changes in the proteins involved in glycogen synthesis or breakdown were identified between the two strains. While no peptides were identified for GlgB, consistent with previous proteomic experiments, the *glgB* transcription peaks early during infection (3-8 hpi), earlier than other glycogen proteins are expressed and before

glycogen is detectable in the inclusion lumen [186, 274]. Why this protein is transcribed and possibly secreted early in infection remains unclear. Additional experiments are needed to assess if GlgB is expressed and localized within the inclusion during infection with the T2S-deficient *Chlamydia* strain, as loss of glycogen branching activities inside the inclusion lumen results in glycogen granule formation.

Table 6: Proteins involved in glycogenesis and glycogenolysis do not change between WT and RSTE4 EBs

434/BU	UW-3/ CX	Gene Name	Peptide Matches	Fold Change Intensity (RSTE4/WT)
CTL0167	CT798	<i>glgA</i>	19	1.27
CTL0298	CT042	<i>glgX</i>	7	-1.38
CTL0500	CT248	<i>glgP</i>	23	-1.24
CTL0750	CT489	<i>glgC</i>	8	1.04
CTL0806	CT544	<i>uhpC</i>	6	-1.06
CTL0547	CT295	<i>mrsA</i>	13	-1.17
CTL0245	CT866	<i>glgB</i>	0	ND*

* No peptides found in dataset, fold change not determined

While a T2S substrate may not be directly involved in glycogenesis and glycogenolysis, substrates may be required for the optimal activity or degradation of Glg proteins during infection; similar regulation is seen in other Gram-negative bacteria [100, 219]. Failure of a T2 substrate to localize to the inclusion lumen during infection could result in the misregulation of Glg proteins and the alteration of the properties of glycogen, leading to the accumulation of granules.

3.5.5 Outer membrane protein levels differ in T2S deficient EBs

Chlamydia attachment to host cells is a two-step process that involves a number of bacterial and host proteins [233, 275-280]. During the first step, MOMP or OmcB mediates reversible attachment via heparan sulfate and glycosaminoglycans (GAGs) on

the host-cell surface [234, 275, 277]. The next, irreversible step, is mediated by species and host specific adhesin-receptor interactions. The Hegemann group has shown all nine Pmp proteins (PmpA-I) of *C. trachomatis* serovar E are mediators of *in vitro* adhesion to epithelial cells [281]. Given the defect in host cell attachment, but not entry (Fig. 17A-B), we hypothesized the outer membrane composition of RSTE4 EBs may differ from WT EBs.

Table 7: Outer membrane protein differences between RSTE4 and WT EBs

434/BU	UW-3/ CX	Gene Name	Peptide Matches	Fold Change Quantification (RSTE4/WT)
CTL0272	CT017	<i>ctad1</i>	9	1.44
CTL0254	CT874	<i>pmpI</i>	27	1.26
CTL0183	CT812	<i>pmpD</i>	40	1.10
CTL0250	CT871	<i>pmpG</i>	46	1.09
CTL0671	CT414	<i>pmpC</i>	47	1.08
CTL0670	CT413	<i>pmpB</i>	60	1.00
CTL0251	CT872	<i>pmpH</i>	39	-1.09
CTL0702	CT443	<i>omcB</i>	62	-1.11
CTL0249	CT870	<i>pmpF</i>	38	-1.15
CTL0248	CT869	<i>pmpE</i>	29	-1.18
CTL0082	CT713	<i>ompB/ MOMP</i>	15	-1.24
CTL0494	CT242	<i>ompH-like</i>	4	-1.61

There were no significant changes in the levels of the Pmp proteins, OmcB, or MOMP between WT and RSTE4 EBs. However, an additive effect is seen in *C. pneumoniae* when recombinant proteins are used to block OmcB and Pmp21 binding sites [282]. The slight variations trending towards a small decrease in the overall abundance of Pmps/OmcB/MOMP present within RSTE4 EBs may have an additive effect, which reduces attachment to host cells. Entry of RSTE4 may not be impacted because of the increase in CtaD1, which has recently been shown to promote bacterial invasion [283].

3.5.6 Accumulated proteins in RSTE4 bacteria have varied functions

Intracellular infection requires the successful interaction with a host cell and numerous substrates of the T2SS have been shown to aid in this process. To identify potential candidate substrates in *C. trachomatis*, we first looked at identified proteins that accumulate in T2S-deficient EBs. Data was log₂ transformed for each protein, then p-values were calculated using a Student's T-test. T-test values were corrected for multiple hypothesis testing using Benjamini Hochberg FDR-correction method. A significant p-value indicates there is low variability between the replicates for each strain and a significant difference between RSTE4 and WT bacteria. The dataset was then filtered to identify candidate differentially expressed proteins, by identifying proteins that fit 2 of the 3 following conditions: 2 or more peptides per protein, a p-value <0.05, and an absolute fold-change >1.5. The fold change calculated using average intensities and quantitation were both considered. In RSTE4 EBs, 65 proteins have a > 1.5-fold increase in T2-deficient bacteria compared to WT (Table 8).

To identify patterns among proteins that accumulate in RSTE4 EBs, we placed the accumulated proteins into functional categories (Fig. 22). The most prominent category, *Chlamydia*-specific hypothetical proteins, accounts for 18% of the selected proteins. Proteins in the cell envelope, those involved in protein folding, assembly, and modification, along with miscellaneous enzymes and conserved proteins, represent additional classes of proteins we hypothesize may contain T2S substrates or be important for the function of the T2SS. Other functional categories that are increased in RSTE4 bacteria include proteins known to be involved in T3S and proteins involved in DNA replication, repair, modification, and recombination. However, none of the proteins in these 2 groups contain predicted Sec-signal peptides (Fig. 22).

Table 8: Proteins accumulated greater than 1.5 fold in RSTE4 EBs compared to WT EBs

434/Bu	Gene Name	Predicted Sec Signal Peptide (Y/N)	Peptide Matches	WT Mean (fmol/ug)	WT SD	RSTE4 Mean (fmol/ug)	RSTE4 SD	WT Mean (Intensity)	WT SD	RSTE4 Mean (Intensity)	RSTE4 SD	Fold Change intensity (RSTE4/WT)	P-value
CTL0018	<i>recA</i>	N	13	5.00	0.34	14.28	1.26	595,640	28,169	1,369,688	72,719	2.30	0.007
CTL0057	<i>parB</i>	N	2	0.81	0.16	1.96	0.54	33,971	7,343	79,912	22,696	2.35	0.066
CTL0071		N	3	3.65	0.07	6.64	0.80	230,393	9,142	405,293	45,072	1.76	0.047
CTL0072	<i>engA</i>	N	5	1.02	0.12	3.38	0.22	75,823	8,388	216,515	14,460	2.86	0.012
CTL0077		N	10	2.54	0.20	5.13	0.23	283,076	9,370	575,177	52,374	2.03	0.026
CTL0078	<i>mreB</i>	N	3	2.39	0.05	3.81	0.51	151,160	4,019	232,943	35,061	1.54	0.105
CTL0093		N	1	NQ	NQ	NQ	NQ	36,455	4,567	55,922	6,392	1.53	0.062
CTL0100	<i>ribD</i>	N	2	0.57	0.11	4.23	0.45	24,133	5,003	172,275	18,978	7.14	0.013
CTL0102		Y	7	1.19	0.08	5.89	0.58	98,678	10,133	415,478	40,418	4.21	0.007
CTL0131	<i>murC-murF</i>	N	2	0.56	0.02	1.10	0.07	23,736	471	44,914	1,713	1.89	0.009
CTL0132		N	1	NQ	NQ	NQ	NQ	151,459	5,576	236,308	26,151	1.56	0.065
CTL0152		Y	3	0.39	0.04	2.86	0.55	24,754	2,905	174,580	31,820	7.05	0.011
CTL0158		N	2	3.05	0.08	6.02	0.73	128,679	5,548	245,338	28,788	1.91	0.04
CTL0188	<i>glmS</i>	N	6	5.04	1.48	9.79	0.93	354,493	103,985	683,494	37,327	1.93	0.119
CTL0199	<i>nrdA</i>	N	5	1.59	0.08	2.68	0.22	124,868	12,011	212,710	4,456	1.70	0.054

434/Bu	Gene Name	Predicted Sec Signal Peptide (Y/N)	Peptide Matches	WT Mean (fmol/ug)	WT SD	RSTE4 Mean (fmol/ug)	RSTE4 SD	WT Mean (Intensity)	WT SD	RSTE4 Mean (Intensity)	RSTE4 SD	Fold Change intensity (RSTE4/WT)	P-value
CTL0233	<i>cpa</i>	Y	16	15.52	1.29	35.82	6.84	1,475,011	151,807	4,105,627	395,036	2.78	0.011
CTL0271		N	1	NQ	NQ	NQ	NQ	6,186	3,706	10,638	3,134	1.72	0.393
CTL0272	<i>Ctad1</i>	N*	9	6.94	1.19	9.98	0.84	534,195	71,632	847,779	37,090	1.59	0.076
CTL0282	<i>trmD</i>	N	1	NQ	NQ	NQ	NQ	576	65	4,373	3,730	7.59	0.133
CTL0290		N	3	1.01	0.02	2.65	0.60	63,569	2,331	162,022	35,722	2.55	0.067
CTL0297		Y	3	1.04	0.22	3.78	0.89	66,111	15,267	231,163	55,099	3.50	0.029
CTL0307	<i>pls3</i>	N	5	6.29	0.76	10.94	2.29	502,150	63,683	751,501	157,773	1.50	0.158
CTL0321	<i>npt1</i>	N	8	16.77	1.04	25.45	1.61	1,668,834	132,035	2,301,218	180,851	1.38	0.047
CTL0322		N	2	1.72	0.46	3.41	0.86	72,437	19,794	139,379	37,513	1.92	0.106
CTL0331	<i>dnaN</i>	N	3	3.27	0.16	5.20	0.45	206,618	8,262	317,821	25,321	1.54	0.031
CTL0373	<i>incG</i>	N	2	1.27	0.18	1.98	0.26	53,525	8,055	80,453	9,877	1.50	0.078
CTL0398		N	6	7.77	0.50	11.17	2.08	838,715	55,955	1,253,268	160,069	1.49	0.071
CTL0400	<i>pkn1</i>	N	2	5.42	0.32	8.55	1.41	392,416	36,353	583,567	83,680	1.49	0.082
CTL0402		N	7	0.63	0.01	2.03	0.09	26,693	584	82,822	5,777	3.10	0.013
CTL0408		N	30	1.24	0.03	3.45	1.04	108,701	4,329	284,424	51,520	2.62	0.052
CTL0476		N	3	2.05	0.65	3.79	0.42	129,929	43,109	231,960	31,270	1.79	0.183

434/Bu	Gene Name	Predicted Sec Signal Peptide (Y/N)	Peptide Matches	WT Mean (fmol/ug)	WT SD	RSTE4 Mean (fmol/ug)	RSTE4 SD	WT Mean (Intensity)	WT SD	RSTE4 Mean (Intensity)	RSTE4 SD	Fold Change intensity (RSTE4/WT)	P-value
CTL0505		Y	1	NQ	NQ	NQ	NQ	103,224	10,461	278,835	26,636	2.70	0.011
CTL0521	<i>murE</i>	N	1	NQ	NQ	NQ	NQ	7,582	750	38,633	1,363	5.10	0.012
CTL0525		N	1	NQ	NQ	NQ	NQ	17,012	3,244	28,977	1,705	1.70	0.083
CTL0526		N	1	NQ	NQ	NQ	NQ	28,695	1,276	54,727	3,022	1.91	0.009
CTL0527	<i>dnaA2</i>	N	3	0.42	0.08	1.61	0.10	26,693	5,377	98,510	8,370	3.69	0.027
CTL0542		N	3	1.25	0.06	2.35	0.20	79,198	4,285	143,876	15,434	1.82	0.029
CTL0562	<i>atpE</i>	N	4	7.04	2.02	11.40	3.48	445,497	127,200	701,398	232,046	1.57	0.267
CTL0583	<i>xseA</i>	N	2	0.75	0.07	2.19	0.55	31,788	3,168	89,209	22,322	2.81	0.065
CTL0609		N	1	NQ	NQ	NQ	NQ	8,712	1,793	59,742	6,578	6.86	0.013
CTL0615	<i>dapA</i>	N	3	1.85	0.06	3.22	0.47	117,202	5,345	197,012	28,380	1.68	0.068
CTL0623	<i>aroB</i>	N	1	NQ	NQ	NQ	NQ	48,062	3,352	100,797	22,061	2.10	0.074
CTL0625		Y	2	1.50	0.43	7.48	3.16	63,521	19,342	306,881	137,248	4.83	0.052
CTL0644		N	3	3.60	0.26	5.60	1.15	227,126	16,475	342,170	69,447	1.51	0.135
CTL0659	<i>lpxK</i>	N	1	NQ	NQ	NQ	NQ	9,892	1,019	29,171	4,579	2.95	0.016
CTL0660	<i>yjfH</i>	N	3	9.53	0.93	21.44	3.95	602,217	58,331	1,307,945	221,300	2.17	0.043
CTL0663	<i>nrdR</i>	N	1	NQ	NQ	NQ	NQ	18,230	2,453	48,787	5,417	2.68	0.015

434/Bu	Gene Name	Predicted Sec Signal Peptide (Y/N)	Peptide Matches	WT Mean (fmol/ug)	WT SD	RSTE4 Mean (fmol/ug)	RSTE4 SD	WT Mean (Intensity)	WT SD	RSTE4 Mean (Intensity)	RSTE4 SD	Fold Change intensity (RSTE4/WT)	P-value
CTL0685		N	1	NQ	NQ	NQ	NQ	10,455	1,896	26,113	4,860	2.50	0.035
CTL0708a	<i>secD/secE</i>	N	5	1.05	0.16	3.41	0.76	88,556	9,964	253,586	58,942	2.86	0.055
CTL0730	<i>recO</i>	N	1	NQ	NQ	NQ	NQ	23,793	2,203	167,132	78,798	7.02	0.084
CTL0731		N*	1	NQ	NQ	NQ	NQ	304	176	2,334	1,128	7.68	0.057
CTL0737		Y	1	NQ	NQ	NQ	NQ	23,889	5,864	95,898	22,010	4.01	0.026
CTL0797	<i>yciA</i>	N	1	NQ	NQ	NQ	NQ	634	418	1,164	241	1.84	0.368
CTL0803	<i>mip</i>	Y	17	25.03	1.04	37.17	1.22	2,312,386	66,213	3,374,981	103,514	1.46	0.009
CTL0809		Y	2	3.54	0.23	5.38	1.03	149,135	9,664	219,156	40,786	1.47	0.135
CTL0832	<i>gspG</i>	N*	2	3.06	0.25	5.47	0.31	128,898	9,781	222,868	11,376	1.73	0.015
CTL0835	<i>gspD</i>	N	2	0.37	0.06	1.32	0.17	15,770	2,820	53,763	7,250	3.41	0.015
CTL0845	<i>minD</i>	N	6	3.50	0.43	7.76	0.91	317,015	19,833	642,968	23,100	2.03	0.011
CTL0863	<i>pal</i>	Y	4	12.15	9.32	27.22	4.73	796,184	599,131	1,727,083	318,171	2.17	0.241
CTL0877	<i>folP</i>	N	6	1.79	0.12	7.80	0.25	154,134	7,944	670,648	36,409	4.35	0.002
CTL0882		N	3	1.12	0.16	2.01	0.18	70,851	11,379	123,019	11,066	1.74	0.065
CTL0883		N	7	4.29	0.25	6.65	0.42	407,433	33,049	615,400	45,927	1.51	0.029
CTL0891		N	4	1.03	0.07	3.13	0.40	66,096	3,942	195,338	20,191	2.96	0.012

434/Bu	Gene Name	Predicted Sec Signal Peptide (Y/N)	Peptide Matches	WT Mean (fmol/ug)	WT SD	RSTE4 Mean (fmol/ug)	RSTE4 SD	WT Mean (Intensity)	WT SD	RSTE4 Mean (Intensity)	RSTE4 SD	Fold Change intensity (RSTE4/WT)	P-value
pL2-03	<i>pORF3/pCT1</i>		17	13.08	1.19	15.56	0.96	1,079,417	77,659	1,662,256	148,367	1.54	0.031
pL2-08			1	NQ	NQ	NQ	NQ	78,802	7,252	189,477	33,766	2.40	0.035

NQ: Not quantified -- only one peptide was found to match

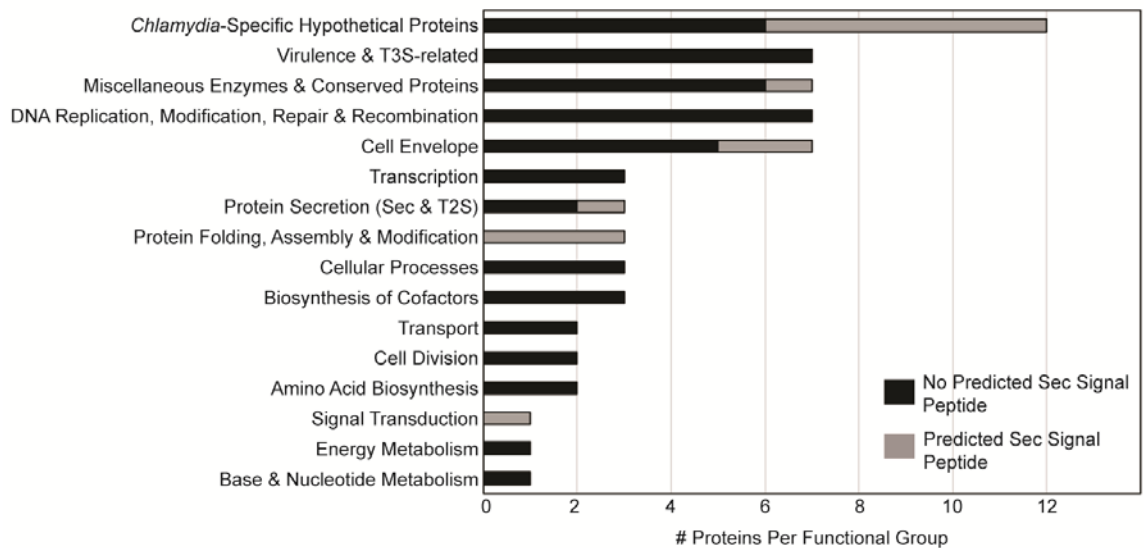


Figure 22: Functional grouping of proteins accumulated in RSTE4 EBs. Based on the mass spectrometry analysis, proteins accumulated greater than 1.5-fold in RSTE4 EBs were classified into functional categories. The presence of a predicted signal peptide, as determined by SignalP, was assessed for each accumulated protein; the number of proteins within a group with a predicted signal sequence is indicated by the gray bar. The most abundant functional group, *Chlamydia*-specific hypothetical proteins, also contains the largest proportion of proteins predicted to translocate to the bacterial periplasm.

3.6 Identifying candidate substrates of the type II secretion system

In *Chlamydia*, proteins secreted by the T2SS are first transported across the inner membrane using the Sec translocase system. Cleavable signal peptides present at the amino-terminal end of T2S substrates allow for targeting to Sec machinery [39]. Computational prediction programs, such as SignalP, identify potential Sec signal sequences [284]. The neural networks behind SignalP generate three different output scores (C-score, Y-score, and S-score) for every position in the input sequence. The C-score helps to distinguish between signal peptide cleavage sites and everything else; the C-max is trained to be highest at the first residue of the mature protein. The S-score differentiates positions within the signal peptide from proteins without signal peptides

and from positions in the mature protein. The Y-score combines the information from the S-score and C-score to predict the cleavage site; the Y-score is the highest immediately after the cleavage site. The final discrimination score (D) uses the Smean and Ymax scores to discriminate signal peptides from non-signal peptides [42, 43, 284]. Using SignalP v3.0, we identified over 60 proteins within the *C. trachomatis* proteome predicted to contain Sec signal peptides (Table 9).

Table 9: *C. trachomatis* proteins predicted to contain Sec signal peptides using SignalP v3.0

434/BU	CMAX	POS	YMAX	POS	SMAX	POS	SMEAN	D	SIGNAL PEPTIDE
CTL0015	0.469	24	0.494	24	0.759	3	0.591	0.53	Y
CTL0016	0.498	23	0.442	23	0.653	2	0.467	0.451	Y
CTL0023	0.468	26	0.476	26	0.57	22	0.461	0.47	Y
CTL0050	0.674	23	0.792	23	0.978	12	0.937	0.861	Y
CTL0082	0.486	27	0.645	27	0.95	17	0.866	0.749	Y
CTL0102	0.64	25	0.715	25	0.911	8	0.841	0.775	Y
CTL0103	0.262	30	0.461	28	0.96	11	0.885	0.66	Y
CTL0110	0.49	21	0.624	21	0.875	11	0.753	0.672	Y
CTL0149	0.618	23	0.715	23	0.935	3	0.864	0.785	Y
CTL0152	0.683	34	0.716	34	0.93	16	0.771	0.742	Y
CTL0163	0.491	23	0.69	23	0.987	20	0.957	0.815	Y
CTL0164	0.341	22	0.507	22	0.904	9	0.803	0.646	Y
CTL0175	0.403	36	0.544	36	0.957	33	0.47	0.509	Y
CTL0183	0.456	31	0.597	31	0.917	29	0.675	0.633	Y
CTL0195	0.159	17	0.37	17	0.905	4	0.865	0.603	Y
CTL0233	0.334	24	0.413	24	0.9	1	0.616	0.508	Y
CTL0248	0.554	19	0.569	19	0.784	1	0.6	0.584	Y
CTL0249	0.553	26	0.653	26	0.907	8	0.818	0.73	Y
CTL0250	0.339	28	0.464	28	0.855	3	0.715	0.582	Y
CTL0251	0.232	25	0.448	25	0.96	20	0.852	0.638	Y
CTL0254	0.21	25	0.392	25	0.85	19	0.745	0.558	Y
CTL0297	0.295	23	0.412	23	0.812	2	0.628	0.514	Y
CTL0323	0.225	34	0.396	34	0.949	23	0.82	0.595	Y
CTL0329	0.581	20	0.732	20	0.966	18	0.909	0.815	Y
CTL0333	0.264	25	0.458	22	0.906	17	0.828	0.632	Y
CTL0339	0.351	34	0.446	34	0.965	17	0.787	0.606	Y

434/BU	CMAX	POS	YMAX	POS	SMAX	POS	SMEAN	D	SIGNAL PEPTIDE
CTL0404	0.788	19	0.854	19	0.945	18	0.916	0.883	Y
CTL0427	0.206	28	0.327	28	0.849	3	0.631	0.47	Y
CTL0433	0.329	27	0.448	27	0.9	14	0.746	0.588	Y
CTL0450	0.201	26	0.375	23	0.932	15	0.841	0.594	Y
CTL0493	0.486	27	0.662	27	0.965	21	0.908	0.778	Y
CTL0494	0.836	20	0.887	20	0.973	10	0.938	0.911	Y
CTL0505	0.23	24	0.442	24	0.971	11	0.892	0.654	Y
CTL0536	0.507	24	0.656	24	0.949	13	0.883	0.763	Y
CTL0563	0.369	23	0.492	23	0.891	11	0.744	0.61	Y
CTL0604	0.42	19	0.555	19	0.921	17	0.746	0.645	Y
CTL0625	0.482	19	0.619	19	0.89	15	0.773	0.692	Y
CTL0636	0.161	23	0.374	23	0.957	5	0.902	0.622	Y
CTL0645	0.507	25	0.647	25	0.932	19	0.824	0.73	Y
CTL0670	0.19	22	0.382	12	0.931	4	0.887	0.619	Y
CTL0671	0.269	21	0.461	21	0.906	1	0.816	0.628	Y
CTL0672	0.362	19	0.499	19	0.807	14	0.657	0.573	Y
CTL0674	0.265	22	0.397	22	0.712	14	0.56	0.457	Y
CTL0700	0.439	22	0.596	22	0.93	18	0.85	0.715	Y
CTL0703	0.163	21	0.368	21	0.927	1	0.857	0.598	Y
CTL0704	0.203	22	0.329	22	0.863	1	0.61	0.461	Y
CTL0714	0.231	20	0.381	20	0.749	11	0.628	0.497	Y
CTL0725	0.164	22	0.35	18	0.904	14	0.858	0.589	Y
CTL0737	0.532	19	0.685	19	0.943	18	0.873	0.773	Y
CTL0803	0.152	31	0.325	20	0.889	1	0.828	0.561	Y
CTL0809	0.638	21	0.742	21	0.954	17	0.86	0.797	Y
CTL0813	0.809	26	0.836	26	0.983	11	0.909	0.87	Y
CTL0814	0.42	24	0.591	24	0.957	12	0.855	0.715	Y
CTL0822	0.354	22	0.573	22	0.964	18	0.936	0.744	Y
CTL0825	0.808	22	0.891	22	0.992	13	0.958	0.922	Y
CTL0829	0.369	22	0.472	22	0.847	3	0.686	0.572	Y
CTL0836	0.456	31	0.441	31	0.807	11	0.567	0.5	Y
CTL0859	0.324	22	0.455	22	0.827	17	0.651	0.547	Y
CTL0862	0.497	25	0.619	25	0.941	2	0.804	0.706	Y
CTL0863	0.244	23	0.437	23	0.945	3	0.844	0.628	Y
CTL0864	0.672	21	0.721	21	0.846	17	0.749	0.734	Y
CTL0868	0.588	21	0.544	21	0.647	18	0.527	0.537	Y
CTL0887	0.472	26	0.652	26	0.973	15	0.907	0.772	Y
CTL0019	0.163	22	0.273	20	0.69	1	0.491	0.354	N*
CTL0061	0.197	22	0.244	22	0.399	18	0.296	0.263	N*

434/BU	CMAX	POS	YMAX	POS	SMAX	POS	SMEAN	D	SIGNAL PEPTIDE
CTL0069	0.17	24	0.175	17	0.443	1	0.234	0.197	N*
CTL0083	0.23	19	0.239	19	0.341	17	0.242	0.24	N*
CTL0113	0.154	24	0.215	24	0.396	22	0.264	0.233	N*
CTL0114	0.15	63	0.14	11	0.312	1	0.185	0.156	N*
CTL0128	0.172	29	0.275	29	0.611	18	0.467	0.346	N*
CTL0129	0.305	27	0.261	27	0.37	12	0.27	0.264	N*
CTL0156	0.224	28	0.17	28	0.298	4	0.172	0.171	N*
CTL0189	0.198	24	0.272	24	0.53	18	0.396	0.318	N*
CTL0226	0.124	18	0.222	18	0.485	16	0.38	0.28	N*
CTL0227	0.194	25	0.193	25	0.265	4	0.2	0.196	N*
CTL0232	0.112	21	0.142	11	0.33	1	0.19	0.16	N*
CTL0262	0.198	23	0.29	23	0.588	1	0.448	0.364	N*
CTL0272	0.162	17	0.259	13	0.62	9	0.47	0.358	N*
CTL0328	0.128	31	0.129	31	0.2	19	0.118	0.125	N*
CTL0369	0.288	18	0.293	18	0.474	13	0.299	0.296	N*
CTL0394	0.12	22	0.206	22	0.512	5	0.395	0.276	N*
CTL0435	0.128	27	0.232	18	0.602	9	0.474	0.346	N*
CTL0456	0.129	27	0.17	11	0.414	1	0.28	0.211	N*
CTL0503	0.151	27	0.24	11	0.723	2	0.577	0.364	N*
CTL0508	0.222	27	0.19	27	0.307	34	0.178	0.186	N*
CTL0509	0.206	30	0.174	30	0.205	23	0.15	0.165	N*
CTL0515	0.233	15	0.299	15	0.505	8	0.369	0.332	N*
CTL0520	0.358	50	0.405	50	0.657	45	0.262	0.352	N*
CTL0523	0.141	25	0.237	25	0.641	2	0.421	0.305	N*
CTL0555	0.211	48	0.257	48	0.418	30	0.229	0.247	N*
CTL0556	0.202	24	0.256	24	0.407	25	0.312	0.277	N*
CTL0605	0.143	22	0.257	22	0.733	1	0.514	0.378	N*
CTL0606	0.186	26	0.186	26	0.317	25	0.147	0.171	N*
CTL0609	0.261	25	0.28	25	0.434	21	0.325	0.296	N*
CTL0614	0.228	24	0.238	24	0.615	5	0.371	0.287	N*
CTL0617	0.12	42	0.189	20	0.404	19	0.306	0.244	N*
CTL0647	0.124	29	0.236	11	0.686	1	0.567	0.358	N*
CTL0658	0.131	29	0.113	11	0.157	3	0.133	0.121	N*
CTL0665	0.191	40	0.166	11	0.496	1	0.256	0.2	N*
CTL0682	0.227	24	0.269	24	0.435	20	0.251	0.262	N*
CTL0721	0.136	26	0.163	17	0.395	1	0.251	0.196	N*
CTL0731	0.301	28	0.346	28	0.505	27	0.322	0.337	N*
CTL0741	0.212	26	0.181	26	0.235	20	0.148	0.168	N*
CTL0754	0.188	19	0.242	19	0.606	15	0.328	0.283	N*

434/BU	C MAX	POS	Y MAX	POS	S MAX	POS	S MEAN	D	SIGNAL PEPTIDE
CTL0755	0.171	40	0.229	11	0.628	9	0.55	0.348	N*
CTL0757	0.103	21	0.167	11	0.414	2	0.28	0.209	N*
CTL0758	0.117	26	0.108	46	0.146	25	0.094	0.103	N*
CTL0796	0.197	19	0.307	19	0.608	17	0.447	0.359	N*
CTL0808	0.132	18	0.146	18	0.279	1	0.179	0.158	N*
CTL0810	0.19	20	0.289	20	0.615	3	0.475	0.358	N*
CTL0815	0.143	30	0.164	11	0.388	2	0.266	0.212	N*
CTL0832	0.353	17	0.25	17	0.257	16	0.183	0.225	N*
CTL0843	0.173	44	0.216	11	0.53	7	0.485	0.316	N*
CTL0852	0.483	35	0.311	35	0.393	3	0.196	0.269	N*

*Signal peptide predicted using eukaryotes organism group, but not Gram-negative organism group; bold indicates cleavage site correlation between C-score and Y-score

Using this information, we narrowed the list of proteins accumulated in RSTE4 EBs to those we predicted contain signal peptides to generate a list of T2S candidate proteins (Figure 22, Table 9). Below is a summary of any previous studies or bioinformatical analyses available that may lend insight into the potential functions of some of the proteins on the list of T2S candidate substrates.

CTL0102/ CT733: Predicted to be a putative lipoprotein with C-terminal region resembling known peroxidases and catalases. Previous studies in *C. trachomatis* identified CT733 in a screen for antibody-inducing antigens using sera from *C. trachomatis* infected patients [285].

Table 10: T2S candidate substrates

434/Bu	UW-3/CX	Gene Name	Peptide Matches	Fold Change intensity (RSTE4/WT)	Fold Change $\mu\text{g}/\text{fmol}$ (RSTE4/WT)	P-value	PhoA Assay Results*
CTL0102	CT733		7	4.21	4.95	0.007	+
CTL0152	CT783		3	7.05	7.31	0.011	+
CTL0233	CT858	<i>cpa</i>	16	2.78	2.31	0.011	+
CTL0272	CT017	<i>ctad1</i>	9	1.59	1.44	0.076	+
CTL0297	CT041		3	3.50	3.62	0.029	+

CTL0505	CT253		1	2.70	ND	0.011	+
CTL0609	CT355		1	6.86	ND	0.013	+
CTL0625	CT371		2	4.83	4.98	0.052	+
CTL0731	CT471		1	7.68	ND	0.057	+
CTL0737	CT476		1	4.01	ND	0.026	+
CTL0803	CT541	<i>mip</i>	17	1.46	1.50	0.009	+
CTL0809	CT547		2	1.47	1.52	0.135	ND
CTL0863	CT600	<i>pal</i>	4	2.17	2.24	0.241	+

ND: not determined

* representative images of colonies in figure 22

CTL0152/ CT783: Predicted to encode a periplasmic disulfide bond isomerase that is known to be expressed at mid-late stages of infection [274]. Second most accumulated in protein in RSTE4 EBs. CTL0149, a reducing disulfide oxidoreductase with only weak isomerase activity [286], is decreased by 1.8-fold in RSTE4 EBs.

CTL0272/ Ctdad1: Recently identified as a *C. trachomatis* adhesion and invasion; binds to integrin β 1 subunit using two N-terminal bacterial SH3 domains [283].

CTL0297/ CT041: Predicted SpoIID domain from AA123-218. SpoIID is a cell wall hydrolase necessary for sporulation and endospore formation in *Bacillus subtilis*; it degrades the glycan strands of the peptidoglycan into disaccharide units [287].

CTL0609/ CT355: PSI-Blast shows similarity to peptidyl-prolyl-isomerases and SurA domain containing proteins; possible periplasmic chaperone.

CTL0625/ CT371: May belong to an operon that contains the coding sequences required for several of the chorismate biosynthesis enzymes. Possible flavin reductase.

CTL0803/ CT541: Mip or machophage infectivity potentiator is a well conserved, surface-associated lipoprotein that has peptidylproline *cis*-*trans*-isomerase (PPIase) activity [288-292]. Its localization to the surface has been described in both *C. trachomatis* (EBs) and *L.pneumophila* [100, 293, 294]. *L. pneumophila* strains containing mutations in Mip had a 40-70% reduction in T2S-dependent phospholipase C activity

[100]. It remains unclear if Mip acts on the T2SS or the exoprotein to promote PLC activity.

CTL0863/ CT600: Peptidoglycan associated lipoprotein (Pal) is an outer membrane anchored protein that faces the periplasm but has subpopulations that are present on the bacterial surface [295]. In *C. trachomatis*, the Tol-Pal system consists of tolQ/tolR/CT598/tolB/pal/CT601/CT602, which are likely in an operon. This system has been suggested to maintain the integrity and stability of the outer membrane and be important for cell division. However, Pal is released into the blood from the bacterial surface in both an infected wound model of monomicrobial sepsis in rats and in a polymicrobial sepsis model in mice [296]. The only other protein from this system present in the proteomics dataset is TolB, whose levels do not change between WT and RSTE4 EBs.

The information from Signal P suggests the signal peptide is cleaved between AA22 and AA23, however Pal identified in the *Chlamydia* outer membrane complex (COMC) fractions of EB contains highly conserved cysteine AA22 and serine AA23 residues that are typically lipidated prior to outer membrane insertion [231]. It is likely that the cleavage site is instead between AA 20 and AA21.

3.6.1 Using an alkaline phosphatase secretion assay to assess if predicted *Chlamydia* Sec signal sequences can drive secretion in *E. coli*

To assess if the signal sequences of the T2S candidate substrates are sufficient for translocation into the bacterial periplasm, we used an *E. coli* based *phoA* gene fusion system. PhoA is an alkaline phosphatase that in the reducing environment of the bacterial cytosol is inactive. However, upon translocation to the oxidizing environment of the periplasm, this protein becomes active and can act on the chromogenic substrate

BCIP, turning the bacteria blue [157, 158, 163, 297]. We fused the N-terminal region containing the predicted signal sequences of the candidate substrates to the C-terminus of PhoA lacking the necessary signal peptide. The PhoA fusion constructs were transformed into an *E. coli* strain (KS272) from which *phoA* has been deleted. The N-terminal region of the T3 substrate, CTL0063 (CT694), functions as a negative control. Of the candidate *C. trachomatis* T2S substrates tested, 11 possessed signal peptides sufficient for periplasmic translocation of PhoA in *E. coli* (Table 10, Fig. 22,23).

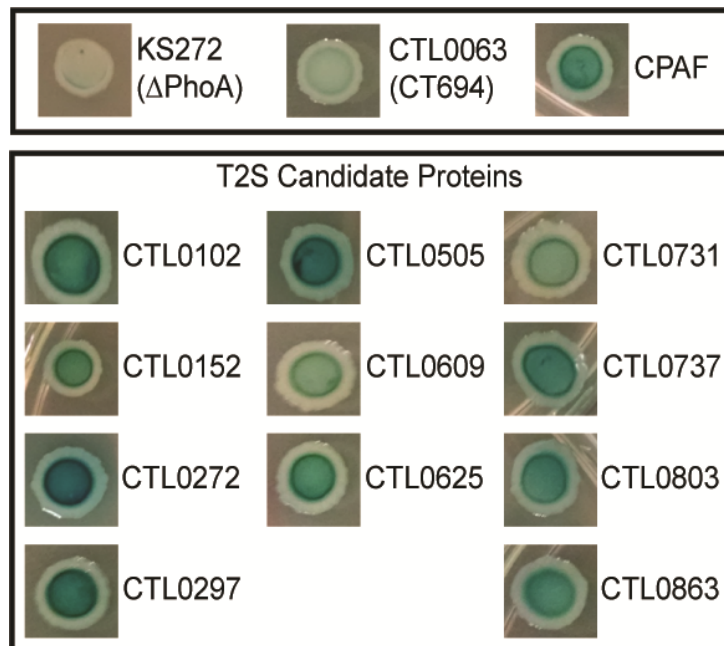


Figure 23: Putative N-terminal signal peptides of T2S candidate substrates are sufficient for translocation of PhoA into the bacterial periplasm. Constructs were made by fusing the predicted signal sequences from the indicated proteins to a truncated PhoA that lacks the signal sequence, followed by transformation into an *E. coli* strain lacking endogenous PhoA. Transformed bacteria were incubated on agar plates containing BCIP. Signal sequences sufficient for Sec mediated PhoA translocation into the bacterial periplasm will result in blue colonies.

3.7 Localization of T2S candidate substrates during infection

We next assessed the localization of candidate substrates during infection in various *C. trachomatis* strains. The *C. trachomatis* strains used for localization analyses

are: L2 (WT), RSTE4, RSTE4^{pGspE}, M380 (*glgB* null mutant), M540 (*glgA* G309S mutant) and a plasmidless strain L2 25667R, referred to as L2R. The CTL2 mutant strain containing a nonsense mutation in *glgB* (M380) controls for any impact on localization caused by glycogen granules within inclusion. The L2 25667R strain is a clinical L2 isolate that lacks the 7.5 Kb plasmid [194]. We have shown this strain, as compared to WT, has a 2-fold or 10-fold reduction in the amount of glycogen during infection in Hela Cas 9 or Gys1KO cells, respectively (Fig. 16B). Finally, in our library of *C. trachomatis* mutants, a strain that contains a mutation in GlgA at amino acid 309 was isolated and characterized to produce up to 2.5-fold less glycogen during infection (Fig. 16B).

We hypothesized a substrate of the T2SS would be localized outside of the bacteria during infection with WT or RSTE4^{pGspE} strains, but would remain associated with the bacteria in the T2S-mutant. Our collaborator, Dr. Guangming Zhong, raised polyclonal mouse antibodies against most proteins from *C. trachomatis* Serovar D, including T2S candidate effector proteins. Antibodies were validated by expressing recombinant *C. trachomatis* His-tagged proteins in *E. coli* (data not shown). Based on the immunoblot validation analyses, six antibodies were used for further immunofluorescence studies.

3.7.1 CT017/Ctad1 and CT783 localize to *C. trachomatis* in infected cells

Using the antibodies described above, the location of CT017/Ctad1 and CT783 during infection was assessed (Fig. 24). While recent studies suggest Ctad1 is an adhesion and invasion factor localized to the cell surface [283], some surface associated outer membrane proteins in other bacteria require the T2SS for proper localization [138]. CT017/Ctad1 was not seen to localize outside of the bacteria after infection with wild

type, T2S mutant or glycogen-deficient strains. However, this does not mean Ctd1 localization is not dependent on T2S; immunofluorescence is not the ideal assay to discriminate between OM or periplasmic localization. The localization of the *C. trachomatis* protein Mip to the EB surface was determined using EB surface biotinylation or surface immunoprecipitation techniques [231, 293].

CTL0152/ CT783, the second most accumulated protein in RSTE4 EBs, also did not localize outside of the bacteria during infection with any of the *C. trachomatis* strains tested; the signal detected from CTL0152/ CT783 always overlaps with the bacterial marker Slc1, a T3S chaperone (Fig. 24). This study suggests CT783 is not secreted by the T2SS. Nonetheless, it may still play a role in secretion of other substrates. In *Pseudomonas*, *Vibrio*, *E. coli*, and *Klebsiella*, disulfide-bond formation is required for the folding, secretion, or activity of T2 substrates [81, 83, 86, 298]. I propose CT783 is functioning as a chaperone to ensure the proper folding of T2S substrates, and its increase in RSTE4 bacteria is a result of substrates accumulating in the periplasm. The construction of CT783 mutant strains using the TargeTron system or the use of the CTL2 mutant library, which contains three strains with predicted non-neutral amino acid substitutions in CT783, will be useful for future investigations to explore this hypothesis [172].

3.7.2 *C. trachomatis* proteins localize to glycogen during infection

A subset of T2S candidate substrates we analyzed localized to glycogen granules that accumulate in RSTE4 infected cells (white arrows, Fig. 25). This localization is not specific to RSTE4, as the substrates were also converged near granules during infections with M380 (*glgB* mutant). For each of these four proteins, CT041, CT355, CT600/Pal, and CT733, Z-stacks were generated. By incrementally

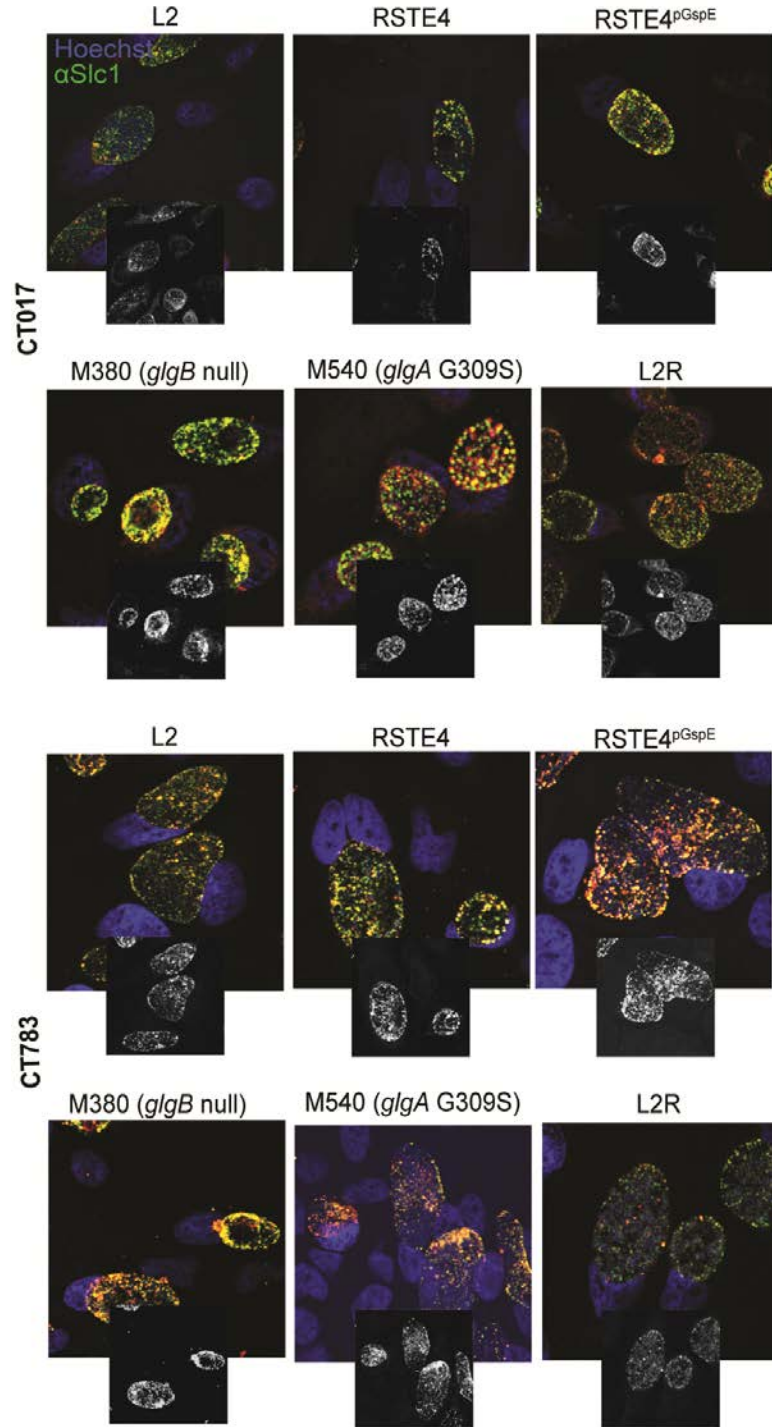


Figure 24: CT783 and CT017 localize prominently to the bacteria during *C. trachomatis* infection. HeLa cells were infected with the indicated strains at an MOI=1 for 48 h and substrate localization visualized using immunofluorescence with specific

antibodies. The insets are the single channels for the substrate only. Tested putative T2S substrate-red; DNA-blue; *Chlamydia*-green.

moving through the focal plane, we were able to determine the localization of the candidate substrate and the bacteria; this ensured candidate protein localization to the granule was not due to an increase in the concentration of bacteria present around the granule (data not shown).

During WT and RSTE4^{pGspE} infections, CT041 does not co-localize with bacteria and is found near the edges of the inclusion. In contrast, inside the inclusion CT355 and CT600/Pal appear to aggregate into large and small clusters, respectively, but show little association with bacteria during infection. However, bacteria are seen to contain CT355 during RSTE4 infection, consistent with the greater than 6-fold increase in EBs isolated from this stain (Table 10). CT733 localizes to both the bacteria and various sized aggregates inside the inclusion in WT and RSTE4^{pGspE} infected cells.

During infection with WT *Chlamydia*, CT355, CT600, and CT733 display areas of extra-bacterial substrate clustering within the inclusion lumen (yellow arrows, Fig. 26). To a lesser extent this accumulation can be seen in cells infected with RSTE4^{pGspE} bacteria. We hypothesized substrates localize to glycogen during infection and are drawn towards granules because of the large quantity of glycogen present. To investigate our hypothesis, we infected cells with two *C. trachomatis* strains (L2R and M540) that produce less glycogen during infection (Fig. 16B).

The localization of CT041 within infected cells does not change in response to glycogen levels within the inclusion lumen. Intriguingly, the aggregation of CT355, CT600, and CT733 in the inclusion lumen during WT infection is not seen during infection with either the plasmidless L2R or *gIa* M540 mutant strain; instead the signal appears to be dispersed throughout the inclusion. This implies the localization of a

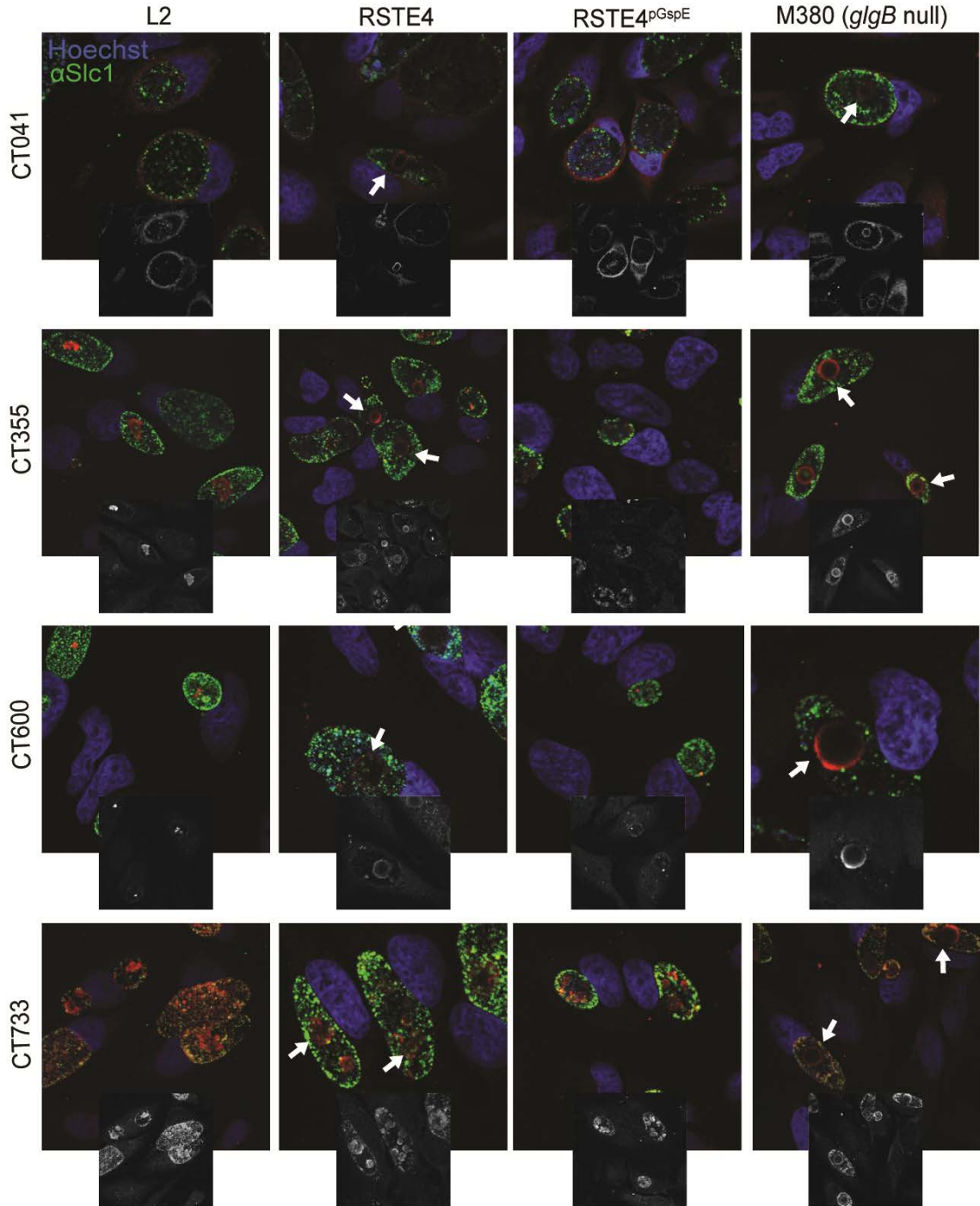


Figure 25: A subset of proteins are localized to glycogen granules during infection with RSTE4 or *glgB* *C. trachomatis* mutants. HeLa cells were infected with the indicated strains at an MOI=1 for 48 h and substrate localization visualized using immunofluorescence with specific antibodies. Glycogen granules present within RSTE4 and *glgB* mutant infected cells are indicated with white arrows. The insets are the single

channels for the substrate only. Tested T2S candidate substrate-red; DNA-blue; *Chlamydia*-green.

subset of proteins differs under conditions where varying amount of glycogen are present within the inclusion lumen (Fig. 26). We hypothesize glycogen plays a role to ensure the proper localization of these proteins during *C. trachomatis* infection.

3.7.3 CPAF expression levels are responsive to glycogen

The potential link between glycogen metabolism and the regulation of secreted proteins correlates with observations our group and others have made regarding CPAF expression levels in the L2R strain (Fig. 27A, bottom row) [191]. Using high-density microarrays, the Caldwell laboratory identified differentially expressed genes at 24hpi in L2 and L2R infected McCoy cells. The transcript levels of *cpa* were increased 2-fold in the plasmidless strain [191]. The increase in *cpa* transcript correlates to a rise in CPAF protein levels during L2R infection (Fig. 27C). This increase appears as early as 12hpi (Fig. 27C). Additionally, immunofluorescence experiments showed enhanced CPAF protein present in the host cytosol of L2R infected cells (Fig. 27A).

As multiple chromosomal genes are regulated by the plasmid, we assessed the contribution of glycogen to the increase in CPAF protein expression by immunoblot and immunofluorescence analyses during infection with the *glgA* M540 mutant strain (Fig. 27A-B). We found CPAF protein levels are increased in cells infected with M540, further supporting the connection between T2S and glycogen metabolism.

3.8 *C. trachomatis* lytic exit is dependent on glycogen

Our work has shown mutations in the T2SS of *C. trachomatis* delay lytic exit from host cell (Fig. 17C). Work by Yang and colleagues implicates both the *Chlamydia* plasmid and CPAF in the regulation of lytic exit [299]. We wanted to evaluate the

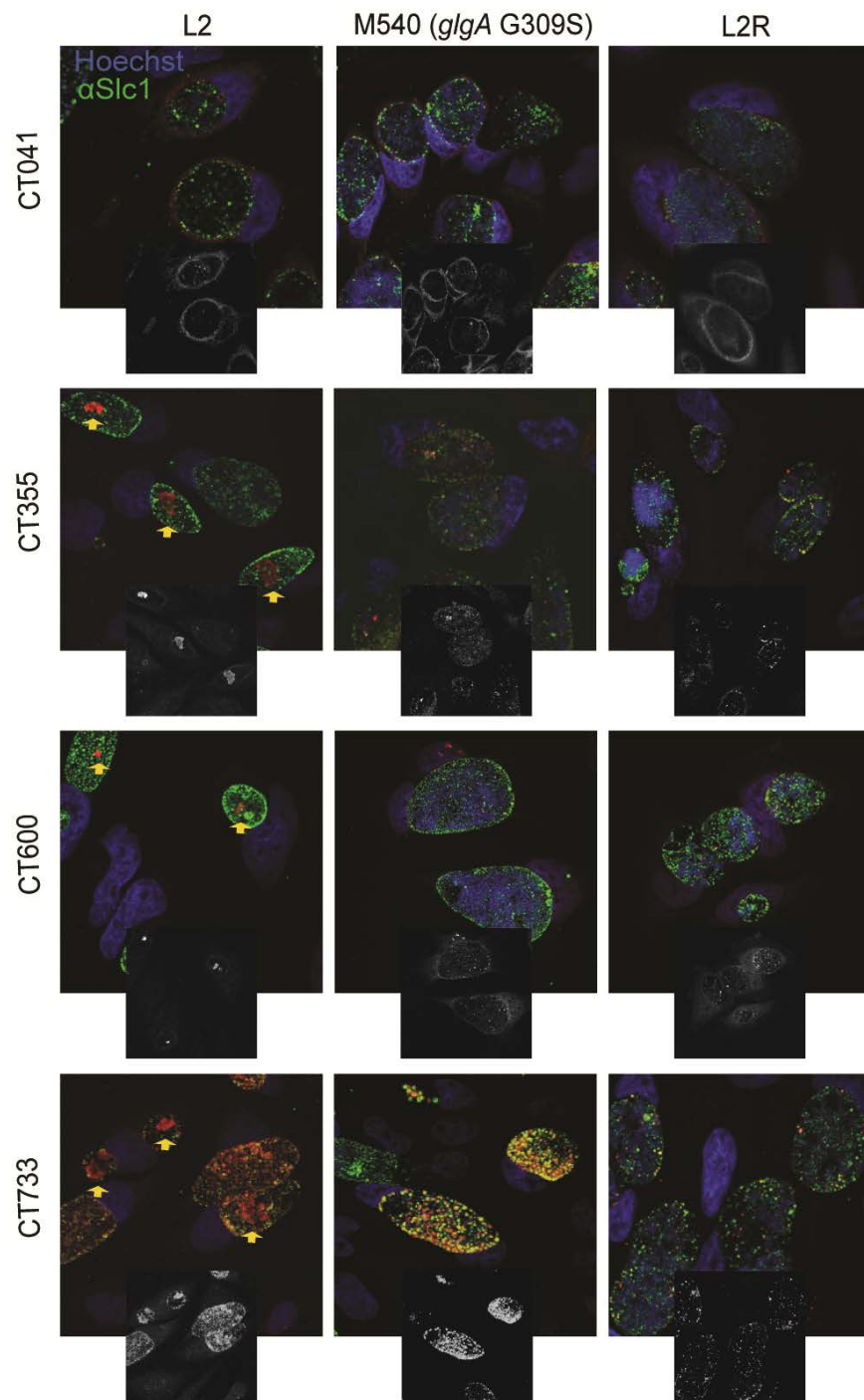


Figure 26: Localization of CT733, CT600, and CT355 within the inclusion is dependent on the presence of glycogen. . HeLa cells were infected with the indicated strains at an MOI=1 for 48 h and substrate localization visualized using immunofluorescence with specific antibodies. Aggregates present within the inclusion lumen of WT infected cells are indicated with yellow arrows. The insets are the single

channels for the substrate only. Tested candidate T2S substrate-red; DNA-blue; *Chlamydia*-green.

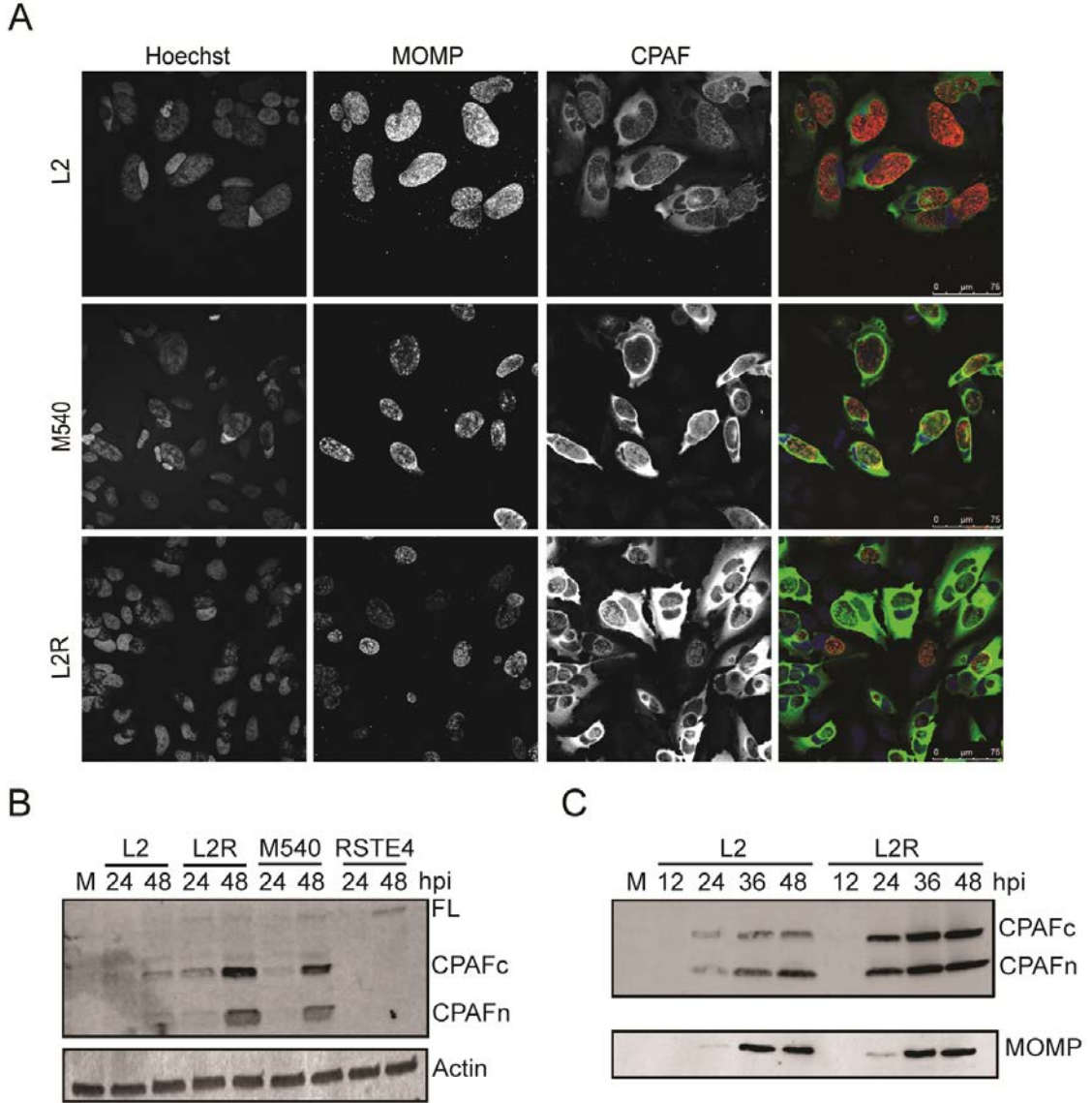


Figure 27: CPAF expression is increased in strains with reduced levels of glycogen. A) HeLa cells were infected with L2, L2R, or the *glgA* mutant M540 for 36 hours. Cells were stained with anti-MOMP (red), anti-CPAF (green), or Hoechst for DNA (blue). Images were taken using the exact same exposure/ acquisition settings on a Leica SP5 confocal microscope. B) Immunoblot analysis of CPAF protein harvested from cells infected at an MOI=1 for 24 or 48 hours. Compared to WT (L2) infection, more processed CPAF is present during infection with the L2R and M540 strains. C) Time course of infection with L2 and L2R strains showing an increase in CPAF protein levels in the plasmidless strain (starting at 12hpi), despite similar levels of the bacterial control MOMP.

contribution of glycogen to this process. We tested the ability of L2R and M540 mutants to exit the host cell by monitoring infected monolayers for lysis (Fig. 28). Analogous to observations by Yang et al., cells infected with L2R did not begin to lyse until after 80 hpi, with lysis of majority of cells by 120 hpi (Fig. 28, top panel). Infection with the M540 mutant paralleled observations with L2R, demonstrating glycogen synthesis and/or the accumulation of glycogen in the inclusion lumen plays a role in the regulation of lytic exit (Fig. 28, bottom panel).

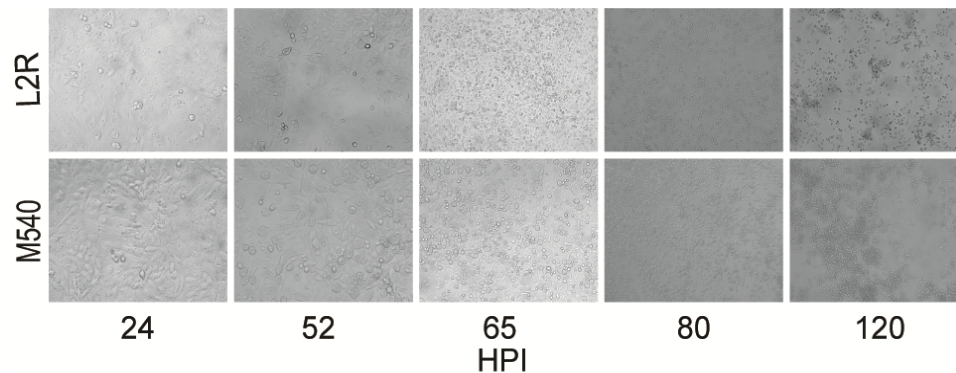


Figure 28: Glcogen synthesis regulates lytic exit. HeLa cells were infected with the specified strains and lysis of infected monolayers was monitored at the indicated times. Infection with the *glgA* mutant, M540, delayed lytic exit from the host cell.

3.9 Discussion

In this work we describe a mutation in GspE, the T2S ATPase of *C. trachomatis*, that impacts attachment to host cells, intracellular growth, the properties of glycogen, and bacterial exit. While we do not know how the G425E mutation influences GspE structure or function, partial rescue of these phenotypes can be accomplished by expressing full length GspE in the RSTE4 background. In complemented cells, individual GspE hexamer complexes may be composed of solely WT or mutant GspE or there may be a mixture of the two types of protein in each hexamer [300]. We postulate in either

scenario efficiency of secretion is reduced, resulting in partial complementation.

One of the more intriguing phenotypes of the RSTE4 mutant is the accumulation of glycogen granules within the inclusion lumen. When this observation was first made, we hypothesized a T2-dependent glycogen hydrolase failed to be secreted during RSTE4 infection [152]. Work by Gehre and colleagues supports secretion of GlgA, GlgB, GlgX, GlgP, and MrsA into the inclusion lumen via the T3SS, not T2 [186]. However, other studies suggest an interplay between the T2 and T3 secretion systems occurs in *Chlamydia*. Previous work in our laboratory implicates CPAF in the cleavage of early T3 effectors including CT005, IncC, and IncD [301]. Recent studies using the Rst5 (CPAF+) and Rst17 (CPAF-) strains further identified 7 midcycle T3S effectors that were lower in abundance in Rst5 infected lysates [219]. Additionally, the T2 and T3 secretion systems interact in other pathogens. In *Xanthomonas campestris* pv *vesicatoria* (*Xcv*) the T2SS promotes translocation of T3 effectors. The authors speculate degradative T2 enzymes may facilitate the assembly of extracellular components of the T3SS during infection in leaves [90]. We propose a T2S-dependent protein promotes the activity of one of the enzymes in the glycogen biosynthesis pathway. Loss of function of GlgB results in the aggregation of insoluble linear glycogen [152]; a similar phenotype would result during RSTE4 infection if a T2S substrate cannot act on GlgP or GlgB. However, we cannot rule out the possibility that the expression or translocation of GlgB is altered during RSTE4 infection, resulting in the accumulation of granules.

Due to glycogen granules co-purifying with EBs during the gradient purification process, we identified proteins associated with glycogen granules in our RSTE4 proteomics dataset (data not shown). CT355 accumulates within RSTE4 bacteria and near glycogen granules during infection (Fig. 25). However, CT041, CT600, and CT733

only localize to granules, not the bacteria. These proteins may not be secreted by the T2SS; localization to the inclusion lumen could occur via OMVs. T2S and OMVs are not mutually exclusive; studies in *V. cholerae* have shown certain T2S substrates are also present in OMVs [302-304]. OMVs carry periplasmic proteins, membrane proteins, and even nonprotein molecules such as LPS and RNA, away from the bacteria [129, 262, 302, 303, 305, 306]. Additionally, OMVs increase when misfolded proteins accumulate in the periplasm [267]. Future studies are needed to assess OMV production and their contents RSTE4 infected cells.

The function of glycogen within the inclusion during *Chlamydia* infection is complex. One possibility is that glycogen inside the inclusion serves as an energy source for EBs during late stages of infection. This hypothesis is supported by very early work from Gordon and Quan that visualized glycogen within the vacuole of numerous *Chlamydia* isolates, including a *C. trachomatis* LGV strain [307]. Using iodine staining they observed relatively few iodine positive inclusions in infected McCoy cells after 4 days of infection. However, there is no quantification at these very late timepoints and it is noted at earlier timepoints there is variation in the depth of iodine staining. Gehre et al. propose the presence of glycogen degrading enzymes GlgX and GlgP, along with MrsA, within the inclusion aids in the generation of free Glc6P, which suggests glycogen is broken down in the inclusion. Additionally, glycogen storage in the inclusion lumen, as opposed to Glc1P or Glc6P storage, allows for maintenance of the osmotic pressure within the inclusion [186].

Glycogen may also contribute to bacterial survival after the inclusion leaves the host cell. *C. trachomatis* exits the host cell via two distinct pathways: lysis and extrusion [200]. During extrusion, a host-membrane encased compartment containing the

inclusion is pinched off, leaving the host cell intact [308]. Extrusions were recently observed to enhance the extracellular survival of *Chlamydia*; 74% of extrusion-derived EBs were viable 4 hours post extrusion compared to 40% of free EBs [309]. Within this transient extracellular niche, glycogen may be an important nutrient source that helps to maintain EB infectivity. Inclusions fated to escape the host via extrusion may need to accumulate more glycogen and could explain the variability of glycogen positive inclusions observed by Gordon and Quan at late stages of infection.

While glycogen may function as a nutrient source to EBs late during infection, it first begins to appear in the inclusion lumen 16-20 hpi, when the bacteria are predominantly RBs [186]. Our work shows there's a defined set of secreted proteins that associate with this polymer during infection and suggests glycogen functions in regulating proteins secreted into the inclusion lumen. Future studies will focus on how these secreted proteins, presumably in complexes with glycogen, contribute to regulating the interactions between *Chlamydia* and its host.

3.10 Materials and Methods

3.10.1 Reagents

Reagents were obtained from the following sources: rabbit anti-*Chlamydia* MOMP (K. Fields, U. of Kentucky), rabbit anti-Slc1 (Valdivia lab), mouse anti-CT017, anti-CT041, anti-CT355, anti-CT600, anti-CT733, and anti-CT783 (G. Zhong, U. of Texas Health and Science Center), mouse anti-LPS (GeneTex), mouse anti-EGFP monoclonal antibody (Clontech), rabbit anti-RpoB/C (M. Tan, UC Irvine), mouse anti-myc (Cell Signaling), rabbit anti-myc (Cell Signaling), anti-IncG (Valdivia Lab), rabbit anti-Tarp, rabbit anti-HtrA (W. Houston, University of Technology Sydney) anti-Gys1 (Cell Signaling), rabbit anti-CPAF (Valdivia lab), Alexa Fluor 555-conjugated anti-mouse,

Alexa Fluor 488-conjugated anti-rabbit, Alexa Fluor 633-conjugated anti-mouse, Hoescht 33258 (Invitrogen), FluorSave Reagent (Calbiochem), Bodipy TR C5 Ceramide (BODIPY TR), BCIP (Sigma), DC Protein Assay (BioRad), and Glycogen Assay Kit (Sigma-Aldrich).

3.9.2 Cell Culture and *Chlamydia* Infections

Cell culture and infections were performed as described in chapter 2, section 2.8.2, with the exception that A2EN cells were maintained in Keratinocyte-SFM supplemented with epidermal growth factor 1-53 and Bovine Pituitary Extract (ThermoFisher). The L2 strain lacking the plasmid, L2 25667R, was first isolated by the de la Maza laboratory [194]. Aside from the expansion of bacteria for elementary body purification, no cycloheximide was use in any of these experiments.

3.9.3 Identification of LGV-L2 mutant strains

Identification. LGV-L2 strain containing the null allele *W222** in *glgB* (CTL0245) and the SNV G309S in *glgA* (CTL0167) were initially identified by whole genome sequencing of a collection of ethyl methyl sulfonate (EMS)-mutagenized and plaque-purified *C. trachomatis* LVG-L2 434/Bu strains (generated as previously described [152, 172]. Strain CTL2-M380 harboring the *glgB* *W222** allele and strain CTL2-M540 harboring the *glgA* *G309S* allele were identified from two independent pools of 20 mutants by Sanger sequencing of each locus. Each strain was harvested from infected Vero cells grown in a 6-well cell culture plate by hypotonic lysis of host cells with 800 μ l of dH₂O per well (for 20 minutes) followed by addition of 200 μ l of 5X sucrose-phosphate-glutamate (SPG) buffer (0.22 M sucrose, 0.01 M potassium phosphate, 0.005 M L-glutamic acid, pH 7.0).

3.9.4 Western blot analyses

Western blot analyses were performed as described in chapter 2, section 2.8.6.

3.9.5 Bacterial growth assays

Vero cells were seeded onto 96 well plates (15,000 cells/well) and 24 h later were infected with each one of the strains analyzed (six biological replicates per time-point) with an MOI~0.6. For determining input IFUs, a separate set of wells was infected in identical conditions. For the calculation of input IFUs, cells infected for 24 hours were fixed with 100% Methanol (EMD Millipore) for 10 minutes on ice and stained with anti-LGV-L2 sera followed by Alexafluor-conjugated secondary antibodies (Invitrogen Life Technologies, Carlsbad, California, USA). Images were acquired in a Zeiss Axioskop 2 upright epifluorescence microscope, at least 5 different fields per replicate. Inclusions were counted by fluorescent microscopy. Input IFUs were very similar among the different strains. Harvesting of output IFUs was done at 48 hpi, as previously described (Nguyen and Valdivia, 2011), aliquoted and saved at -80C until IFU analysis. Output IFUs obtained were calculated by infecting serial dilutions of harvested seeds in Vero cells seeded onto 96 well plates. After 24-30 hpi, cells were fixed, stained, and counted (as previously indicated). To determine the infectious progeny generated per bacterium, total number of infected progeny released (output) was divided by the total number of infectious particles in the first sample (input).

3.9.6 Microscopy

Indirect immunofluorescence. HeLa cells were grown on glass coverslips and infected at the indicated MOI. Cells were fixed with 3% formaldehyde/0.025% glutaraldehyde in phosphate-buffered saline (PBS) for 20 min and permeabilized with 0.2% Triton X-100. After blocking with 5% bovine serum albumin (BSA)-PBS, cells were

stained with specific antibodies followed by Alexa-conjugated secondary antibodies ((Invitrogen Life Technologies, Carlsbad, California, USA) at room temperature. Host and bacterial DNA were stained with 1 μ M Hoechst in PBS (Invitrogen). Infected cells were imaged with a Zeiss AxioScope epifluorescence microscope and Axiovision v3.0 software or Leica DMI6000CS inverted confocal microscope and Leica LAS AF v2.6 software.

Periodic Acid Schiff stain. Formaldehyde/glutaraldehyde fixed infected cells were washed twice in 70% ethanol, followed by incubation in 1% periodic acid (Sigma) at room temperature. Cells were washed with 70% ethanol and stained with 0.5% basic fuchsin (Sigma). After three washes in 70% ethanol, cells were prepared for immunofluorescence staining.

Transmission electron microscopy. Infected cells were fixed with 2.5% glutaraldehyde/ 0.05%malachite green (EMS) in 0.1Msodium cacodylate buffer (pH 6.8) and then post-fixed with the following stains: 0.5% osmium tetroxide/0.8% potassium ferricyanide in 0.1M sodiumcacodylate; 1%tannicacid; and 1%uranyl acetate. Samples were dehydrated with graded amounts of ethanol and embedded in Spur resin. Ultrathin sections were processed, poststained with uranyl acetate and lead citrate, and imaged on a Tecnai G2 Twin microscope (FEI).

3.9.7 Attachment and Entry Assays

Attachment. 0.2×10^6 A2EN cells grown on coverslips in a 24 well plate were infected at an MOI of 50 with purified EBs. Infections were allowed to rock at 24°C for 1 hour. Following infection, cells were washed 3x PBS to ensure removal of non-specifically bound bacteria prior to fixation and staining with anti-MOMP antibodies.

Bacterial attached to all cells within a minimum of 5 fields, 3 biological replicates were counted.

Entry. Cells were grown and infected exactly as in the attachment assay, but were incubated for 1 hr at 37°C in an atmosphere containing 5% CO₂ prior to fixation. Following fixation, cells were incubated in blocking solution for 20 min, stained with mouse anti-LPS antibodies to identify external bacteria, and then washed 3x with PBS. Cells were then permeabilized, blocked, and stained with rabbit anti-MOMP before incubation with Alexa secondary antibodies (goat anti-mouse AlexaFluor 488, goat anti-rabbit AlexaFluor 555). Total bacteria attached to and internalized into each cell within the field was counted for a minimum of 5 fields, 3 biological replicates.

3.9.8 Quantification of Exit

0.2e6 HeLa cells were seeded and infected MOI of 1. At various timepoints post infection, cells monolayers were imaged and the supernatant removed. To determine recoverable IFUs, supernatants were spun at 10,000g, 15 min, 4°C to pellet the bacteria and resuspended in 50 µ 1x SPG. IFUs were enumerated in a similar manner to the bacterial growth assays: infection with serial dilutions in 96 well plates of confluent Vero cell monolayers. At 24hpi, cells were fixed and stained with anti-Slc1 antibodies. The number of inclusions per well was calculated and used to enumerate the total IFUs in the 50ul of resuspended supernatant.

3.9.9 Preparation of *C. trachomatis* Total Protein Extracts

To prepare total protein extracts for LC/LC-MS/MS, EBs were suspended in lysis buffer (20 mM Tris-HCl pH 8.0, 5 mM EDTA, 50 mM NaCl, 15 mM DTT, 0.06 mM 2-Mercaptoethanol, 1 mM Na₃VO₄, 50 mM NaF, 100 mM NH₄HCO₃, 0.5% RapiGest SF Surfactant [Waters Corp., Milford, Maryland, USA] in 100 mM NH₄HCO₃), briefly

sonicated on ice, heated at 65°C for 10 min and then boiled for 5 min in water. Lysates were centrifuged at 25 000 g (10 min, 4°C) to remove insoluble debris and supernatants were stored at -80°C. The Duke Proteomics Core Facility (DPCF) received 6 samples, three elementary body (EB) preparations each from two strains of *C. trachomatis*, RifR and RSTE4. Protein yield was between 47 and 62 ug for all samples, determined using a mini-Bradford assay (BioRad). 30 ug from each was pipetted out for digestion and protein concentration was normalized to approximately 0.5 ug/uL using 0.5% Rapigest in 50 mM AmBic, then samples were reduced with 10 mM DTT at 80C for 15 min and alkylated with 60 mM iodoacetamide at room temperature in the dark for 30 min (it is necessary to overalkylate because lysis buffer already contains 15 mM DTT). Samples were then subjected to trypsin digestion overnight at 37°C at an enzyme to protein ratio (w/w) of 1:50. After digestion, all samples were acidified to 1% TFA/2% ACN and heated to 60C for 2 hours to hydrolyze Rapigest, spun at 15000 rpm to isolate the soluble supernatant, then taken to dryness in a speed vac. Samples were resuspended at 1 ug/uL in 200 mM Ammonium Formate (pH 10) in a buffer containing 25 fmol/uL ADH1_YEAST (MassPrep, Waters) as a surrogate standard. A QC Pool, containing 4 uL from each sample, was generated to use for column conditioning and technical reproducibility assessment.

3.9.10 LC-MC Data Collection

Quantitative two-dimensional liquid chromatography – tandem mass spectrometry (LC/LC-MS/MS) was performed on 5 µg of protein digest per sample in singlicate, and the pool was analyzed in triplicate with 5 ug injections (once each at beginning, middle, and end of the queue). The method uses two-dimensional liquid chromatography in a high-low pH reversed phase/reversed phase configuration on a

nanoAcquity UPLC system (Waters Corp) coupled to a Synapt G2 HDMS high resolution accurate mass tandem mass spectrometer (Waters Corp.) with nanoelectrospray ionization in a manner similar to previously described [1-3]. Peptides were first trapped at 2 μ l/min at 97/3 v/v water/MeCN in 20 mM ammonium formate (pH 10) on a 5 μ m XBridge BEH130 C18 300 μ m \times 50 mm column (Waters). A series of step-elutions of MeCN at 2 μ l/min was used to elute peptides from the 1st dimension column. Ten steps of 7.4%, 10.8%, 12.6%, 14.0%, 15.3%, 16.7%, 18.3%, 20.4%, 23.5% and 50.0% MeCN were utilized for the unbiased analyses; these percentages were optimized to deliver an approximately equal load to the 2nd dimension column for each fraction. For 2nd dimension separation, the eluent from the 1st dimension was first diluted 10-fold online with 99.8/0.1/0.1 v/v/v water/MeCN/formic acid and trapped on a 5 μ m Symmetry C18 180 μ m \times 20 mm trapping column (Waters). The 2nd dimension separations were performed on a 1.7 μ m Acquity BEH130 C18 75 μ m \times 150 mm column (Waters) using a linear gradient of 7 to 35% MeCN with 0.1% formic acid over 37 min, at a flow rate of 0.5 μ l/min and column temperature of 35 $^{\circ}$ C. Data collection on the Synapt G2 mass spectrometer was performed in ion-mobility assisted data-independent acquisition (HDMSE) mode, using 0.6 second alternating cycle time between low (6V) and high (27-50V) collision energy (CE) in the transfer region after the ion mobility cell. Scans performed at low CE measure peptide accurate mass and intensity (abundance), while scans at elevated CE allow for qualitative identification of the resulting peptide fragments via database searching. The pool was also injected once by DDA data acquisition at the beginning of the run queue for column conditioning and supplemental qualitative-only peptide identifications. The total analysis cycle time for each sample injection was approximately 10 hours.

3.9.11 LC-MS Data Processing and Protein Quantification

Samples were run in an order to minimize batch effect (QC pool, RifR1, GspE1, RifR2, QC pool, GspE2, RifR3, GspE3, QC Pool). Following the 10 analyses, data were imported into Rosetta Elucidator v3.3 (Rosetta Biosoftware, Inc), and all LC/LC-MS runs were aligned based on the accurate mass and retention time of detected ions (“features”) using PeakTeller algorithm (Elucidator). The relative peptide abundance was calculated based on area-under-the-curve (AUC) of aligned features across all runs. The overall dataset had over 942,000 quantified features, and high collision energy (peptide fragment) data was collected as 283,638 spectra for sequencing by database searching. This MS/MS data was searched against a custom database containing NCBI ref seq CT434/Bu sequences appended to SwissProt entries with *homo sapiens* taxonomy which also contains a reversed-sequence “decoy” database for false positive rate determination as well as several proteins used as surrogate standards (database is available at https://discovery.genome.duke.edu/express/resources/3640/ChI_CT434_sp_hum_Mix1_rev_011714.fasta). ProteinLynx Global Server v2.5.2 (PLGS) was utilized to produce fragment ion spectra from the ion-mobility MSE runs, and to perform the database searches. Included in the database searches were variable modifications on M (oxidation) and N/Q (deamidation). After individual peptide scoring using PeptideProphet algorithm (Elucidator), the data was annotated at a 1% peptide false discovery rate. This analysis yielded identifications for 7,046 peptides and 1,246 proteins across all samples. For quantitative processing, the data was first curated to contain only high quality peptides with appropriate chromatographic peak shape, peptide quantities across all ten LC/LC fractions were summed, and the dataset was intensity scaled to the robust mean

across all samples analyzed. the final quantitative dataset for the dataset was based on 6,917 peptides and contains 1,237 proteins (774 proteins contained at least 2 unique peptides). Fold-change was calculated as the ratio of average WT intensities over average of RSTE4 intensities, or the inverse reciprocal. Data was log₂ transformed for each protein, then p-values were calculated using a Student's T-test. T-test values were corrected for multiple hypothesis testing using Benjamini Hochberg FDR-correction method. Protein quantification was performed exactly as previously described [188]. Proteins with only one peptide to match were eliminated from the quantitative analysis. Next, based on the historic response factor of the instrument utilized (2050 ±400 counts fmol⁻¹, n = 117) we calculated the fmol of each protein in the sample. Using each protein's molecular weight from the database, this fmol quantity was converted to nanograms, and by summing these values for each analysis we calculate the total ng in each sample. Finally, to calculate the species-specific protein expression for each sample, the fmol value for each protein was divided by the ng sum for only the species of interest, and scaled by 1000 to yield fmol µg⁻¹. Data was log₂ transformed for each protein, then p-values were calculated using a Student's T-test. T-test values were corrected for multiple hypothesis testing using Benjamini Hochberg FDR-correction method.

3.9.12 Sec Signal Prediction and Assessment

Signal P v3.0 analysis. The first 70AA of each protein in the *C. trachomatis* L2/434/Bu genome (entry TC00645 at www.genome.jp, RS: NC_010287) was placed in multi-FASTA format to facilitate analysis though SignalP v3.0 using the following settings: Gram-negative bacteria, short output format, sensitive D-cutoff values, and no

graphics [284]. SignalP v3.0 was used as v4.1 did not recognize the signal sequence present in CPAF (CTL0233).

PhoA assay. The *E. coli phoA* gene without the signal peptide region (AA1-21) was inserted into the *EcoRI/KpnI* sites of pFLAG-CTC (Sigma) to create the recombinant plasmid pFLAG-PhoAnoss that has a FLAG tag at the C-terminus. Predicted signal sequences from candidate effector proteins were PCR amplified from L2 gDNA, digested, and cloned into the *NdeI/HindIII* sites. Finished constructs were transformed into KS272 *E. coli* strain ($\Delta(lacIPOZY)X74 galE galK thi rpsL \Delta phoA$) that lacks endogenous *phoA*. This strain is streptomycin resistant. Transformed constructs were grown overnight in liquid culture at 37°C and plated the next day onto LB agar plates containing 50µg/ml BCIP. Plates were incubated for 24 hours at 30°C prior to assessment of color.

3.9.13 Glycogen Quantification Assays

Glycogen quantification assay was performed per manufacturer's instruction. Briefly, HeLa Cas9 or Gys1 cells were seeded in a 6-well plate until confluency and mock-infected or infected at an MOI=1 for 40 hours. All samples were done in duplicate with technical triplicates. At 40hpi, cells were washed with cold ultra-pure water twice and harvested in 100µl cold ultra-pure water prior to being flash frozen in liquid nitrogen. Flash freezing prevents glycogen breakdown while all samples are collected. Samples are then boiled for 5 minutes and centrifuged at 4°C, 13,000g, for 5 min. 80µl is removed from each tube and aliquoted for the glycogen quantification assay and the DC protein assay. 4ul of sample was used for each assay. Total µg of glycogen present within the well was normalized to µg of total protein.

4. Future Perspectives

4.1 *The path forward with CPAF*

In this work, we describe and establish tools that can be widely used to define the mechanisms by which CPAF contributes to *Chlamydia* pathogenesis, namely the Rst5 (CPAF+), Rst17 (CPAF-) and CTL2 *cpa:cat* strains. However, questions endure as to how CPAF accesses the host cytosol and why its described activity appears to be constrained to the inclusion lumen, despite immunofluorescence evidence from multiple groups (using different antibodies) suggesting it is present in the host cytosol by 16-24 hpi.

4.1.1 Using Rst5 and Rst17 to define the function of CPAF during *C. trachomatis* infection

Since the publication of this work, the Rst5 (CPAF+) and Rst17 (CPAF-) strains have been made available to numerous groups for further investigation of the role of CPAF during *C. trachomatis* infection. Using these strains, the Zhong laboratory provided further support for the importance of CPAF in *Chlamydia* pathogenesis using a genital tract mouse infection model [123]. In this model, CPAF promotes survival in the lower genital tract of mice, however when both Rst5 and Rst17 are inoculated directly into the upper genital tract, no significant difference in bacterial shedding is observed [123].

CPAF activity also represents a mechanism by which *Chlamydia* can regulate the T3SS and T3 effector proteins. Patton and colleagues infected HeLa cells with both Rst5 and Rst17 prior to harvesting cells in hot SDS buffer, conditions we have shown inactivate CPAF [219]. Proteomic analysis revealed both human and *C. trachomatis* proteins differ in abundance during infection with these two strains. Both components

and chaperones of the T3SS (CT860, CT579, CT665, CT667, and CT860), along with midcycle T3 effector proteins (CT620, CT621, CT711, and CT847) were lower in abundance during Rst5 infections, suggesting CPAF-dependent degradation [219]. However, it is not known if this effect is a direct or indirect consequence of the loss of CPAF.

When host proteins were analyzed, Patton et al. observed only 6 proteins were reduced in abundance during WT infection. Expectedly, they did not see cleavage of vimentin; this analysis was performed at 30hpi and we have shown vimentin cleavage occurs after inclusion rupture (Fig.12). While our data suggests CPAF is not involved in dampening an already activated NFκB response, their studies suggest CPAF plays an indirect role in blocking the initial nuclear translocation of p65 [219]. This study represents only a snapshot of CPAF's involvement during infection. It is possible at other timepoints different sets of host and bacterial proteins would be identified.

Through experiments with the Rst5 and Rst17 mutant strains, CPAF has also been implicated to play a role in the regulation of lytic exit [299] and in the induction of multinucleation during infection [310].

4.2 The *C. trachomatis* type II secretion system

Many questions remain about the T2SS and its substrates in *Chlamydia*, but also in other Gram-negative bacteria. To date, no "T2S signal" has been defined, although proteomic approaches have made impressive advancements in identifying a breadth of substrates. As knowledge expands and more secreted proteins are recognized, structural similarities may come to light. Additionally, numerous secreted proteins remain uncharacterized and further studies may reveal involvement of the T2SS in novel pathogenic activities.

4.2.1 Identifying components of the T2SS

Although we know *C. trachomatis* has an active T2SS, some of the components required for its function are still unknown. The signal peptidases LepB and LspA may be responsible for the function of the prepilin peptidase, GspO. However, other structural components that cannot be identified from homology searches of the *C. trachomatis* genome include GspM and GspL, the latter of which is known to directly interact with the N1 domain of GspE. Without this interaction, ATP hydrolysis is not coupled to the inner membrane platform and the required conformational changes in the T2SS to extend the pseudopilus do not occur.

Among a library of ~1,000 fully sequenced, *C. trachomatis* mutants, I isolated a set of mutant strains with lesions in *gspCDEF*, along with *CT567*. However, T2S remained functional in each of these strains, as assessed by CPAF localization (data not shown). Additionally, no T2S genes were identified by screening 24,000 plaques of EMS mutagenized *C. trachomatis* strains for the glycogen accumulation phenotype (data not shown). A more promising strategy to identify and verify T2S components is to express tagged variants in *C. trachomatis*, followed by immunoprecipitation and mass spectrometry approaches to identify interacting partners.

4.2.2 Identifying novel effector proteins

One class of substrates unlikely to be identified in our approach are surface-associated T2S proteins. If OM associated proteins do not detach from the surface of WT bacteria, there may not appear to be a difference in abundance between WT and RSTE4 EBs. In *Shewanella oneidensis*, surface membrane proteins were identified by using a membrane-impermeable chemical probe followed by ¹⁶O/¹⁸O labeling. Enriched proteins were then quantified using the accurate mass and time tag approach. Using this

method, the dependence of 4 surface associated proteins on T2S was confirmed [311]. A modified approach could be used in *C. trachomatis* WT and RSTE4 strains to identify this class of T2S proteins.

Further investigations are also needed into the T2S candidate substrates identified in this work. The localization of 6 candidates during *C. trachomatis* infection was not determined and the subcellular localization of Ctad1 (periplasm vs surface) in RSTE4 bacteria remains to be elucidated. Additionally, tagged variants of CT041, CT355, CT600, and CT733 should be expressed in WT and RSTE4 strains to confirm their localization. A similar approach can be taken to identify the localization of CT795, Tsp, and CT311.

A question remains as to whether substrates are physically associated with glycogen. Establishing protocols for the purification of glycogen granules may help to answer these questions. Alternatively, the human protein phosphatase 1 (PP1) contains a glycogen-binding domain [312]. Whether this domain can be incorporated into a protocol to isolate glycogen, and therefore its associated proteins, remains to be seen.

An interesting set of experiments surrounds OMV purification during infection with RSTE4 mutants. A protocol has already been described for purification of membrane vesicles in *C. trachomatis* [265], although their approach adds ampicillin as a stressor to promote vesicle production. Given the state of the RSTE4 periplasm, ampicillin may not be needed to increase vesiculation. I hypothesize CT041, CT733, and CT600 are contained within OMVs.

4.2.3 Investigating the role of glycogen during *C. trachomatis* infection

The regulation of secreted proteins by glycogen is intriguing, especially

considering previous work indicates changing glucose concentrations during infection, and by proxy glycogen levels, does not alter glycogen metabolism gene expression [313]. Careful studies examining the impact of changing glycogen levels on CPAF transcript and protein expression need to be done; this can be accomplished by varying the glucose concentrations of cell culture media. Many substrates of the T2SS are important for nutrient acquisition and low glucose levels correspond with lower levels of glycogen. An increase in CPAF production may be a response to limited nutrients (ie glucose) present within the inclusion. If this is the case, an exacerbation of the growth defect of CPAF-deficient strains may occur when limited glucose is available during infection.

During infection, the microbiota present in the vaginal tract will interact with *Chlamydia*. Certain species of normal vaginal flora are known to have protective functions against infection, including *Lactobacillus* species [314-316]. In particular, *L. crispatus* has a strong inhibitory effect on *Chlamydia* infectivity *in vitro* [317]. Glucose depletion may represent a mechanism by which this inhibition occurs, as addition of glucose to *L. crispatus* supernatants leads to a significant increase in the infectivity of *C. trachomatis* [317]. In an *in vivo* setting, increased glucose consumption by *L. crispatus* could impact the growth of *Chlamydia* by decreasing this energy source; glucose fermentation by *Lactobacilli* would also create an unfavorable environment as fermentation leads to the formation of lactic acid. In these conditions, an increase in CPAF production may promote *C. trachomatis* infection by degrading or modifying factors that constitute danger signals to be sensed by immune cells (HMGB1, anti-microbial peptides, secreted bacterial effectors, ect), modifying physical barriers that limit bacterial dispersal, or by a yet unknown mechanism that affects the growth of normal

vaginal microbiota. Additionally, studies suggest CPAF promotes survival in the lower genital tract of mice, where majority of the vaginal flora resides; the upper genital tract is a more sterile environment where CPAF has been shown to not be essential for survival [123].

Overall, we have identified that CPAF activity is largely contained within the inclusion lumen until late stages of infection, used quantitative proteomics to identify proteins that accumulate in a *C. trachomatis* T2S-mutant strain, and proposed a new function for glycogen within the inclusion lumen.

References

1. Silhavy TJ, Kahne D, Walker S. The bacterial cell envelope. *Cold Spring Harb Perspect Biol.* 2010;2(5):a000414.
2. Costa TR, Felisberto-Rodrigues C, Meir A, Prevost MS, Redzej A, Trokter M, et al. Secretion systems in Gram-negative bacteria: structural and mechanistic insights. *Nat Rev Microbiol.* 2015;13(6):343-59.
3. Arts J, van Boxtel R, Filloux A, Tommassen J, Koster M. Export of the pseudopilin XcpT of the *Pseudomonas aeruginosa* type II secretion system via the signal recognition particle-Sec pathway. *J Bacteriol.* 2007;189(5):2069-76.
4. Palmer T, Berks BC. The twin-arginine translocation (Tat) protein export pathway. *Nat Rev Micro.* 2012;10(7):483-96.
5. Lycklama ANJA, Driessen AJ. The bacterial Sec-translocase: structure and mechanism. *Philos Trans R Soc Lond B Biol Sci.* 2012;367(1592):1016-28.
6. Douzi B, Filloux A, Voulhoux R. On the path to uncover the bacterial type II secretion system. *Philos Trans R Soc Lond B Biol Sci.* 2012;367(1592):1059-72.
7. Korotkov KV, Gonen T, Hol WG. Secretins: dynamic channels for protein transport across membranes. *Trends Biochem Sci.* 2011;36(8):433-43.
8. Strozen TG, Stanley H, Gu Y, Boyd J, Bagdasarian M, Sandkvist M, et al. Involvement of the GspAB complex in assembly of the type II secretion system secretin of *Aeromonas* and *Vibrio* species. *J Bacteriol.* 2011;193(9):2322-31.
9. Strozen TG, Li G, Howard SP. YghG (GspSbeta) is a novel pilot protein required for localization of the GspSbeta type II secretion system secretin of enterotoxigenic *Escherichia coli*. *Infect Immun.* 2012;80(8):2608-22.
10. Dunstan RA, Heinz E, Wijeyewickrema LC, Pike RN, Purcell AW, Evans TJ, et al. Assembly of the type II secretion system such as found in *Vibrio cholerae* depends on the novel Pilotin AspS. *PLoS Pathog.* 2013;9(1):e1003117.
11. Harding CM, Kinsella RL, Palmer LD, Skaar EP, Feldman MF. Medically Relevant *Acinetobacter* Species Require a Type II Secretion System and Specific Membrane-Associated Chaperones for the Export of Multiple Substrates and Full Virulence. *PLoS Pathog.* 2016;12(1):e1005391.
12. Johnson TL, Waack U, Smith S, Mobley H, Sandkvist M. *Acinetobacter baumannii* is dependent on the type II secretion system and its substrate LipA for lipid utilization and in vivo fitness. *J Bacteriol.* 2015.

13. Filloux A. The underlying mechanisms of type II protein secretion. *Biochim Biophys Acta*. 2004;1694(1-3):163-79.
14. Nunn DN, Lory S. Components of the protein-excretion apparatus of *Pseudomonas aeruginosa* are processed by the type IV prepilin peptidase. *Proc Natl Acad Sci U S A*. 1992;89(1):47-51.
15. Roelofs KG, Jones CJ, Helman SR, Shang X, Orr MW, Goodson JR, et al. Systematic Identification of Cyclic-di-GMP Binding Proteins in *Vibrio cholerae* Reveals a Novel Class of Cyclic-di-GMP-Binding ATPases Associated with Type II Secretion Systems. *PLoS Pathog*. 2015;11(10):e1005232.
16. Korotkov KV, Sandkvist M, Hol WG. The type II secretion system: biogenesis, molecular architecture and mechanism. *Nat Rev Microbiol*. 2012;10(5):336-51.
17. Nivaskumar M, Francetic O. Type II secretion system: a magic beanstalk or a protein escalator. *Biochim Biophys Acta*. 2014;1843(8):1568-77.
18. Marsh JW, Taylor RK. Identification of the *Vibrio cholerae* type 4 prepilin peptidase required for cholera toxin secretion and pilus formation. *Mol Microbiol*. 1998;29(6):1481-92.
19. Durand E, Michel G, Voulhoux R, Kurner J, Bernadac A, Filloux A. XcpX controls biogenesis of the *Pseudomonas aeruginosa* XcpT-containing pseudopilus. *J Biol Chem*. 2005;280(36):31378-89. doi: 10.1074/jbc.M505812200.
20. Camberg JL, Sandkvist M. Molecular analysis of the *Vibrio cholerae* type II secretion ATPase EpsE. *J Bacteriol*. 2005;187(1):249-56.
21. Sandkvist M, Bagdasarian M, Howard SP, DiRita VJ. Interaction between the autokinase EpsE and EpsL in the cytoplasmic membrane is required for extracellular secretion in *Vibrio cholerae*. *EMBO J*. 1995;14(8):1664-73.
22. Sandkvist M, Keith JM, Bagdasarian M, Howard SP. Two regions of EpsL involved in species-specific protein-protein interactions with EpsE and EpsM of the general secretion pathway in *Vibrio cholerae*. *J Bacteriol*. 2000;182(3):742-8.
23. Abendroth J, Murphy P, Sandkvist M, Bagdasarian M, Hol WG. The X-ray structure of the type II secretion system complex formed by the N-terminal domain of EpsE and the cytoplasmic domain of EpsL of *Vibrio cholerae*. *J Mol Biol*. 2005;348(4):845-55.
24. Shiue SJ, Kao KM, Leu WM, Chen LY, Chan NL, Hu NT. XpsE oligomerization triggered by ATP binding, not hydrolysis, leads to its association with XpsL. *EMBO J*. 2006;25(7):1426-35.

25. Gray MD, Bagdasarian M, Hol WG, Sandkvist M. In vivo cross-linking of EpsG to EpsL suggests a role for EpsL as an ATPase-pseudopilin coupling protein in the Type II secretion system of *Vibrio cholerae*. *Mol Microbiol.* 2011;79(3):786-98.
26. Py B, Loiseau L, Barras F. An inner membrane platform in the type II secretion machinery of Gram-negative bacteria. *EMBO Rep.* 2001;2(3):244-8.
27. Johnson TL, Scott ME, Sandkvist M. Mapping critical interactive sites within the periplasmic domain of the *Vibrio cholerae* type II secretion protein EpsM. *J Bacteriol.* 2007;189(24):9082-9.
28. Camberg JL, Johnson TL, Patrick M, Abendroth J, Hol WG, Sandkvist M. Synergistic stimulation of EpsE ATP hydrolysis by EpsL and acidic phospholipids. *EMBO J.* 2007;26(1):19-27.
29. Possot OM, Vignon G, Bomchil N, Ebel F, Pugsley AP. Multiple interactions between pullulanase secretion components involved in stabilization and cytoplasmic membrane association of Pule. *J Bacteriol.* 2000;182(8):2142-52.
30. Korotkov KV, Johnson TL, Jobling MG, Pruneda J, Pardon E, Heroux A, et al. Structural and functional studies on the interaction of GspC and GspD in the type II secretion system. *PLoS Pathog.* 2011;7(9):e1002228.
31. Shevchik VE, Robert-Baudouy J, Condemine G. Specific interaction between OutD, an *Erwinia chrysanthemi* outer membrane protein of the general secretory pathway, and secreted proteins. *Embo j.* 1997;16(11):3007-16.
32. Viarre V, Cascales E, Ball G, Michel GP, Filloux A, Voulhoux R. HxcQ liposecretin is self-piloted to the outer membrane by its N-terminal lipid anchor. *J Biol Chem.* 2009;284(49):33815-23.
33. Tosi T, Nickerson NN, Mollica L, Jensen MR, Blackledge M, Baron B, et al. Pilotin-secretin recognition in the type II secretion system of *Klebsiella oxytoca*. *Mol Microbiol.* 2011;82(6):1422-32.
34. Gu S, Rehman S, Wang X, Shevchik VE, Pickersgill RW. Structural and functional insights into the pilotin-secretin complex of the type II secretion system. *PLoS Pathog.* 2012;8(2):e1002531.
35. Possot OM, Letellier L, Pugsley AP. Energy requirement for pullulanase secretion by the main terminal branch of the general secretory pathway. *Mol Microbiol.* 1997;24(3):457-64.
36. Letellier L, Howard SP, Buckley JT. Studies on the energetics of proaerolysin secretion across the outer membrane of *Aeromonas* species. Evidence for a requirement for both the protonmotive force and ATP. *J Biol Chem.* 1997;272(17):11109-13.

37. Campos M, Cisneros DA, Nivaskumar M, Francetic O. The type II secretion system - a dynamic fiber assembly nanomachine. *Res Microbiol.* 2013;164(6):545-55.
38. d'Enfert C, Chapon C, Pugsley AP. Export and secretion of the lipoprotein pullulanase by *Klebsiella pneumoniae*. *Mol Microbiol.* 1987;1(1):107-16.
39. Kudva R, Denks K, Kuhn P, Vogt A, Muller M, Koch HG. Protein translocation across the inner membrane of Gram-negative bacteria: the Sec and Tat dependent protein transport pathways. *Res Microbiol.* 2013;164(6):505-34.
40. Cline K. Mechanistic Aspects of Folded Protein Transport by the Twin Arginine Translocase (Tat). *J Biol Chem.* 2015;290(27):16530-8.
41. Bendtsen JD, Nielsen H, Widdick D, Palmer T, Brunak S. Prediction of twin-arginine signal peptides. *BMC Bioinformatics.* 2005;6:167.
42. Emanuelsson O, Brunak S, von Heijne G, Nielsen H. Locating proteins in the cell using TargetP, SignalP and related tools. *Nat Protoc.* 2007;2(4):953-71.
43. Petersen TN, Brunak S, von Heijne G, Nielsen H. SignalP 4.0: discriminating signal peptides from transmembrane regions. *Nat Methods.* 2011;8(10):785-6.
44. Bagos PG, Nikolaou EP, Liakopoulos TD, Tsirigos KD. Combined prediction of Tat and Sec signal peptides with hidden Markov models. *Bioinformatics.* 2010;26(22):2811-7.
45. Juncker AS, Willenbrock H, Von Heijne G, Brunak S, Nielsen H, Krogh A. Prediction of lipoprotein signal peptides in Gram-negative bacteria. *Protein Sci.* 2003;12(8):1652-62.
46. Bagos PG, Tsirigos KD, Liakopoulos TD, Hamodrakas SJ. Prediction of lipoprotein signal peptides in Gram-positive bacteria with a Hidden Markov Model. *J Proteome Res.* 2008;7(12):5082-93.
47. Voulhoux R, Ball G, Ize B, Vasil ML, Lazdunski A, Wu LF, et al. Involvement of the twin-arginine translocation system in protein secretion via the type II pathway. *EMBO J.* 2001;20(23):6735-41.
48. Martinez A, Ostrovsky P, Nunn DN. Identification of an additional member of the secretin superfamily of proteins in *Pseudomonas aeruginosa* that is able to function in type II protein secretion. *Mol Microbiol.* 1998;28(6):1235-46.
49. Rossier O, Cianciotto NP. The *Legionella pneumophila* *tatB* gene facilitates secretion of phospholipase C, growth under iron-limiting conditions, and intracellular infection. *Infect Immun.* 2005;73(4):2020-32.

50. Hirst TR, Holmgren J. Conformation of protein secreted across bacterial outer membranes: a study of enterotoxin translocation from *Vibrio cholerae*. *Proc Natl Acad Sci U S A*. 1987;84(21):7418-22.
51. Hardie KR, Schulze A, Parker MW, Buckley JT. *Vibrio* spp. secrete proaerolysin as a folded dimer without the need for disulphide bond formation. *Mol Microbiol*. 1995;17(6):1035-44.
52. Chapon V, Simpson HD, Morelli X, Brun E, Barras F. Alteration of a single tryptophan residue of the cellulose-binding domain blocks secretion of the *Erwinia chrysanthemi* Cel5 cellulase (ex-EGZ) via the type II system. *J Mol Biol*. 2000;303(2):117-23.
53. Palomaki T, Saarilahti HT. The extreme C-terminus is required for secretion of both the native polygalacturonase (PehA) and PehA-Bla hybrid proteins in *Erwinia carotovora* subsp. *carotovora*. *Mol Microbiol*. 1995;17(3):449-59.
54. Sauvonnet N, Pugsley AP. Identification of two regions of *Klebsiella oxytoca* pullulanase that together are capable of promoting beta-lactamase secretion by the general secretory pathway. *Mol Microbiol*. 1996;22(1):1-7.
55. McVay CS, Hamood AN. Toxin A secretion in *Pseudomonas aeruginosa*: the role of the first 30 amino acids of the mature toxin. *Mol Gen Genet*. 1995;249(5):515-25.
56. Voulhoux R, Taupiac MP, Czjzek M, Beaumelle B, Filloux A. Influence of deletions within domain II of exotoxin A on its extracellular secretion from *Pseudomonas aeruginosa*. *J Bacteriol*. 2000;182(14):4051-8.
57. Palomaki T, Pickersgill R, Riekkari R, Romantschuk M, Saarilahti HT. A putative three-dimensional targeting motif of polygalacturonase (PehA), a protein secreted through the type II (GSP) pathway in *Erwinia carotovora*. *Mol Microbiol*. 2002;43(3):585-96.
58. Pineau C, Guschinskaya N, Robert X, Gouet P, Ballut L, Shevchik VE. Substrate recognition by the bacterial type II secretion system: more than a simple interaction. *Mol Microbiol*. 2014;94(1):126-40.
59. Wohner G, Wober G. Biosynthesis of pullulanase, an outer membrane enzyme in *Klebsiella*. Differential effect of translation and transcription inhibitors on synthesis of enzymes in cytoplasm, periplasm, cytoplasmic and outer membrane. *Mol Cell Biochem*. 1979;24(2):83-91.
60. De SN. Enterotoxicity of bacteria-free culture-filtrate of *Vibrio cholerae*. *Nature*. 1959;183(4674):1533-4. Epub 1959/05/30.
61. Andro T, Chambost JP, Kotoujansky A, Cattaneo J, Bertheau Y, Barras F, et al. Mutants of *Erwinia chrysanthemi* defective in secretion of pectinase and cellulase. *J Bacteriol*. 1984;160(3):1199-203.

62. Zhong G, Liu L, Fan T, Fan P, Ji H. Degradation of transcription factor RFX5 during the inhibition of both constitutive and interferon gamma-inducible major histocompatibility complex class I expression in chlamydia-infected cells. *J Exp Med.* 2000;191(9):1525-34.
63. Sandkvist M, Morales V, Bagdasarian M. A protein required for secretion of cholera toxin through the outer membrane of *Vibrio cholerae*. *Gene.* 1993;123(1):81-6.
64. Snaveley EA, Kokes M, Dunn JD, Saka HA, Nguyen BD, Bastidas RJ, et al. Reassessing the role of the secreted protease CPAF in *Chlamydia trachomatis* infection through genetic approaches. *Pathog Dis.* 2014;71(3):336-51.
65. Liles MR, Edelstein PH, Cianciotto NP. The prepilin peptidase is required for protein secretion by and the virulence of the intracellular pathogen *Legionella pneumophila*. *Mol Microbiol.* 1999;31(3):959-70.
66. Dowling JN, Saha AK, Glew RH. Virulence factors of the family Legionellaceae. *Microbiological reviews.* 1992;56(1):32-60. Epub 1992/03/01.
67. Kok RG, van Thor JJ, Nugteren-Roodzant IM, Vosman B, Hellingwerf KJ. Characterization of lipase-deficient mutants of *Acinetobacter calcoaceticus* BD413: identification of a periplasmic lipase chaperone essential for the production of extracellular lipase. *J Bacteriol.* 1995;177(11):3295-307.
68. Kok RG, van Thor JJ, Nugteren-Roodzant IM, Brouwer MB, Egmond MR, Nudel CB, et al. Characterization of the extracellular lipase, LipA, of *Acinetobacter calcoaceticus* BD413 and sequence analysis of the cloned structural gene. *Mol Microbiol.* 1995;15(5):803-18.
69. Wortman AT, Somerville CC, Colwell RR. Chitinase determinants of *Vibrio vulnificus*: gene cloning and applications of a chitinase probe. *Appl Environ Microbiol.* 1986;52(1):142-5.
70. Connell TD, Metzger DJ, Lynch J, Folster JP. Endochitinase is transported to the extracellular milieu by the eps-encoded general secretory pathway of *Vibrio cholerae*. *J Bacteriol.* 1998;180(21):5591-600.
71. Tan KS, Chen Y, Lim YC, Tan GY, Liu Y, Lim YT, et al. Suppression of host innate immune response by *Burkholderia pseudomallei* through the virulence factor TssM. *J Immunol.* 2010;184(9):5160-71.
72. El Khattabi M, Van Gelder P, Bitter W, Tommassen J. Role of the lipase-specific foldase of *Burkholderia glumae* as a steric chaperone. *J Biol Chem.* 2000;275(35):26885-91.
73. Pauwels K, Sanchez del Pino MM, Feller G, Van Gelder P. Decoding the folding of *Burkholderia glumae* lipase: folding intermediates en route to kinetic stability. *PLoS One.* 2012;7(5):e36999.

74. Sikora AE. Proteins secreted via the type II secretion system: smart strategies of *Vibrio cholerae* to maintain fitness in different ecological niches. *PLoS Pathog.* 2013;9(2):e1003126.
75. Sikora AE, Zielke RA, Lawrence DA, Andrews PC, Sandkvist M. Proteomic analysis of the *Vibrio cholerae* type II secretome reveals new proteins, including three related serine proteases. *J Biol Chem.* 2011;286(19):16555-66.
76. Liu H, Zhang S, Schell MA, Denny TP. Pyramiding unmarked deletions in *Ralstonia solanacearum* shows that secreted proteins in addition to plant cell-wall-degrading enzymes contribute to virulence. *Mol Plant Microbe Interact.* 2005;18(12):1296-305.
77. Poueymiro M, Genin S. Secreted proteins from *Ralstonia solanacearum*: a hundred tricks to kill a plant. *Curr Opin Microbiol.* 2009;12(1):44-52.
78. Evans FF, Raftery MJ, Egan S, Kjelleberg S. Profiling the secretome of the marine bacterium *Pseudoalteromonas tunicata* using amine-specific isobaric tagging (iTRAQ). *J Proteome Res.* 2007;6(3):967-75.
79. DebRoy S, Dao J, Soderberg M, Rossier O, Cianciotto NP. *Legionella pneumophila* type II secretome reveals unique exoproteins and a chitinase that promotes bacterial persistence in the lung. *Proc Natl Acad Sci U S A.* 2006;103(50):19146-51.
80. Bortoli-German I, Brun E, Py B, Chippaux M, Barras F. Periplasmic disulphide bond formation is essential for cellulase secretion by the plant pathogen *Erwinia chrysanthemi*. *Mol Microbiol.* 1994;11(3):545-53.
81. Pugsley AP, Bayan N, Sauvonnet N. Disulfide bond formation in secretory component PulK provides a possible explanation for the role of DsbA in pullulanase secretion. *J Bacteriol.* 2001;183(4):1312-9.
82. Peek JA, Taylor RK. Characterization of a periplasmic thiol:disulfide interchange protein required for the functional maturation of secreted virulence factors of *Vibrio cholerae*. *Proc Natl Acad Sci U S A.* 1992;89(13):6210-4.
83. Okamoto K, Baba T, Yamanaka H, Akashi N, Fujii Y. Disulfide bond formation and secretion of *Escherichia coli* heat-stable enterotoxin II. *J Bacteriol.* 1995;177(16):4579-86.
84. Yamanaka H, Nomura T, Fujii Y, Okamoto K. Extracellular secretion of *Escherichia coli* heat-stable enterotoxin I across the outer membrane. *J Bacteriol.* 1997;179(11):3383-90.
85. Brumlik MJ, van der Goot FG, Wong KR, Buckley JT. The disulfide bond in the *Aeromonas hydrophila* lipase/acyltransferase stabilizes the structure but is not required for secretion or activity. *J Bacteriol.* 1997;179(10):3116-21.

86. Liebeton K, Zacharias A, Jaeger KE. Disulfide bond in *Pseudomonas aeruginosa* lipase stabilizes the structure but is not required for interaction with its foldase. *J Bacteriol.* 2001;183(2):597-603.
87. Martinez A, Ostrovsky P, Nunn DN. LipC, a second lipase of *Pseudomonas aeruginosa*, is LipB and Xcp dependent and is transcriptionally regulated by pilus biogenesis components. *Mol Microbiol.* 1999;34(2):317-26.
88. Chen YS, Bastidas RJ, Saka HA, Carpenter VK, Richards KL, Plano GV, et al. The *Chlamydia trachomatis* type III secretion chaperone Slc1 engages multiple early effectors, including TepP, a tyrosine-phosphorylated protein required for the recruitment of Crkl-II to nascent inclusions and innate immune signaling. *PLoS Pathog.* 2014;10(2):e1003954.
89. Shutinoski B, Schmidt MA, Heusipp G. Transcriptional regulation of the Yts1 type II secretion system of *Yersinia enterocolitica* and identification of secretion substrates. *Mol Microbiol.* 2010;75(3):676-91.
90. Szczesny R, Jordan M, Schramm C, Schulz S, Cogež V, Bonas U, et al. Functional characterization of the Xcs and Xps type II secretion systems from the plant pathogenic bacterium *Xanthomonas campestris* pv *vesicatoria*. *New Phytol.* 2010;187(4):983-1002.
91. Ball G, Durand E, Lazdunski A, Filloux A. A novel type II secretion system in *Pseudomonas aeruginosa*. *Mol Microbiol.* 2002;43(2):475-85.
92. Ball G, Viarre V, Garvis S, Voulhoux R, Filloux A. Type II-dependent secretion of a *Pseudomonas aeruginosa* DING protein. *Res Microbiol.* 2012;163(6-7):457-69.
93. Soderberg MA, Cianciotto NP. A *Legionella pneumophila* peptidyl-prolyl cis-trans isomerase present in culture supernatants is necessary for optimal growth at low temperatures. *Appl Environ Microbiol.* 2008;74(5):1634-8.
94. Soderberg MA, Dao J, Starckenburg SR, Cianciotto NP. Importance of type II secretion for survival of *Legionella pneumophila* in tap water and in amoebae at low temperatures. *Appl Environ Microbiol.* 2008;74(17):5583-8.
95. Soderberg MA, Rossier O, Cianciotto NP. The type II protein secretion system of *Legionella pneumophila* promotes growth at low temperatures. *J Bacteriol.* 2004;186(12):3712-20.
96. Cianciotto NP. Type II Secretion and *Legionella* Virulence. *Molecular Mechanisms of Legionella Pathogenesis.* Springer. 2014; 376:81-102.
97. Tyson JY, Pearce MM, Vargas P, Bagchi S, Mulhern BJ, Cianciotto NP. Multiple *Legionella pneumophila* Type II secretion substrates, including a novel protein, contribute to differential infection of the amoebae *Acanthamoeba castellanii*,

- Hartmannella vermiformis, and Naegleria lovaniensis. Infect Immun. 2013;81(5):1399-410.
98. Tyson JY, Vargas P, Cianciotto NP. The novel Legionella pneumophila type II secretion substrate NttC contributes to infection of amoebae Hartmannella vermiformis and Willaertia magna. Microbiology. 2014;160(Pt 12):2732-44.
99. Lang C, Rastew E, Hermes B, Siegbrecht E, Ahrends R, Banerji S, et al. Zinc metalloproteinase ProA directly activates Legionella pneumophila PlaC glycerophospholipid:cholesterol acyltransferase. J Biol Chem. 2012;287(28):23464-78.
100. Debroy S, Aragon V, Kurtz S, Cianciotto NP. Legionella pneumophila Mip, a surface-exposed peptidylproline cis-trans-isomerase, promotes the presence of phospholipase C-like activity in culture supernatants. Infect Immun. 2006;74(9):5152-60.
101. Omsland A, Cockrell DC, Fischer ER, Heinzen RA. Sustained axenic metabolic activity by the obligate intracellular bacterium Coxiella burnetii. J Bacteriol. 2008;190(9):3203-12.
102. Omsland A. Axenic growth of Coxiella burnetii. Adv Exp Med Biol. 2012;984:215-29.
103. Stead CM, Omsland A, Beare PA, Sandoz KM, Heinzen RA. Sec-mediated secretion by Coxiella burnetii. BMC Microbiol. 2013;13:222.
104. Aragon V, Kurtz S, Cianciotto NP. Legionella pneumophila major acid phosphatase and its role in intracellular infection. Infect Immun. 2001;69(1):177-85.
105. Cianciotto N, Eisenstein BI, Engleberg NC, Shuman H. Genetics and molecular pathogenesis of Legionella pneumophila, an intracellular parasite of macrophages. Mol Biol Med. 1989;6(5):409-24.
106. Cianciotto NP. Type II secretion: a protein secretion system for all seasons. Trends Microbiol. 2005;13(12):581-8. doi: 10.1016/j.tim.2005.09.005.
107. Dorsey FC, Fischer JF, Fleckenstein JM. Directed delivery of heat-labile enterotoxin by enterotoxigenic Escherichia coli. Cell Microbiol. 2006;8(9):1516-27.
108. Grys TE, Siegel MB, Lathem WW, Welch RA. The StcE protease contributes to intimate adherence of enterohemorrhagic Escherichia coli O157:H7 to host cells. Infect Immun. 2005;73(3):1295-303.
109. Iwobi A, Heesemann J, Garcia E, Igwe E, Noelting C, Rakin A. Novel virulence-associated type II secretion system unique to high-pathogenicity Yersinia enterocolitica. Infect Immun. 2003;71(4):1872-9.

110. Karaba SM, White RC, Cianciotto NP. *Stenotrophomonas maltophilia* encodes a type II protein secretion system that promotes detrimental effects on lung epithelial cells. *Infect Immun.* 2013;81(9):3210-9.
111. Overbye LJ, Sandkvist M, Bagdasarian M. Genes required for extracellular secretion of enterotoxin are clustered in *Vibrio cholerae*. *Gene.* 1993;132(1):101-6.
112. Patrick M, Gray MD, Sandkvist M, Johnson TL. Type II Secretion in *Escherichia coli*. *EcoSal Plus.* 2010;4(1).
113. Sandkvist M, Bagdasarian M, Howard SP. Characterization of the multimeric Eps complex required for cholera toxin secretion. *Int J Med Microbiol.* 2000;290(4-5):345-50.
114. Xu XJ, Ferguson MR, Popov VL, Houston CW, Peterson JW, Chopra AK. Role of a cytotoxic enterotoxin in *Aeromonas*-mediated infections: development of transposon and isogenic mutants. *Infect Immun.* 1998;66(8):3501-9.
115. Somvanshi VS, Viswanathan P, Jacobs JL, Mulks MH, Sundin GW, Ciche TA. The type 2 secretion Pseudopilin, *gspJ*, is required for multihost pathogenicity of *Burkholderia cenocepacia* AU1054. *Infect Immun.* 2010;78(10):4110-21.
116. Ho TD, Davis BM, Ritchie JM, Waldor MK. Type 2 secretion promotes enterohemorrhagic *Escherichia coli* adherence and intestinal colonization. *Infect Immun.* 2008;76(5):1858-65.
117. Baldi DL, Higginson EE, Hocking DM, Praszkie J, Cavaliere R, James CE, et al. The type II secretion system and its ubiquitous lipoprotein substrate, SslE, are required for biofilm formation and virulence of enteropathogenic *Escherichia coli*. *Infect Immun.* 2012;80(6):2042-52.
118. Tomas A, Lery L, Regueiro V, Perez-Gutierrez C, Martinez V, Moranta D, et al. Functional Genomic Screen Identifies *Klebsiella pneumoniae* Factors Implicated in Blocking Nuclear Factor kappaB (NF-kappaB) Signaling. *J Biol Chem.* 2015;290(27):16678-97.
119. McCoy-Simandle K, Stewart CR, Dao J, DebRoy S, Rossier O, Bryce PJ, et al. *Legionella pneumophila* type II secretion dampens the cytokine response of infected macrophages and epithelia. *Infect Immun.* 2011;79(5):1984-97.
120. Mulcahy H, Charron-Mazenod L, Lewenza S. *Pseudomonas aeruginosa* produces an extracellular deoxyribonuclease that is required for utilization of DNA as a nutrient source. *Environ Microbiol.* 2010;12(6):1621-9.
121. Jyot J, Balloy V, Jouvion G, Verma A, Touqui L, Huerre M, et al. Type II secretion system of *Pseudomonas aeruginosa*: in vivo evidence of a significant role in death due to lung infection. *J Infect Dis.* 2011;203(10):1369-77.

122. Hwang W, Lee NY, Kim J, Lee MA, Kim KS, Lee KH, et al. Functional characterization of EpsC, a component of the type II secretion system, in the pathogenicity of *Vibrio vulnificus*. *Infect Immun*. 2011;79(10):4068-80.
123. Yang Z, Tang L, Shao L, Zhang Y, Zhang T, Schenken R, et al. The Chlamydia-Secreted Protease CPAF Promotes Chlamydial Survival in the Mouse Lower Genital Tract. *Infect Immun*. 2016;84(9):2697-702.
124. Hassan S, Shevchik VE, Robert X, Hugouvieux-Cotte-Pattat N. PelN is a new pectate lyase of *Dickeya dadantii* with unusual characteristics. *J Bacteriol*. 2013;195(10):2197-206.
125. Kariola T, Palomaki TA, Brader G, Palva ET. *Erwinia carotovora* subsp. *carotovora* and *Erwinia*-derived elicitors HrpN and PehA trigger distinct but interacting defense responses and cell death in *Arabidopsis*. *Mol Plant Microbe Interact*. 2003;16(3):179-87.
126. Sauvonnet N, Poquet I, Pugsley AP. Extracellular secretion of pullulanase is unaffected by minor sequence changes but is usually prevented by adding reporter proteins to its N- or C-terminal end. *J Bacteriol*. 1995;177(18):5238-46.
127. Ray SK, Rajeshwari R, Sonti RV. Mutants of *Xanthomonas oryzae* pv. *oryzae* deficient in general secretory pathway are virulence deficient and unable to secrete xylanase. *Mol Plant Microbe Interact*. 2000;13(4):394-401.
128. Wang N, Ozer EA, Mandel MJ, Hauser AR. Genome-wide identification of *Acinetobacter baumannii* genes necessary for persistence in the lung. *MBio*. 2014;5(3):e01163-14.
129. Sole M, Scheibner F, Hoffmeister AK, Hartmann N, Hause G, Rother A, et al. *Xanthomonas campestris* pv. *vesicatoria* Secretes Proteases and Xylanases via the Xps Type II Secretion System and Outer Membrane Vesicles. *J Bacteriol*. 2015;197(17):2879-93.
130. Alrahman MA, Yoon SS. Identification of essential genes of *Pseudomonas aeruginosa* for its growth in airway mucus. *J Microbiol*. 2017;55(1):68-74.
131. Park BR, Zielke RA, Wierzbicki IH, Mitchell KC, Withey JH, Sikora AE. A metalloprotease secreted by the type II secretion system links *Vibrio cholerae* with collagen. *J Bacteriol*. 2015;197(6):1051-64.
132. Elhosseiny NM, El-Tayeb OM, Yassin AS, Lory S, Attia AS. The secretome of *Acinetobacter baumannii* ATCC 17978 type II secretion system reveals a novel plasmid encoded phospholipase that could be implicated in lung colonization. *Int J Med Microbiol*. 2016;306(8):633-41.

133. Kuhle K, Krausze J, Curth U, Rossle M, Heuner K, Lang C, et al. Oligomerization inhibits *Legionella pneumophila* PlaB phospholipase A activity. *J Biol Chem*. 2014;289(27):18657-66.
134. Aragon V, Rossier O, Cianciotto NP. *Legionella pneumophila* genes that encode lipase and phospholipase C activities. *Microbiology*. 2002;148(Pt 7):2223-31.
135. DeShazer D, Brett PJ, Burtnick MN, Woods DE. Molecular characterization of genetic loci required for secretion of exoproducts in *Burkholderia pseudomallei*. *J Bacteriol*. 1999;181(15):4661-4.
136. Lazdunski A, Guzzo J, Filloux A, Bally M, Murgier M. Secretion of extracellular proteins by *Pseudomonas aeruginosa*. *Biochimie*. 1990;72(2-3):147-56.
137. Rossier O, Dao J, Cianciotto NP. A type II secreted RNase of *Legionella pneumophila* facilitates optimal intracellular infection of *Hartmannella vermiformis*. *Microbiology*. 2009;155(Pt 3):882-90.
138. Rondelet A, Condemine G. Type II secretion: the substrates that won't go away. *Res Microbiol*. 2013;164(6):556-61.
139. Roy K, Hamilton DJ, Munson GP, Fleckenstein JM. Outer membrane vesicles induce immune responses to virulence proteins and protect against colonization by enterotoxigenic *Escherichia coli*. *Clin Vaccine Immunol*. 2011;18(11):1803-8.
140. Johnson AM, Kaushik RS, Francis DH, Fleckenstein JM, Hardwidge PR. Heat-labile enterotoxin promotes *Escherichia coli* adherence to intestinal epithelial cells. *J Bacteriol*. 2009;191(1):178-86.
141. Sandkvist M, Michel LO, Hough LP, Morales VM, Bagdasarian M, Koomey M, et al. General secretion pathway (*eps*) genes required for toxin secretion and outer membrane biogenesis in *Vibrio cholerae*. *J Bacteriol*. 1997;179(22):6994-7003.
142. Adderley-Kelly B, Stephens EM. Chlamydia: A major health threat to adolescents and young adults. *ABNF J*. 2005;16(3):52-5.
143. Prevention CfDCa. Sexually Transmitted Disease Surveillance 2014. Atlanta: U.S. Department of Health and Human Services; 2015.
144. Mylonas I. Female genital *Chlamydia trachomatis* infection: where are we heading? *Arch Gynecol Obstet*. 2012;285(5):1271-85.
145. Schachter J. The intracellular life of *Chlamydia*. *Curr Top Microbiol Immunol*. 1988;138:109-39.
146. Hodinka RL, Davis CH, Choong J, Wyrick PB. Ultrastructural study of endocytosis of *Chlamydia trachomatis* by McCoy cells. *Infect Immun*. 1988;56(6):1456-63.

147. Bastidas RJ, Elwell CA, Engel JN, Valdivia RH. Chlamydial intracellular survival strategies. *Cold Spring Harb Perspect Med*. 2013;3(5):a010256.
148. Valdivia RH. Chlamydia effector proteins and new insights into chlamydial cellular microbiology. *Curr Opin Microbiol*. 2008;11(1):53-9.
149. Betts-Hampikian HJ, Fields KA. The Chlamydial Type III Secretion Mechanism: Revealing Cracks in a Tough Nut. *Front Microbiol*. 2010;1:114.
150. Stephens RS, Kalman S, Lammel C, Fan J, Marathe R, Aravind L, et al. Genome sequence of an obligate intracellular pathogen of humans: *Chlamydia trachomatis*. *Science*. 1998;282(5389):754-9.
151. Mueller KE, Plano GV, Fields KA. New frontiers in type III secretion biology: the *Chlamydia* perspective. *Infect Immun*. 2014;82(1):2-9.
152. Nguyen BD, Valdivia RH. Virulence determinants in the obligate intracellular pathogen *Chlamydia trachomatis* revealed by forward genetic approaches. *Proc Natl Acad Sci U S A*. 2012;109(4):1263-8. doi: 10.1073/pnas.1117884109.
153. Rockey DD, Heinzen RA, Hackstadt T. Cloning and characterization of a *Chlamydia psittaci* gene coding for a protein localized in the inclusion membrane of infected cells. *Mol Microbiol*. 1995;15(4):617-26.
154. Misaghi S, Balsara ZR, Catic A, Spooner E, Ploegh HL, Starnbach MN. *Chlamydia trachomatis*-derived deubiquitinating enzymes in mammalian cells during infection. *Mol Microbiol*. 2006;61(1):142-50.
155. Clifton DR, Fields KA, Grieshaber SS, Dooley CA, Fischer ER, Mead DJ, et al. A chlamydial type III translocated protein is tyrosine-phosphorylated at the site of entry and associated with recruitment of actin. *Proc Natl Acad Sci U S A*. 2004;101(27):10166-71.
156. Dong F, Pirbhai M, Zhong Y, Zhong G. Cleavage-dependent activation of a chlamydia-secreted protease. *Mol Microbiol*. 2004;52(5):1487-94.
157. Lei L, Qi M, Budrys N, Schenken R, Zhong G. Localization of *Chlamydia trachomatis* hypothetical protein CT311 in host cell cytoplasm. *Microb Pathog*. 2011;51(3):101-9.
158. Qi M, Lei L, Gong S, Liu Q, DeLisa MP, Zhong G. *Chlamydia trachomatis* secretion of an immunodominant hypothetical protein (CT795) into host cell cytoplasm. *J Bacteriol*. 2011;193(10):2498-509.
159. Lu C, Lei L, Peng B, Tang L, Ding H, Gong S, et al. *Chlamydia trachomatis* GlgA is secreted into host cell cytoplasm. *PLoS One*. 2013;8(7):e68764.
160. Wolf K, Betts HJ, Chellas-Gery B, Hower S, Linton CN, Fields KA. Treatment of *Chlamydia trachomatis* with a small molecule inhibitor of the *Yersinia* type III secretion

system disrupts progression of the chlamydial developmental cycle. *Mol Microbiol.* 2006;61(6):1543-55.

161. Muschiol S, Bailey L, Gylfe A, Sundin C, Hultenby K, Bergstrom S, et al. A small-molecule inhibitor of type III secretion inhibits different stages of the infectious cycle of *Chlamydia trachomatis*. *Proc Natl Acad Sci U S A.* 2006;103(39):14566-71.

162. Paetzel M, Goodall JJ, Kania M, Dalbey RE, Page MG. Crystallographic and biophysical analysis of a bacterial signal peptidase in complex with a lipopeptide-based inhibitor. *J Biol Chem.* 2004;279(29):30781-90.

163. Chen D, Lei L, Lu C, Flores R, DeLisa MP, Roberts TC, et al. Secretion of the chlamydial virulence factor CPAF requires the Sec-dependent pathway. *Microbiology.* 2010;156(Pt 10):3031-40.

164. Sixt BS, Valdivia RH. Molecular Genetic Analysis of *Chlamydia* Species. *Annu Rev Microbiol.* 2016;70:179-98.

165. Johnson CM, Fisher DJ. Site-specific, insertional inactivation of *incA* in *Chlamydia trachomatis* using a group II intron. *PLoS One.* 2013;8(12):e83989.

166. Wang Y, Kahane S, Cutcliffe LT, Skilton RJ, Lambden PR, Clarke IN. Development of a transformation system for *Chlamydia trachomatis*: restoration of glycogen biosynthesis by acquisition of a plasmid shuttle vector. *PLoS Pathog.* 2011;7(9):e1002258.

167. Wang Y, Kahane S, Cutcliffe LT, Skilton RJ, Lambden PR, Persson K, et al. Genetic transformation of a clinical (genital tract), plasmid-free isolate of *Chlamydia trachomatis*: engineering the plasmid as a cloning vector. *PLoS One.* 2013;8(3):e59195.

168. Wickstrum J, Sammons LR, Restivo KN, Hefty PS. Conditional gene expression in *Chlamydia trachomatis* using the tet system. *PLoS One.* 2013;8(10):e76743.

169. Mueller KE WK, Fields KA. Gene Deletion by Fluorescence-Reported Allelic Exchange Mutagenesis in *Chlamydia trachomatis*. *mBio.* 2016;7(1):e01817-15.

170. Demars R, Weinfurter J, Guex E, Lin J, Potucek Y. Lateral gene transfer in vitro in the intracellular pathogen *Chlamydia trachomatis*. *J Bacteriol.* 2007;189(3):991-1003.

171. Kari L, Goheen MM, Randall LB, Taylor LD, Carlson JH, Whitmire WM, et al. Generation of targeted *Chlamydia trachomatis* null mutants. *Proc Natl Acad Sci U S A.* 2011;108(17):7189-93.

172. Kokes M, Dunn JD, Granek JA, Nguyen BD, Barker JR, Valdivia RH, et al. Integrating chemical mutagenesis and whole-genome sequencing as a platform for forward and reverse genetic analysis of *Chlamydia*. *Cell Host Microbe.* 2015;17(5):716-25.

173. Rajaram K, Giebel AM, Toh E, Hu S, Newman JH, Morrison SG, et al. Mutational Analysis of the *Chlamydia muridarum* Plasticity Zone. *Infect Immun*. 2015;83(7):2870-81.
174. Bauler LD, Hackstadt T. Expression and targeting of secreted proteins from *Chlamydia trachomatis*. *J Bacteriol*. 2014;196(7):1325-34.
175. Voth DE, Beare PA, Howe D, Sharma UM, Samoilis G, Cockrell DC, et al. The *Coxiella burnetii* cryptic plasmid is enriched in genes encoding type IV secretion system substrates. *J Bacteriol*. 2011;193(7):1493-503.
176. Mueller KE, Fields KA. Application of beta-lactamase reporter fusions as an indicator of effector protein secretion during infections with the obligate intracellular pathogen *Chlamydia trachomatis*. *PLoS One*. 2015;10(8):e0135295.
177. Zhong G, Fan P, Ji H, Dong F, Huang Y. Identification of a chlamydial protease-like activity factor responsible for the degradation of host transcription factors. *J Exp Med*. 2001;193(8):935-42. Epub 2001/04/17.
178. Dong F, Sharma J, Xiao Y, Zhong Y, Zhong G. Intramolecular dimerization is required for the chlamydia-secreted protease CPAF to degrade host transcriptional factors. *Infect Immun*. 2004;72(7):3869-75.
179. Huang Z, Feng Y, Chen D, Wu X, Huang S, Wang X, et al. Structural basis for activation and inhibition of the secreted chlamydia protease CPAF. *Cell Host Microbe*. 2008;4(6):529-42.
180. Jorgensen I, Valdivia RH. Pmp-like proteins Pls1 and Pls2 are secreted into the lumen of the *Chlamydia trachomatis* inclusion. *Infect Immun*. 2008;76(9):3940-50.
181. Bednar MM, Jorgensen I, Valdivia RH, McCafferty DG. Chlamydia protease-like activity factor (CPAF): characterization of proteolysis activity in vitro and development of a nanomolar affinity CPAF zymogen-derived inhibitor. *Biochemistry*. 2011;50(35):7441-3.
182. Chen AL, Johnson KA, Lee JK, Sutterlin C, Tan M. CPAF: a Chlamydial protease in search of an authentic substrate. *PLoS Pathog*. 2012;8(8):e1002842.
183. Dong F, Zhong Y, Arulanandam B, Zhong G. Production of a proteolytically active protein, chlamydial protease/proteasome-like activity factor, by five different *Chlamydia* species. *Infect Immun*. 2005;73(3):1868-72.
184. Kawana K, Quayle AJ, Ficarra M, Ibane JA, Shen L, Kawana Y, et al. CD1d degradation in *Chlamydia trachomatis*-infected epithelial cells is the result of both cellular and chlamydial proteasomal activity. *J Biol Chem*. 2007;282(10):7368-75.

185. Thomson NR, Holden MT, Carder C, Lennard N, Lockey SJ, Marsh P, et al. *Chlamydia trachomatis*: genome sequence analysis of lymphogranuloma venereum isolates. *Genome Res.* 2008;18(1):161-71.
186. Gehre L, Gorgette O, Perrinet S, Prevost MC, Ducatez M, Giebel AM, et al. Sequestration of host metabolism by an intracellular pathogen. *Elife.* 2016;5:e12552.
187. Omsland A, Sager J, Nair V, Sturdevant DE, Hackstadt T. Developmental stage-specific metabolic and transcriptional activity of *Chlamydia trachomatis* in an axenic medium. *Proc Natl Acad Sci U S A.* 2012;109(48):19781-5.
188. Saka HA, Thompson JW, Chen YS, Kumar Y, Dubois LG, Moseley MA, et al. Quantitative proteomics reveals metabolic and pathogenic properties of *Chlamydia trachomatis* developmental forms. *Mol Microbiol.* 2011;82(5):1185-203.
189. Skipp PJ, Hughes C, McKenna T, Edwards R, Langridge J, Thomson NR, et al. Quantitative Proteomics of the Infectious and Replicative Forms of *Chlamydia trachomatis*. *PLoS One.* 2016;11(2):e0149011.
190. O'Connell CM, Nicks KM. A plasmid-cured *Chlamydia muridarum* strain displays altered plaque morphology and reduced infectivity in cell culture. *Microbiology.* 2006;152(Pt 6):1601-7.
191. Carlson JH, Whitmire WM, Crane DD, Wicke L, Virtaneva K, Sturdevant DE, et al. The *Chlamydia trachomatis* plasmid is a transcriptional regulator of chromosomal genes and a virulence factor. *Infect Immun.* 2008;76(6):2273-83.
192. Ricci S, Ratti G, Scarlato V. Transcriptional regulation in the *Chlamydia trachomatis* pCT plasmid. *Gene.* 1995;154(1):93-8.
193. Song L, Carlson JH, Whitmire WM, Kari L, Virtaneva K, Sturdevant DE, et al. *Chlamydia trachomatis* plasmid-encoded Pgp4 is a transcriptional regulator of virulence-associated genes. *Infect Immun.* 2013;81(3):636-44.
194. Peterson EM, Markoff BA, Schachter J, de la Maza LM. The 7.5-kb plasmid present in *Chlamydia trachomatis* is not essential for the growth of this microorganism. *Plasmid.* 1990;23(2):144-8.
195. Gong S, Yang Z, Lei L, Shen L, Zhong G. Characterization of *Chlamydia trachomatis* plasmid-encoded open reading frames. *J Bacteriol.* 2013;195(17):3819-26.
196. O'Connell CM, Ingalls RR, Andrews CW, Jr., Scurlock AM, Darville T. Plasmid-deficient *Chlamydia muridarum* fail to induce immune pathology and protect against oviduct disease. *J Immunol.* 2007;179(6):4027-34.
197. Belland R, Ojcius DM, Byrne GI. *Chlamydia*. *Nat Rev Microbiol.* 2004;2(7):530-1. Epub 2004/07/14.

198. Darville T, Hiltke TJ. Pathogenesis of genital tract disease due to *Chlamydia trachomatis*. *J Infect Dis*. 2010;201 Suppl 2:S114-25. Epub 2010/06/05.
199. Hu VH, Harding-Esch, E. M., Burton, M. J., Bailey, R. L., Kadimpeul, J. and Mabey, D. C. W. Epidemiology and control of trachoma: systematic review. *Tropical Medicine & International Health* 2010. p. 673–91.
200. Hybiske K, Stephens RS. Mechanisms of host cell exit by the intracellular bacterium *Chlamydia*. *Proc Natl Acad Sci U S A*. 2007;104(27):11430-5.
201. Giles DK, Whittimore JD, LaRue RW, Raulston JE, Wyrick PB. Ultrastructural analysis of chlamydial antigen-containing vesicles everting from the *Chlamydia trachomatis* inclusion. *Microbes Infect*. 2006;8(6):1579-91.
202. Giles DK, Wyrick PB. Trafficking of chlamydial antigens to the endoplasmic reticulum of infected epithelial cells. *Microbes Infect*. 2008;10(14-15):1494-503. Epub 2008/10/04.
203. Sandkvist M. Type II secretion and pathogenesis. *Infect Immun*. 2001;69(6):3523-35.
204. Zhong G, Fan P, Ji H, Dong F, Huang Y. Identification of a chlamydial protease-like activity factor responsible for the degradation of host transcription factors. *J Exp Med*. 2001;193(8):935-42. Epub 2001/04/17.
205. Shaw AC, Vandahl BB, Larsen MR, Roepstorff P, Gevaert K, Vandekerckhove J, et al. Characterization of a secreted *Chlamydia* protease. *Cell Microbiol*. 2002;4(7):411-24.
206. Pirbhai M, Dong F, Zhong Y, Pan KZ, Zhong G. The secreted protease factor CPAF is responsible for degrading pro-apoptotic BH3-only proteins in *Chlamydia trachomatis*-infected cells. *J Biol Chem*. 2006;281(42):31495-501.
207. Christian JG, Vier J, Paschen SA, Hacker G. Cleavage of the NF- κ B-family protein p65/RelA by the chlamydial protease chlamydial protease-like activity factor (CPAF) impairs pro-inflammatory signalling in cells infected with chlamydiae. *J Biol Chem*. 2010.
208. Kumar Y, Valdivia RH. Actin and intermediate filaments stabilize the *Chlamydia trachomatis* vacuole by forming dynamic structural scaffolds. *Cell Host Microbe*. 2008;4(2):159-69.
209. Dong F, Su H, Huang Y, Zhong Y, Zhong G. Cleavage of host keratin 8 by a *Chlamydia*-secreted protease. *Infect Immun*. 2004;72(7):3863-8. Epub 2004/06/24.
210. Sun J, Kintner J, Schoborg RV. The host adherens junction molecule nectin-1 is downregulated in *Chlamydia trachomatis*-infected genital epithelial cells. *Microbiology*. 2008;154(Pt 5):1290-9.

211. Yu H, Schwarzer K, Forster M, Kniemeyer O, Forsbach-Birk V, Straube E, et al. Role of high-mobility group box 1 protein and poly(ADP-ribose) polymerase 1 degradation in *Chlamydia trachomatis*-induced cytopathicity. *Infect Immun*. 2010;78(7):3288-97.
212. Paschen SA, Christian JG, Vier J, Schmidt F, Walch A, Ojcius DM, et al. Cytopathicity of *Chlamydia* is largely reproduced by expression of a single chlamydial protease. *J Cell Biol*. 2008;182(1):117-27. Epub 2008/07/16.
213. Brown HM, Knowlton AE, Grieshaber SS. Chlamydial infection induces host cytokinesis failure at abscission. *Cell Microbiol*. 2012;14(10):1554-67.
214. Christian JG, Heymann J, Paschen SA, Vier J, Schauenburg L, Rupp J, et al. Targeting of a chlamydial protease impedes intracellular bacterial growth. *PLoS Pathog*. 2011;7(9):e1002283.
215. Paschen SA, Christian JG, Vier J, Schmidt F, Walch A, Ojcius DM, et al. Cytopathicity of *Chlamydia* is largely reproduced by expression of a single chlamydial protease. *J Cell Biol*. 2008;182(1):117-27. 10.1083/jcb.200804023. PubMed PMID: 18625845; PubMed Central PMCID: PMC2447887.
216. Zhong G. *Chlamydia trachomatis* secretion of proteases for manipulating host signaling pathways. *Front Microbiol*. 2011;2:14.
217. Zhong G. Killing me softly: chlamydial use of proteolysis for evading host defenses. *Trends Microbiol*. 2009;17(10):467-74.
218. Jorgensen I, Bednar MM, Amin V, Davis BK, Ting JP, McCafferty DG, et al. The *Chlamydia* protease CPAF regulates host and bacterial proteins to maintain pathogen vacuole integrity and promote virulence. *Cell Host Microbe*. 2011;10(1):21-32.
219. Patton MJ, McCorrister S, Grant C, Westmacott G, Fariss R, Hu P, et al. Chlamydial Protease-Like Activity Factor and Type III Secreted Effectors Cooperate in Inhibition of p65 Nuclear Translocation. *MBio*. 2016;7(5).
220. Hou S, Lei L, Yang Z, Qi M, Liu Q, Zhong G. *Chlamydia trachomatis* outer membrane complex protein B (OmcB) is processed by the protease CPAF. *J Bacteriol*. 2013;195(5):951-7.
221. Qi M, Gong S, Lei L, Liu Q, Zhong G. A *Chlamydia trachomatis* OmcB C-terminal fragment is released into the host cell cytoplasm and is immunogenic in humans. *Infect Immun*. 2011;79(6):2193-203.
222. Chen AL, Johnson KA, Lee JK, Sutterlin C, Tan M. CPAF: a *Chlamydial* protease in search of an authentic substrate. *PLoS Pathog*. 2012;8(8):e1002842.

223. Nguyen BD, Valdivia RH. Virulence determinants in the obligate intracellular pathogen *Chlamydia trachomatis* revealed by forward genetic approaches. *Proc Natl Acad Sci U S A*. 2012;109(4):1263-8.
224. Dong F, Pirbhai M, Zhong Y, Zhong G. Cleavage-dependent activation of a chlamydia-secreted protease. *Mol Microbiol*. 2004;52(5):1487-94.
225. Byrne GI, Ojcius DM. Chlamydia and apoptosis: life and death decisions of an intracellular pathogen. *Nat Rev Microbiol*. 2004;2(10):802-8.
226. Sharma M, Rudel T. Apoptosis resistance in Chlamydia-infected cells: a fate worse than death? *FEMS Immunol Med Microbiol*. 2009;55(2):154-61.
227. Fischer SF, Vier J, Kirschnek S, Klos A, Hess S, Ying S, et al. Chlamydia inhibit host cell apoptosis by degradation of proapoptotic BH3-only proteins. *J Exp Med*. 2004;200(7):905-16.
228. Pirbhai M, Dong F, Zhong Y, Pan KZ, Zhong G. The secreted protease factor CPAF is responsible for degrading pro-apoptotic BH3-only proteins in Chlamydia trachomatis-infected cells. *J Biol Chem*. 2006;281(42):31495-501.
229. Fan T, Lu H, Hu H, Shi L, McClarty GA, Nance DM, et al. Inhibition of apoptosis in chlamydia-infected cells: blockade of mitochondrial cytochrome c release and caspase activation. *J Exp Med*. 1998;187(4):487-96.
230. Christian J, Vier J, Paschen SA, Hacker G. Cleavage of the NF-kappaB family protein p65/RelA by the chlamydial protease-like activity factor (CPAF) impairs proinflammatory signaling in cells infected with Chlamydiae. *J Biol Chem*. 2010;285(53):41320-7.
231. Liu X, Afrane M, Clemmer DE, Zhong G, Nelson DE. Identification of Chlamydia trachomatis outer membrane complex proteins by differential proteomics. *J Bacteriol*. 2010;192(11):2852-60.
232. Qi M, Gong S, Lei L, Liu Q, Zhong G. A Chlamydia trachomatis OmcB C-terminal fragment is released into the host cell cytoplasm and is immunogenic in humans. *Infect Immun*. 2011;79(6):2193-203.
233. Stephens RS, Koshiyama K, Lewis E, Kubo A. Heparin-binding outer membrane protein of chlamydiae. *Mol Microbiol*. 2001;40(3):691-9.
234. Fechtner T, Stallmann S, Moelleken K, Meyer KL, Hegemann JH. Characterization of the interaction between the chlamydial adhesin OmcB and the human host cell. *J Bacteriol*. 2013;195(23):5323-33.
235. Hou S, Lei L, Yang Z, Qi M, Liu Q, Zhong G. Chlamydia trachomatis outer membrane complex protein B (OmcB) is processed by the protease CPAF. *J Bacteriol*. 2013;195(5):951-7.

236. Lotze MT, Tracey KJ. High-mobility group box 1 protein (HMGB1): nuclear weapon in the immune arsenal. *Nat Rev Immunol.* 2005;5(4):331-42.
237. Heuer D, Rejman Lipinski A, Machuy N, Karlas A, Wehrens A, Siedler F, et al. Chlamydia causes fragmentation of the Golgi compartment to ensure reproduction. *Nature.* 2009;457(7230):731-5.
238. Dong F, Su H, Huang Y, Zhong Y, Zhong G. Cleavage of host keratin 8 by a Chlamydia-secreted protease. *Infect Immun.* 2004;72(7):3863-8.
239. Kumar Y, Valdivia RH. Actin and intermediate filaments stabilize the Chlamydia trachomatis vacuole by forming dynamic structural scaffolds. *Cell Host Microbe.* 2008;4(2):159-69.
240. Goodchild RE, Dauer WT. The AAA+ protein torsinA interacts with a conserved domain present in LAP1 and a novel ER protein. *J Cell Biol.* 2005;168(6):855-62.
241. Saka HA, Thompson JW, Chen YS, Kumar Y, Dubois LG, Moseley MA, et al. Quantitative proteomics reveals metabolic and pathogenic properties of Chlamydia trachomatis developmental forms. *Mol Microbiol.* 2011;82(5):1185-203.
242. Zhong G, Liu L, Fan T, Fan P, Ji H. Degradation of transcription factor RFX5 during the inhibition of both constitutive and interferon gamma-inducible major histocompatibility complex class I expression in chlamydia-infected cells. *J Exp Med.* 2000;191(9):1525-34.
243. Wang Y, Kahane S, Cutcliffe LT, Skilton RJ, Lambden PR, Clarke IN. Development of a transformation system for Chlamydia trachomatis: restoration of glycogen biosynthesis by acquisition of a plasmid shuttle vector. *PLoS Pathog.* 2011;7(9):e1002258.
244. Conrad T, Yang Z, Ojcius D, Zhong G. A path forward for the chlamydial virulence factor CPAF. *Microbes Infect.* 2013.
245. Murthy AK, Guentzel MN, Zhong G, Arulanandam BP. Chlamydial protease-like activity factor--insights into immunity and vaccine development. *J Reprod Immunol.* 2009;83(1-2):179-84.
246. Murthy AK, Li W, Guentzel MN, Zhong G, Arulanandam BP. Vaccination with the defined chlamydial secreted protein CPAF induces robust protection against female infertility following repeated genital chlamydial challenge. *Vaccine.* 2011;29(14):2519-22.
247. Nguyen BD, Valdivia RH. Forward genetic approaches in Chlamydia trachomatis. *J Vis Exp.* 2013;(80):e50636.
248. Malhotra M, Sood S, Mukherjee A, Muralidhar S, Bala M. Genital Chlamydia trachomatis: an update. *Indian J Med Res.* 2013;138(3):303-16.

249. Peabody CR, Chung YJ, Yen MR, Vidal-Ingigliardi D, Pugsley AP, Saier MH, Jr. Type II protein secretion and its relationship to bacterial type IV pili and archaeal flagella. *Microbiology*. 2003;149(Pt 11):3051-72.
250. Prain CJ, Pearce JH. Ultrastructural studies on the intracellular fate of *Chlamydia psittaci* (strain guinea pig inclusion conjunctivitis) and *Chlamydia trachomatis* (strain lymphogranuloma venereum 434): modulation of intracellular events and relationship with endocytic mechanism. *J Gen Microbiol*. 1989;135(7):2107-23.
251. Patel AL, Chen X, Wood ST, Stuart ES, Arcaro KF, Molina DP, et al. Activation of epidermal growth factor receptor is required for *Chlamydia trachomatis* development. *BMC Microbiol*. 2014;14:277.
252. Housby JN, Thomas JD, Wharam SD, Reeves PJ, Salmond GP. Conditional mutations in OutE and OutL block exoenzyme secretion across the *Erwinia carotovora* outer membrane. *FEMS Microbiol Lett*. 1998;165(1):91-102.
253. Green ER, Meccas J. Bacterial Secretion Systems: An Overview. *Microbiol Spectr*. 2016;4(1). doi: 10.1128/microbiolspec.VMBF-0012-2015.
254. Tsukazaki T, Nureki O. The mechanism of protein export enhancement by the SecDF membrane component. *Biophysics (Nagoya-shi)*. 2011;7:129-33.
255. Sikora AE, Beyhan S, Bagdasarian M, Yildiz FH, Sandkvist M. Cell envelope perturbation induces oxidative stress and changes in iron homeostasis in *Vibrio cholerae*. *J Bacteriol*. 2009;191(17):5398-408.
256. Karunakaran KP, Noguchi Y, Read TD, Cherkasov A, Kwee J, Shen C, et al. Molecular analysis of the multiple GroEL proteins of *Chlamydiae*. *J Bacteriol*. 2003;185(6):1958-66.
257. Hanson BR, Tan M. Transcriptional regulation of the *Chlamydia* heat shock stress response in an intracellular infection. *Mol Microbiol*. 2015;97(6):1158-67.
258. Wilson AC, Tan M. Stress response gene regulation in *Chlamydia* is dependent on HrcA-CIRCE interactions. *J Bacteriol*. 2004;186(11):3384-91.
259. Marsh JW, Wee BA, Tyndall JD, Lott WB, Bastidas RJ, Caldwell HD, et al. A *Chlamydia trachomatis* strain with a chemically generated amino acid substitution (P370L) in the *cthtrA* gene shows reduced elementary body production. *BMC Microbiol*. 2015;15:194.
260. Patel P, De Boer L, Timms P, Huston WM. Evidence of a conserved role for *Chlamydia* HtrA in the replication phase of the chlamydial developmental cycle. *Microbes Infect*. 2014;16(8):690-4.

261. Wu X, Lei L, Gong S, Chen D, Flores R, Zhong G. The chlamydial periplasmic stress response serine protease cHtrA is secreted into host cell cytosol. *BMC Microbiol.* 2011;11:87.
262. Schwechheimer C, Kuehn MJ. Outer-membrane vesicles from Gram-negative bacteria: biogenesis and functions. *Nat Rev Microbiol.* 2015;13(10):605-19.
263. Giles DK, Whittimore JD, LaRue RW, Raulston JE, Wyrick PB. Ultrastructural analysis of chlamydial antigen-containing vesicles everting from the *Chlamydia trachomatis* inclusion. *Microbes Infect.* 2006;8(6):1579-91.
264. Matsumoto A, Manire GP. Electron microscopic observations on the effects of penicillin on the morphology of *Chlamydia psittaci*. *J Bacteriol.* 1970;101(1):278-85.
265. Frohlich KM, Hua Z, Quayle AJ, Wang J, Lewis ME, Chou CW, et al. Membrane vesicle production by *Chlamydia trachomatis* as an adaptive response. *Front Cell Infect Microbiol.* 2014;4:73.
266. Bonnington KE, Kuehn MJ. Outer Membrane Vesicle Production Facilitates LPS Remodeling and Outer Membrane Maintenance in *Salmonella* during Environmental Transitions. *MBio.* 2016;7(5).
267. Schwechheimer C, Kuehn MJ. Synthetic effect between envelope stress and lack of outer membrane vesicle production in *Escherichia coli*. *J Bacteriol.* 2013;195(18):4161-73.
268. Macdonald IA, Kuehn MJ. Stress-induced outer membrane vesicle production by *Pseudomonas aeruginosa*. *J Bacteriol.* 2013;195(13):2971-81.
269. McBroom AJ, Johnson AP, Vemulapalli S, Kuehn MJ. Outer membrane vesicle production by *Escherichia coli* is independent of membrane instability. *J Bacteriol.* 2006;188(15):5385-92.
270. Dutta S, Iida K, Takade A, Meno Y, Nair GB, Yoshida S. Release of Shiga toxin by membrane vesicles in *Shigella dysenteriae* serotype 1 strains and in vitro effects of antimicrobials on toxin production and release. *Microbiol Immunol.* 2004;48(12):965-9.
271. Maredia R, Devineni N, Lentz P, Dallo SF, Yu J, Guentzel N, et al. Vesiculation from *Pseudomonas aeruginosa* under SOS. *ScientificWorldJournal.* 2012;2012:402919.
272. Wang J, Frohlich KM, Buckner L, Quayle AJ, Luo M, Feng X, et al. Altered protein secretion of *Chlamydia trachomatis* in persistently infected human endocervical epithelial cells. *Microbiology.* 2011;157(Pt 10):2759-71.
273. da Cunha M, Milho C, Almeida F, Pais SV, Borges V, Mauricio R, et al. Identification of type III secretion substrates of *Chlamydia trachomatis* using *Yersinia enterocolitica* as a heterologous system. *BMC Microbiol.* 2014;14:40.

274. Belland RJ, Zhong G, Crane DD, Hogan D, Sturdevant D, Sharma J, et al. Genomic transcriptional profiling of the developmental cycle of *Chlamydia trachomatis*. *Proc Natl Acad Sci U S A*. 2003;100(14):8478-83.
275. Moelleken K, Hegemann JH. The *Chlamydia* outer membrane protein OmcB is required for adhesion and exhibits biovar-specific differences in glycosaminoglycan binding. *Mol Microbiol*. 2008;67(2):403-19.
276. Stephens RS, Poteralski JM, Olinger L. Interaction of *Chlamydia trachomatis* with mammalian cells is independent of host cell surface heparan sulfate glycosaminoglycans. *Infect Immun*. 2006;74(3):1795-9.
277. Su H, Raymond L, Rockey DD, Fischer E, Hackstadt T, Caldwell HD. A recombinant *Chlamydia trachomatis* major outer membrane protein binds to heparan sulfate receptors on epithelial cells. *Proc Natl Acad Sci U S A*. 1996;93(20):11143-8. PubMed PMID: 8855323; PubMed Central PMCID: PMC38298.
278. Kihlstrom E, Majeed M, Rozalska B, Wadstrom T. Binding of *Chlamydia trachomatis* serovar L2 to collagen types I and IV, fibronectin, heparan sulphate, laminin and vitronectin. *Zentralbl Bakteriol*. 1992;277(3):329-33.
279. Abromaitis S, Stephens RS. Attachment and entry of *Chlamydia* have distinct requirements for host protein disulfide isomerase. *PLoS Pathog*. 2009;5(4):e1000357.
280. Conant CG, Stephens RS. *Chlamydia* attachment to mammalian cells requires protein disulfide isomerase. *Cell Microbiol*. 2007;9(1):222-32.
281. Becker E, Hegemann JH. All subtypes of the Pmp adhesin family are implicated in chlamydial virulence and show species-specific function. *Microbiologyopen*. 2014;3(4):544-56.
282. Molleken K, Schmidt E, Hegemann JH. Members of the Pmp protein family of *Chlamydia pneumoniae* mediate adhesion to human cells via short repetitive peptide motifs. *Mol Microbiol*. 2010;78(4):1004-17.
283. Stallmann S, Hegemann JH. The *Chlamydia trachomatis* Ctad1 invasin exploits the human integrin beta1 receptor for host cell entry. *Cell Microbiol*. 2016;18(5):761-75.
284. Bendtsen JD, Nielsen H, von Heijne G, Brunak S. Improved prediction of signal peptides: SignalP 3.0. *J Mol Biol*. 2004;340(4):783-95.
285. Finco O, Frigimelica E, Buricchi F, Petracca R, Galli G, Faenzi E, et al. Approach to discover T- and B-cell antigens of intracellular pathogens applied to the design of *Chlamydia trachomatis* vaccines. *Proc Natl Acad Sci U S A*. 2011;108(24):9969-74.
286. Mac TT, von Hacht A, Hung KC, Dutton RJ, Boyd D, Bardwell JC, et al. Insight into disulfide bond catalysis in *Chlamydia* from the structure and function of DsbH, a novel oxidoreductase. *J Biol Chem*. 2008;283(2):824-32.

287. Gutierrez J, Smith R, Pogliano K. SpoIID-mediated peptidoglycan degradation is required throughout engulfment during *Bacillus subtilis* sporulation. *J Bacteriol.* 2010;192(12):3174-86.
288. Lundemose AG, Rouch DA, Penn CW, Pearce JH. The *Chlamydia trachomatis* Mip-like protein is a lipoprotein. *J Bacteriol.* 1993;175(11):3669-71.
289. Lundemose AG, Kay JE, Pearce JH. *Chlamydia trachomatis* Mip-like protein has peptidyl-prolyl cis/trans isomerase activity that is inhibited by FK506 and rapamycin and is implicated in initiation of chlamydial infection. *Mol Microbiol.* 1993;7(5):777-83.
290. Lundemose AG, Rouch DA, Birkelund S, Christiansen G, Pearce JH. *Chlamydia trachomatis* Mip-like protein. *Mol Microbiol.* 1992;6(17):2539-48.
291. Bangsberg JM, Cianciotto NP, Hindersson P. Nucleotide sequence analysis of the *Legionella micdadei* mip gene, encoding a 30-kilodalton analog of the *Legionella pneumophila* Mip protein. *Infect Immun.* 1991;59(10):3836-40.
292. Cianciotto NP, Bangsberg JM, Eisenstein BI, Engleberg NC. Identification of mip-like genes in the genus *Legionella*. *Infect Immun.* 1990;58(9):2912-8.
293. Neff L, Daher S, Muzzin P, Spenato U, Gulacar F, Gabay C, et al. Molecular characterization and subcellular localization of macrophage infectivity potentiator, a *Chlamydia trachomatis* lipoprotein. *J Bacteriol.* 2007;189(13):4739-48.
294. Cianciotto NP, Stamos JK, Kamp DW. Infectivity of *Legionella pneumophila* mip mutant for alveolar epithelial cells. *Curr Microbiol.* 1995;30(4):247-50.
295. Michel LV, Shaw J, MacPherson V, Barnard D, Bettinger J, D'Arcy B, et al. Dual orientation of the outer membrane lipoprotein Pal in *Escherichia coli*. *Microbiology.* 2015;161(6):1251-9.
296. Hellman J, Warren HS. Outer membrane protein A (OmpA), peptidoglycan-associated lipoprotein (PAL), and murein lipoprotein (MLP) are released in experimental Gram-negative sepsis. *J Endotoxin Res.* 2001;7(1):69-72.
297. d'Enfert C, Pugsley AP. A gene fusion approach to the study of pullulanase export and secretion in *Escherichia coli*. *Mol Microbiol.* 1987;1(2):159-68.
298. Sauvonnnet N, Pugsley AP. The requirement for DsbA in pullulanase secretion is independent of disulphide bond formation in the enzyme. *Mol Microbiol.* 1998;27(3):661-7.
299. Yang C, Starr T, Song L, Carlson JH, Sturdevant GL, Beare PA, et al. Chlamydial Lytic Exit from Host Cells Is Plasmid Regulated. *MBio.* 2015;6(6):e01648-15.

300. Lu C, Turley S, Marionni ST, Park YJ, Lee KK, Patrick M, et al. Hexamers of the type II secretion ATPase GspE from *Vibrio cholerae* with increased ATPase activity. *Structure*. 2013;21(9):1707-17.
301. Jorgensen I, Bednar MM, Amin V, Davis BK, Ting JP, McCafferty DG, et al. The *Chlamydia* protease CPAF regulates host and bacterial proteins to maintain pathogen vacuole integrity and promote virulence. *Cell Host Microbe*. 2011;10(1):21-32.
302. Rompikuntal PK, Vdovikova S, Duperthuy M, Johnson TL, Ahlund M, Lundmark R, et al. Outer Membrane Vesicle-Mediated Export of Processed PrtV Protease from *Vibrio cholerae*. *PLoS One*. 2015;10(7):e0134098.
303. Altindis E, Fu Y, Mekalanos JJ. Proteomic analysis of *Vibrio cholerae* outer membrane vesicles. *Proc Natl Acad Sci U S A*. 2014;111(15):E1548-56.
304. Chatterjee D, Chaudhuri K. Association of cholera toxin with *Vibrio cholerae* outer membrane vesicles which are internalized by human intestinal epithelial cells. *FEBS Lett*. 2011;585(9):1357-62.
305. Jung AL, Hoffmann K, Herkt CE, Schulz C, Bertrams W, Schmeck B. *Legionella pneumophila* Outer Membrane Vesicles: Isolation and Analysis of Their Pro-inflammatory Potential on Macrophages. *J Vis Exp*. 2017;(120).
306. Sjostrom AE, Sandblad L, Uhlin BE, Wai SN. Membrane vesicle-mediated release of bacterial RNA. *Sci Rep*. 2015;5:15329.
307. Gordon FB, Quan AL. Occurrence of Glycogen in Inclusions of the Psittacosis-Lymphogranuloma Venereum-Trachoma Agents. *J Infect Dis*. 1965;115:186-96.
308. Zuck M, Sherrid A, Suchland R, Ellis T, Hybiske K. Conservation of extrusion as an exit mechanism for *Chlamydia*. *Pathog Dis*. 2016;74(7).
309. Zuck M, Ellis T, Venida A, Hybiske K. Extrusions are phagocytosed and promote *Chlamydia* survival within macrophages. *Cell Microbiol*. 2017;19(4).
310. Brown HM, Knowlton AE, Snavelly E, Nguyen BD, Richards TS, Grieshaber SS. Multinucleation during *C. trachomatis* infections is caused by the contribution of two effector pathways. *PLoS One*. 2014;9(6):e100763.
311. H. Zhang RNB, W.J. Qian, M.E. Monroe, S.O. Purvine, R.J. Moore, M.A. Gritsenko, L. Shi, et al. Quantitative analysis of cell surface membrane proteins using membrane-impermeable chemical probe coupled with ¹⁸O labeling. *Proteome Res*. 2011;9.
312. Souchet M, Legave M, Jullian N, Bertrand HO, Bril A, Berrebi-Bertrand I. Structure of the human glycogen-associated protein phosphatase 1 regulatory subunit hGM: homology modeling revealed an (alpha/beta)₈-barrel-like fold in the multidomain protein. *Protein Sci*. 1999;8(12):2570-9.

313. Iliffe-Lee ER, McClarty G. Regulation of carbon metabolism in *Chlamydia trachomatis*. *Mol Microbiol.* 2000;38(1):20-30.
314. Kuczkowska K, Myrbraten I, Overland L, Eijsink VGH, Follmann F, Mathiesen G, et al. *Lactobacillus plantarum* producing a *Chlamydia trachomatis* antigen induces a specific IgA response after mucosal booster immunization. *PLoS One.* 2017;12(5):e0176401.
315. Martius J, Krohn MA, Hillier SL, Stamm WE, Holmes KK, Eschenbach DA. Relationships of vaginal *Lactobacillus* species, cervical *Chlamydia trachomatis*, and bacterial vaginosis to preterm birth. *Obstet Gynecol.* 1988;71(1):89-95.
316. Gong Z, Luna Y, Yu P, Fan H. *Lactobacilli* inactivate *Chlamydia trachomatis* through lactic acid but not H₂O₂. *PLoS One.* 2014;9(9):e107758.
317. Nardini P, Nahui Palomino RA, Parolin C, Laghi L, Foschi C, Cevenini R, et al. *Lactobacillus crispatus* inhibits the infectivity of *Chlamydia trachomatis* elementary bodies, in vitro study. *Sci Rep.* 2016;6:29024.

Biography

Emily Snavelly was born in 1988 and grew up near Rapid City, SD. She attended college at Dartmouth College in Hanover, NH and graduated with a B.A and high honors in Biology in 2010. She came to graduate school at Duke University and joined Raphael Valdivia's laboratory in the Spring of 2011. After graduate school, she is pursuing an APHL/CDC Antimicrobial Resistance Fellowship at the Wadsworth Center in Albany, NY.